EXCITATION OF WAVE PACKETS AND RANDOM DISTURBANCES IN A BOUNDARY LAYER

by

Christopher E. Costis

Thesis submitted to the Graduate Faculty of the
Virginia Polytechnic Institute and State University
in partial fulfillment of the requirements of the degree of

MASTER OF SCIENCE
in
Engineering Mechanics

APPROVED:

W. S. Saric, Chairman

Th. Herbert

D. P. Telionis

May 1982
Blacksburg, Virginia

ACKNOWLEDGEMENTS

The completion of the work described here could have only been possible with the special help and cooperation of all those involved in the project. For this cooperation the author is very grateful and would like to express his sincere thanks collectively.

A very special thanks is due to the author's advisor, Professor William S. Saric, for his advice and assistance. The author would also like to extend special thanks to and for their assistance and their valuable pieces of advice.

The author also wishes to thank Professor D. Telionis and Carol Saric for their moral support and also and for their patience and skill in the typing of the thesis.

This work was supported under NASA-Langley Research Center Grant No.

TABLE OF CONTENTS

TABLE OF CONTENTS (continued)

CHAPTER 1

INTRODUCTION

In the flows past solid bodies, a very frequently encountered phenomenon is the transition of the boundary layer from laminar to turbulent flow. The presence of pressure gradients, the surface roughness and the free-stream turbulence are just a few of the factors that influence transition. The lower skin friction and heat transfer of laminar boundary layers compared with that of turbulent ones, and the resulting practical application to drag reduction of vehicles and airplanes is a great motivation for further study of the problem of transition.

A simple model for the study of the transition is a flat plate in a uniform flow with no pressure gradient. The fundamental idea, that small disturbances present in a laminar boundary layer may eventually lead to transition, was first proposed by Tollmien (1929) & Schlichting (1933). However, the first credible experimental investigation came with the work of Schubauer & Skramstad (1947). They verified aspects of the theory of Tollmien & Schlichting by introducing sinusoidal velocity fluctuations into the boundary layer by using the vibrating-ribbon technique and observing the subsequent growth of the disturbances. This work represents the first experimental verification of neutral stability points for the case of the flat plate with and without pressure gradient.

Another fundamental contribution in the investigation of the nature of the transition was done by Klebanoff & Tidstrom (1959). They were the first to observe that well controlled two-dimensional initial disturbances quickly transform into three-dimensional configurations. This work was followed by Klebanoff et al. (1962), Kovasznay et al. (1962), Hama & Nutant (1963) and others. The primary purpose of these efforts was the understanding of the mechanism that causes the transformation into 3-D configurations, as well as the justification of a theoretical model that would explain the phenomenon. An interesting result of the measurements was that 3-D configurations develop when the amplitude of the disturbances approaches 1% of the value of the free-stream velocity.

The theory of Tollmien (1929) & Schlichting (1933) and experimental verification by Schubauer & Skramstad (1947), Ross et al. (1970), Kachanov et al. (1975), & Strazisar et al. (1975) have established that growth or decay of disturbances depends not only on spatial location i.e., the Reynolds number, but also on frequency. At a given Reynolds number there is a discrete frequency band of disturbances which are amplified while all others are damped. Figs. 1.1 and 1.2 show a typical profile of a disturbance and the spatial growth of its maximum. Likewise, for a given frequency, there is a region from R_I to R_{II} which has amplified waves while outside this region the waves decay. This is the behavior predicted by the neutral stability curve shown in Fig. 1.3. Figure 1.3 gives the neutral stability curves, found by parallel and nonparallel linear theory (e.g. Saric & Nayfeh,

1977). The difference between the two theories is that in the parallel theory the growth of the boundary-layer thickness is not taken into account and the boundary-layer flow is considered as parallel. A simple example of a theoretical calculation, using the prallel theory, is given in chapter three.

The experimental and theoretical studies on boundary-layer stability and transition have been in constant growth during the last few years. Modern, low-turbulence wind tunnels, as well as digital computers have made additional contributions to the knowledge about the phenomena. Although the modern electronic equipment make the acquisition of experimental data more precise and quick, some of the classic techniques are still in use. The introduction of the velocity fluctuations by the vibrating-ribbon technique is still in use and it seems that it provides greater advantages compared to other methods, like introduction of sound disturbances or local periodic injection of fluid in the boundary layer. The technique consists of a ribbon placed transverse to the mean flow at a fixed distance from the plate. An alternating current is passed through the ribbon and magnets placed on the back of the plate create a constant magnetic field within which the ribbon is located. Due to the Lorentz force, a force acts on the ribbon and vibrates it at the frequency of the AC current.

The technique is useful for introducing controlled 2-D disturbances into the boundary layer. In order to create 3-D disturbances, the vibrating ribbon may be placed on the flat plate at an angle different than 90 degrees with the mean flow. This setup will produce an

organized 3-D pattern. Moreover, by reversing the polarity of some of the magnets, it is possible to vibrate the ribbon in higher modes than the fundamental. However, these methods have problems and the simplest method is one in which strips of tape are placed under the vibrating ribbon as first done by Klebanoff & Tidstrom (1959).

An interesting feature of the vibrating-ribbon technique is the ability of introducing fluctuations of the mean flow at more than a single frequency. Having an easy way to introduce waves of two or more frequencies at the same time, wave interactions can be studied and non-linear theories can be tested (Saric & Reynolds, 1980).

The purpose of the present work is to demonstrate the abilities of the vibrating ribbon to produce many types of disturbances, like higher frequency ones, random or step-function form, if it is combined with modern electronic equipment and data-acquisition systems. It started as an attempt to develop a method to create a 3-D disturbance pattern which would replace the old technique that uses strips of tape under the vibrating ribbon. The work continued with the development of a quick method of locating the neutral stability curve by using random excitation on the ribbon. Also, some interesting phenomena are observed by exciting the vibrating ribbon with a DC current having a form of a step function.

In chapter 2 of the present work, there is a brief description of the experimental facilities. Chapter 3 contains a description of the theory of Tollmien-Schlichting waves as well as an attempt to model the vibrating ribbon by a spring-mass-dashpot system. In chapter 4

are the results of the random excitation of the vibrating ribbon and in chapter 5 the step excitation results are presented. Some concluding remarks are given in chapter 6.

CHAPTER 2

EXPERIMENTAL FACILITIES AND APPARATUS

2.1 The Wind Tunnel Facilities

The experiments are performed in the VPI & SU Stability Wind Tunnel. The layout of the facility is shown in Fig. 2.1. Recent studies (Reynolds 1979) indicate that the tunnel is able to provide very good flow quality. The free-stream turbulence level is found to be in the range of .02% - .04% of the free-stream velocity. Bradshaw (1965) shows that the optimum damping screens must have an open-area ratio greater than 0.57 in order to be able to effectively reduce free-stream turbulendce. The damping screens in the VPI & SU tunnel have an open-area ration of 0.60 and are quite effective in reducing the turbulence level and permit accurate transition experiments.

The facility is a closed loop with an air-exchange tower which is open to the atmosphere. The tunnel circuit has no heat exchanger for temperature control, however, temperature stability is maintained by partial air replacement via the air-exchange tower.

The test section is 7.3 m long with a constant square cross-section of 1.83 m. The test section is enclosed in an air-tight control room. Thus, having the control room at the same static pressure as the test section, the problem of air leakage of the test-section flow is minimized.

The flow is driven by a 4.3 m diameter propeller that has eight constant-pitch blades. The fan is able to provide stable free-stream

velocities in the test section in the range of 4.6 m/s to 67 m/s. Measurements of the free-stream turbulence are shown in the table 2.1 and are due to Reynolds (1979).

2.2 The Model

The wind-tunnel model is a 1.83 x 3.7 m flat plate with a leading edge. The model is a panel that consists of a 19 mm paper honeycomb core covered by two, 1 mm thick aluminum sheets. One of the outer surfaces of the plate is polished flat. The leading edge of the flat plate is designed to minimize the pressure rise in the stagnation region and to be insensitive to leading-edge separation at slight angles of attack. The leading edge shown in Fig. 2.2 has the form of semi-elliptical cylinder with a ratio of major to minor axes of 67:1.

In order to produce the zero-pressure-gradient condition under the influence of the growing wall boundary layers, the plate is placed at a small angle of attack with respect to the free-stream direction. Ninety-three pressure ports are used to check the pressure gradient on the surface of the plate. The distribution of the pressure ports is shown in Fig. 2.3. A trailing-edge flap permits the adjustment of the overall circulation and the location of the attachment line.

2.3 Vibrating Ribbion

The introduction of the disturbances is done by the traditional vibrating-ribbon technique. The material of the ribbon is a phosphor-bronze alloy which is 0.025 mm thick and has a width of 2.5 mm.

The magnetic field is produced by thirty-two electromagnets placed under the vibrating ribbon on the back face of the plate (Fig. 2.4). The vibrating ribbon is insulated from the plate and the free vibrating length was 0.3 mm and this length is centered at midspan of the plate. The response of the vibrating ribbon due to various current inputs is measured by using an inductance probe mounted inside the plate and under the mid-point of the free-vibration length (Appendix 1).

2.4 Traversing Mechanism and Test-Section Configuration

The boundary-layer measurements are performed using hot-wire anemometers. A two-dimensional traversing mechanism is used to position the hot-wire probe at the desired location. The traversing mechanism is moved in the x-direction by gliding on two steel rods placed in the interior of the wind tunnel while driven by a stepping motor (Fig. 2.5). The probe is placed on a specially designed sting which is moved in the y-direction by a stepping motor and a lead screw. The stepping motors are controlled from the control room through the traverse controller. The traverse controller is intervaced with the HP COMPUTER to provide an automatic placement of the hot-wire probe at a fixed location and permits the acquisition of velocity profiles using software programming. The programmable motion of the hot-wire probe is limited to the y-direction, while the x-position is determined manually. Appendix 1 gives a list of all of the electronic equipment that was used.

CHAPTER 3

THEORETICAL ANALYSIS

3.1 Neutral Stability Curve

The general dimensionless form of the Navier-Stokes equation is

$$\nabla \cdot \underset{\sim}{v}^* = 0 \tag{3.1.1}$$

$$\frac{\partial \underset{\sim}{v}^*}{\partial t} + \underset{\sim}{v}^* \cdot \nabla \underset{\sim}{v}^* = -\nabla p^* + \frac{1}{Re} \nabla^2 \underset{\sim}{v}^* \tag{3.1.2}$$

where $\underset{\sim}{v}^*$ is the dimensionless velocity vector, p^* is the dimensionless pressure and Re is the Reynolds number. Considering the class of stationary basic states we can assume that each flow quantity is the sum of a mean-flow term $\underset{\sim}{v}(\underset{\sim}{r})$, $p(\underset{\sim}{r})$ and a fluctuating term $\underset{\sim}{v}'(\underset{\sim}{r},t)$, $p'(\underset{\sim}{r},t)$ or:

$$\underset{\sim}{v}^*(\underset{\sim}{r},t) = \underset{\sim}{v}(\underset{\sim}{r}) + \underset{\sim}{v}'(\underset{\sim}{r},t), \quad p^*(\underset{\sim}{r},t) = p(\underset{\sim}{r}) + p'(\underset{\sim}{r},t) \tag{3.1.3}$$

Introducing the expressions (3.1.3) into (3.1.1) and (3.1.2), assuming the mean-flow quantities to be solutions of the Navier-Stokes equations and separating the time-independent terms from the time-dependent terms the equations for the stationary and fluctuating quantities are given as:

Stationary:
$$\nabla \cdot \underset{\sim}{v} = 0 \tag{3.1.4}$$

$$\underset{\sim}{v} \cdot \nabla \underset{\sim}{v} + \langle \underset{\sim}{v}' \cdot \nabla \underset{\sim}{v}' \rangle + \nabla p - \frac{1}{Re} \nabla^2 \underset{\sim}{v} = 0 \tag{3.1.5}$$

Fluctuating: $\nabla \cdot \underset{\sim}{v}' = 0$

$$\frac{\partial v'}{\partial t} + \underset{\sim}{v}' \cdot \nabla \underset{\sim}{v} + \underset{\sim}{v} \cdot \nabla \underset{\sim}{v}' + \underset{\sim}{v}' \cdot \nabla v' - \langle \underset{\sim}{v}' \cdot \nabla \underset{\sim}{v}' \rangle + \\ + \nabla p' - \frac{1}{Re} \nabla^2 \underset{\sim}{v}' = 0$$

Where the symbol $\langle \rangle$ denotes a time average. For infinitesimal disturbances, products of the fluctuating quantities can be neglected; i.e. the terms $\underset{\sim}{v}' \cdot \nabla \underset{\sim}{v}'$ can be neglected in comparison to the linear terms.

A further simplification of the equation can be done by assuming parallel flow. This is true for the class of one-dimensional flows where:

$$U = U(y), \; W = W(y), \; V = 0 \qquad (3.1.6)$$

In this case the convective acceleration terms vanish in the basic-state equations and the equations for the disturbances take the form

$$\frac{\partial u'}{\partial x} + \frac{\partial v'}{\partial y} + \frac{\partial w'}{\partial z} = 0 \qquad (3.1.7)$$

$$\frac{\partial u'}{\partial t} + U \frac{\partial u'}{\partial x} + W \frac{\partial u'}{\partial z} + v' \frac{\partial u}{\partial y} = \frac{\partial p'}{\partial x} + \frac{1}{Re} \nabla^2 u' \qquad (3.1.8)$$

$$\frac{\partial v'}{\partial t} + U \frac{\partial v'}{\partial x} + W \frac{\partial v'}{\partial z} = - \frac{\partial p}{\partial y} + \frac{1}{Re} \nabla^2 v' \qquad (3.1.9)$$

$$\frac{\partial w'}{\partial t} + U \frac{\partial w'}{\partial x} + W \frac{\partial w'}{\partial y} + v' \frac{\partial w}{\partial y} = - \frac{\partial p}{\partial z} + \frac{1}{Re} \nabla^2 w' \qquad (3.1.10)$$

Since the above stability equations are linear and since the coefficients are functions of y only we assume disturbances of the form

$$q'(x,y,z,t) = q(y) \exp\left[i(k_x x + k_z z - \omega t)\right] \quad (3.1.11)$$

where q' is a typical disturbance quantity, k_x and k_z are the dimensionless wavenumbers in the x and z direction respectively and ω is the dimensionless frequency. Disturbances can be classified into: disturbances with (i) temporal amplification, (ii) spatial amplification and (iii) both temporal and spatial amplification.

The spatial amplification class corresponds more closely to the boundary-layer situation. In this case ω is assumed to be real while k_x and k_z complex. The real parts of k_x and k_z represents the physical wavenumbers of the disturbances while their imaginary parts represent the decay or amplification rates in the x and z directions.

Expressing each disturbance quantity in the sinusoidal form and substituting the result into the disturbance equations, we obtain the equations:

$$i\,k_x + i\,k_z w + Dv = 0 \quad (3.1.12)$$

$$i(k_x U + k_z W - \omega)u + (DU)v = i\,k_x p + \frac{1}{Re}(D^2 - k^2)u \quad (3.1.13)$$

$$i(k_x U + k_z W - \omega)v = - Dp + \frac{1}{Re}(D^2 - k^2)v \quad (3.1.14)$$

$$i(k_x U + k_z W - \omega)w + (DW)v = - i\,k_z p + \frac{1}{Re}(D^2 - k^2)w \quad (3.1.15)$$

where the operator D is defined as $D = \frac{d}{dy}$ and $k = k_x^2 + k_z^2$. To complete the problem formulation, the boundary conditions have to be specified. The usual no-slip and no penetration conditions can be expressed as:

$$u(0) = v(0) = w(0) = 0 \qquad (3.1.16)$$

Far away from the body the disturbances have to decay, or

$$u(\infty) = v(\infty) = w(\infty) = 0 \qquad (3.1.17)$$

The system of equations (3.1.12) - (3.1.17) form an eigenvalue system of equations. For given values of dimensionless frequency ω (real) and Re the equations can be solved and the k_x and k_z can be determined. Two of these equations can also be combined into a single equation known as the Orr-Somerfeld equation.

The stability results usually are presented in the form of a curve as shown in Fig. 3.1. This curve presents graphically the state of each disturbance of given k_z as a function of frequency and Re. For a given frequency the points outside of the curve are the points were the disturbances decay, as they move toward greater Re numbers while the points inside the curve represent the points where the disturbances grow. The points on the curve are the points of neutral stability. In Figure 3.1 the stability curve for the special case of the Blasius boundary-layer flow is presented. The abscissa is scaled

for the quantity $R = (Re_x)^{1/2}$ while the ordinate represents the non-dimensional frequency corresponding to this $k_z = 0$.

$$F = \frac{2\pi f \nu}{V^2}$$

The solid line represents the locus of neutral stability points for the case of parallel theory, while the dotted-line is the locus of neutral stability points for the nonparallel theory (Saric & Nayfeh 1977). Within the curves the flow is unstable while it is stable outside of the curves. For the case of 2-D flow equations 3.1.12, 3.1.13 and 3.1.14 can be combined in the Orr-Sommerfeld equations. By introducing

$$u' = \frac{\partial \psi}{\partial y} = \phi'(y)\, e^{i(kx - \omega t)}$$

$$v' = -\frac{\partial \psi}{\partial x} = -ik\,\phi(y)\, e^{i(kx - \omega t)}$$

into the three separate differential equations, the Orr-Sommerfeld equation is derived. It is stated as:

$$(D^2 - k^2)\phi - ik\,Re[U - \omega/k)(D^2 - k^2)\phi - (D^2U)\phi] = 0 \qquad (3.1.18)$$

The boundary conditions remain

$$\begin{aligned} &y = 0 \;:\; u' = v' = 0 \;,\; \phi = 0 \;,\; \phi' = 0 \\ &y \to \infty \;:\; u' \to 0 \;,\; v' \to 0 \;,\; \phi \to 0 \end{aligned} \qquad (3.1.19)$$

The stability problem is thus reduced to an eigenvalue problem stated by Eqn. (3.1.18) with the boundary conditions (3.1.19). For specified mean flow U(y), Reynolds number Re and frequency ω, the solution of (3.1.18) furnishes the eigenfunction $\phi(y)$ and the complex eigenvalue:

$$k = k_r + i\, k_i$$

For each pair of values (w,Re) k_r represents the phase velocity of the prescribed disturbance, whereas the sign of k_i determines whether the wave is amplified ($k_i > 0$), as it happens in the region between the neutral stability curve, or damped ($k_i < 0$) as it is outside of it. The limiting case $k_i = 0$ corresponds to neutral disturbances.

3.2 Step-function force on the vibrating ribbon. Asymptotic behavior of the introduced disturbance.

The behaviour of small-amplitude disturbances in a given parallel mean flow is governed by the previous described set of equations, which are linearized with respect to the disturbance amplitude. A disturbance can be forced either by a modification to the equation by the addition of some body-force terms, or by a change in the boundary conditions so that they are no longer homogeneous. If the second way is adopted the boundary conditions to simulate the excitation of the mean flow by a vibrating ribbon can be written:

$$\text{at the wall: } y = 0 \quad , \quad u = \partial\psi(0;\, x,t)/\partial y = 0$$

$$v = \partial\psi(0;\, x,t)/\partial x = Q(x,t)$$

where $Q(x,t)$ is some specified forcing function. Far from the wall the perturbation must decay:

$$u = \partial\psi(y_1;\, x,t)/\partial y \to 0 \quad \text{and} \quad v = -\partial\psi(y_1;\, x,t)/\partial x \to 0, \; y_1 \to \infty$$

A form of $Q(x,t)$ which will simulate ribbon vibrating near the surface is:

$$Q(x,t) = \delta(x) \cos \omega_1 t \quad (t > 0)$$

It is of interest to find the asymptotic solution for large t and thus x.

The perturbation stream function of the disturbance can be defined as:

$$\Psi(y;\, x,t) = c_1 \int_{-\infty}^{+\infty} c_2 \int_{-\infty}^{+\infty} \Phi(y;\, k,\omega) \exp\left[i(kx - \omega t)\right] dk d\omega \qquad (3.2.1)$$

where Φ is the transform of the perturbation stream function. If it is assumed that Φ is continuous and has continuous derivatives along c_1 and c_2 (c_1 and c_2 are the paths of integration), 3.1.8 can be substituted into the linearized equations of motion for parallel mean flows to yield the Orr-Sommerfeld equation given in 3.1.18. So far it is assumed that k and ω are complex. In terms of Φ the boundary conditions are:

$$\Phi(y_1;\, k,\omega) \to 0 \quad \Phi'(y_1;\, k,\omega) \to 0 \quad y_1 \to 0$$

$$\Phi'(0;\, k,\omega) = 0 \quad \text{at } y = 0$$

The remaining boundary value of $\Phi(0;\, k,w)$ is obtained by inverting 3.2.1 from 3.2.1:

$$-\frac{\partial \Psi(0;\, x,t)}{\partial x} = -i\, c_1 \int_{-\infty}^{+\infty} c_2 \int_{-\infty}^{+\infty} k\Phi(0;\, k,\omega)\, \exp[i(kx - \omega t)]\, dk d\omega$$

It can be shown (Gaster, 1965) that the integral is analytic over the entire k complex plane and in the upper half of ω complex plane. Thus the Fourier inversion formula can be applied to obtain:

$$-i\alpha\, \Phi(0;\, k,w) = \frac{1}{4\pi^2} \int_{-\infty}^{+\infty} \int_{-\infty}^{+\infty} \delta x\, \cos\omega_1 t\, \exp[-i(kx - 2t)]\, dx dt$$

$$\Phi(0;\, k,\omega) = -\frac{\omega}{4\pi^2 k(\omega^2 - \omega_1^2)} \qquad (3.2.2)$$

provided that $\mathrm{Im}(\omega)$ is greater than zero so that the integral converges as $t \to \infty$.

Using equations 3.2.1 and 3.2.2 an expression for $v(y;\, x,t)$ can be obtained:

$$v(y;\, x,t) = \frac{i}{4\pi^2} c_1 \int_{-\infty}^{+\infty} c_2 \int_{-\infty}^{+\infty} \frac{\omega}{\omega^2 - \omega_1^2} \frac{\Phi(y;\, k,\omega)}{\Phi(0;\, k,\omega)} \exp[i(kx - \omega t)]\, dk d\omega$$

Gaster (1965) found that the asymptotic solution of the above integral has the form:

$$v(y;\, x,t) = \mathrm{Re}\left\{\frac{i}{2}\,\frac{\Phi(y;\, k(\omega_1),\, \omega_1)}{\partial\Phi(0;\, k(\omega_1),\, \omega_1)/\partial k}\,\exp[\,i(k(\omega_1)x - \omega_1 t]\right\}$$

It has to be noted that the mode will have a wavenumber identical to that of the free eigenmode which has the same frequency on the ribbon.

A two dimensional step input may be represented by a boundary perturbation of the form:

$$\frac{\partial\psi}{\partial y} = 0 \qquad -\frac{\partial\psi}{\partial x} = \delta(x)\;\delta(t)$$

It has to be mentioned that even if the vibrating-ribbon force input has a step-function form the boundary perturbation is still ths same as before since the disturbance is caused by a sudden displacement and it is not influenced by the final location of the vibrating ribbon.

The delta function may be written in the form of an integral

$$\delta(t) = \frac{1}{\pi}\int_{-\infty}^{+\infty} \cos(\omega t)\; H(t)\,d\omega$$

and the asymptotic form of the stream function can be obtained as an integral:

$$v = \mathrm{Re}\left\{\int_{-\infty}^{+\infty} \frac{-i\;\Phi(y,\, k(\omega),\, \omega)\;H(x)}{\partial\Phi(0;\, k(\omega),\, \omega)/\partial k}\,\exp\{\,i[\,k(\omega)x - \omega t\}\,d\omega\right\}$$

If ω^* is the value of w where the exponential term becomes stationary or where:

$$\frac{dk(\omega^*)}{d\omega} - \frac{t}{x} = 0$$

then Gaster (1968) has given an asymptotic value of the above integral.

$$v = Re\left\{\frac{\exp\{i[k(\omega^*)x - \omega^* t]\}}{d^2k(\omega^*)/d\omega} + H.O.T.\right\}$$

This represents a traveling system of wave which is amplified in space and time. Along rays in the (x,t)-plane ω^* is constant and the system appears as a simple traveling wave with wave-number $k_r(\omega^*)$, frequency w* and amplification rate

$$-[k_i(\omega^*)x - \omega_i^* t]$$

The amplification rate may be written in terms of temporal growth as

$$-\left[k_i(\omega^*)\frac{\partial \omega_r}{\partial k_r}(\omega^*) - \omega_i^*\right]$$

or spatial growth

$$-\left[k_i(\omega^*) - \omega_i^*\frac{\partial k_r}{\partial \omega_r}(\omega^*)\right]$$

The previous analysis explains the creation of traveling wave-packets from impulse surface disturbances. It is an interesting fact that not only impulse but also step-function form disturbances can create wave packets. Physically this can be explained by considering

only the motion of the vibrating ribbon causing disturbances and not its final position in the flow.

3.3 Vibrating-Ribbon Model

The vibrating ribbon is modeled by a spring-dashpot-mass system as shown in Figure 3.3.1.

For such a linear system the output spectral density $S_y(\omega)$ for a single-degree-of-freedom oscillation, when it is excited by a forcing function $x(t)$ whose spectral density is $S_x(\omega)$ is:

$$S_y(\omega) = |H(\omega)|^2 \, S_x(\omega) \tag{3.3.1}$$

where $H(\omega)$ is the complex frequency-response function. The equation of motion for the system is:

$$m\ddot{y} + c\dot{y} + Ey = x(t) \tag{3.3.2}$$

To find $H(\omega)$, put $x(t) = e^{i\omega t}$ and $y(t) = H(\omega)e^{i\omega t}$ in the equation of motion (3.3.2) to obtain

$$(-m\omega^2 + ci\omega + E)\ H(\omega) = 1 \tag{3.3.3}$$

and

$$H(\omega) = \frac{1}{-m\omega^2 + ic\omega + E} \tag{3.3.4}$$

3.4.1 Random-Input Forcing Function

In the case of a random forcing function the input spectral density $S_x(\omega) = S_0$ and hence the output spectral density is:

$$S_y(\omega) = \frac{S_0}{(E - m\omega^2)^2 + c^2\omega^2} \qquad (3.3.5)$$

A typical picture of this output spectral density is given in Figure 3.3.2. The peak value occurs for small damping when:

$$w \approx \sqrt{\frac{E}{m}} = \omega_n \qquad (3.3.6)$$

and its height is:

$$S_y(\omega_n) = \frac{S_0}{c^2\omega^2_n} = \frac{S_0 m}{c^2 E} \qquad (3.3.7)$$

By knowing the spectrum of the response of the ribbon to a random input, the modulus of elasticity E is calculated from the frequency which corresponds to the peak value and the damping parameter c is calculated from the magnitude of the peak value $S_y(\omega_n)$. It is understood for the case of the vibrating ribbon that E is a function of the tension applied on the ribbon.

A very simple algorithm is developed to calculate for given ω_n, S_0, m, $S_y(\omega_n)$ the physical parameters of the model. Also a comparison between the output spectral density $S_y(\omega)$ and the real output of the vibrating ribbon is obtained.

A difficulty of this simulation arises in the calculation of S_0 which depends upon the density of the magnetic field--a rather diffi-

cult quantity to be measured. Thus, the value of $S_y(\omega)$ was employed for an arbitrary value of ω.

Thus, from (3.3.6) the calculation of E can be done and using (3.3.5) for a given value of ω and (3.3.7) for ω_n the value of c can be found. in Fig. 3.3.2 and 3.3.3 the results of the model and the ribbon are presented.

3.4.2 Step Input Forcing Function

The equation of motion of the system is:

$$m\ddot{y} + c\dot{y} + Ey = \ddot{x}(t)$$

where x(t) is the force acting on the system and it has the form:

$$\ddot{x}(t) = \begin{cases} 0 & \text{for } t < 0 \\ x_o & \text{for } t \geq 0 \end{cases}$$

The frequency response function $H(\omega)$ relating the output y(t) to the input acceleration x(t), from vibration analysis is:

$$H(\omega) = \frac{1}{(E - m\omega^2)^2 + c^2\omega^2}$$

It is also known from vibration analysis that the relation between input and output spectral densities are

$$Y(\omega) = H(\omega)\ x(\omega)$$

where $Y(\omega)$ is the output and $x(\omega)$ is the input spectral density found from the Fourier transform of input and output signal of the time domain:

$$x(\omega) = \frac{x_0}{2\pi\omega}$$

and thus

$$Y(\omega) = \frac{1}{(E - m\omega^2)^2 + c^2\omega^2} \cdot \frac{x_0}{2\pi\omega} \qquad (3.3.8)$$

For the evaluation of x_0, one point of the experimentally found spectrum is compared. A simple computer program has been developed for the calculation of $S_y(\omega)$, $|Y(\omega)|$, $H(\omega)$. The experimental spectrum and that of the model are given in Figs. 3.3.4 and 3.3.5.

The reason for developing the vibrating-ribbon model is that the type of the disturbance introduced by the ribbon can be found and easily verified. This is another advantage of the vibrating-ribbon method of excitation compared to other types of excitation like the introduction of acoustic pulses.

From the final form of the equations for the random excitation and the step-function excitation four unknowns for each case have to be determined. The m, E, c, S_0 for the case of random excitation and m, E, c, x_0 for the step-function excitation. In the developed algorithm the values of m/c, E/c, S_0/c and x_0/c are to be determined and in general this can be done by employing three points of the experimentally found spectra. However, if one of the tuning frequencies is employed then only two other points are necessary. For this case the tuning frequency, the amplitude at the tuning frequency and the ampli-

tude at another frequency are employed for the determination of the parameters.

In the comparison of experimental with the theoretical data, the employed points coalesce but the other points do not agree perfectly. But qualitatively the comparison can be used to give the type of excitation with great confidence.

CHAPTER 4

RANDOM EXCITATION OF THE VIBRATING RIBBON

4.1 Basic Idea

The random oscillation of the ribbon introduces a random two-dimensional disturbance in the mean flow. According to Fourier analysis, this random disturbance may be considered as the superposition of an infinite number of sinusoidal disturbances, of the form mentioned in the analysis of section 3.1.

If the amplitude of the random disturbance is kept low, then non-linear interactions among the waves of different frequency (Kachanov et al., 1980; Saric & Reynolds, 1980) is avoided and the amplitude of the disturbance of a particular frequency is considered as an independent sinusoidal wave. This grows or decays as the Reynolds number increases, according to its frequency, regardless of what happens to the other waves. In this way the spatial behavior of waves of many frequencies can be examined at the same time and many neutral stability points can be obtained with one x-direction "sweep" of the plate.

4.2 Experimental Procedure

The purpose of this experiment is to find neutral stability points for the case of the Blasius boundary layer.

The random signal is provided by the HP5420 SPECTRUM ANALYSER. The random signal is amplified by a power amplifier and the output voltage of the amplifier is applied to the vibrating ribbon. A con-

stant DC current is passed through the 32 magnets on the back of the plate and thus the vibrating ribbon is kept in a constant magnetic field. According to the Lorentz law, the superposition of a random current traverse to a constant magnetic field produces a random forcing function on the ribbon.

The proximitor probe, (described in Section A.16 of Appendix 1) placed under the ribbon at midspan of the free vibrating length, measures the instantaneous ribbon amplitude which in turn is analysed to determine the ribbon response to the random forcing function. This is described in section 3.3.1. The proximitor output is connected to the TEKTRONIX OSCILLOSCOPE to the HP SPECTRUM ANALYZER. The output of the ribbon excitation is taken in the "time-domain" or in the "frequency-domain" modes of the spectrum analyser. Figure 3.3.3 shows the vibrating ribbon response to random excitation. From that spectrum it is obvious that for the frequencies from 0 Hz to 150 Hz, the response amplitude is almost flat. For the applied tension on the ribbon of approximately 30 Nts the frequency of the maximum amplitude is found to be around 180 Hz.

Measurements of the mean flow and the fluctuations of the mean flow are taken by the DISA HOT-WIRE ANEMOMETER. The hot-wire probe is mounted on the traverse mechanism and it is able to move in the x-direction and in the y-direction. The signal from the hot-wire anemometer after linearization is fed into the TEKTRONIX OSCILLOSCOPE and into the HP SPECTRUM ANALYZER. As in the case of the ribbon response, it is possible to have the behavior of the disturbances of the mean

flow, at any location, in the time domain and in the frequency domain at the same time. Fig. 4.1 shows the Data Acquisition instrumentation. The signal of the probe after the linearizer is amplified and it is driven to the HP SPECTRUM ANALYZER which is interfaced with the HP COMPUTER.

Spectra of the fluctuations in the mean flow are taken every 10 cm downstream of the location of the vibrating ribbon. At every x-location, spectra are taken at four y-directions which correspond to four values of the mean flow. Fig. 4.2 shows the four y-positions where measurementns are taken with respect to the mean flow and the corresponding value of single-frequency disturbances in the region of Tollmien-Schlichting wave development.

The spectra of the random fluctuation of the mean flow, at every location, are stored on a magnetic tape. Interfacing the HP SPECTRUM ANALYSER with the HP COMPUTER makes possible the use of software programming to have the disturbance behavior at any x-location for any desired frequency. This is done for every constant y-location of the hot-wire. Thus, from these spectra the growth or the decay of a disturbance of a particular frequency with respect to the Reynolds number is examined. A typical curve of the amplitude growth with Reynolds number is seen in Fig. 1.2.

According to the basic idea the position of the maximum of those constant-frequency amplitude curves will correspond to points of the second branch of the stability curve (R_{II}) while the minimum corresponds to branch I. The complete effort is easily done by programming

the HP COMPUTER. In Appendix 3 and 4 are given the modes of the HP SPECTRUM ANALYZER for the random excitation and for the step input force function respectively.

Some of the data are given in Tables 4.1 for U_∞ = 16 m/s, 4.2 for the case of U_∞ = 15 m/s and 4.3 for the case of U_∞ = 10 m/s. In the tables .1 and 4.2 for a certain frequency the $R = (Re)^{1/2}$ for the neutral points found by the experiment are compared with those given by the non-parallel theory. In table 4.3 for a given R the comparison is done between the dimensionless frequencies F. Some of the data points are given on the stability curve in Fig. 4.4. Figure 4.3 shows the way in which Neutral-Stability points are found. First the distance from the wall is selected, i.e. 0.4 of U_∞. Then the frequency of a disturbance whose amplitude is to be determined is selected i.e. 80 Hz. Then the HP SPECTRUM ANALYZER interfaced with the HP COMPUTER is ordered to select from the magnetic tape the spectra for the selected velocity, and distance from the wall and for each one of them, which corresponds to a certain distance from the leading edge, to find the amplitude of the disturbance of the selected frequency. Having the amplitude as a function of distance from leading edge maximum or minimum may be found, which correspond to neutral-stability points. Using software programming the process can be repeated automatically for any number of frequencies, distance from the wall or free-stream velocities.

4.3 Comparison

In Tables 4.1, 4.2, 4.3 as well as in Fig. 4.1, the comparison between the experimentally found neutral stability points and those found by the non-parallel theory is given. In general there is a good agreement between the stability points of the second branch but not so good agreement with the first branch.

Many factors may influence this deviation such as the existence of small pressure gradient or local distortion of the disturbance profile due to nonparallel effects (Saric & Nayfeh, 1977). However, the comparison of the results found by this method to those in Fig. 1.3, found by classical methods leads to the conclusion that the present method has great advantages in the measurement of neutral stability points because of its speed. Moreover, the current method of examining waves of all frequencies at the same time can be extended to different types of linear stability experiments since it can provide data on all the frequencies at the same time. Also, it can be a good reason for further research in the field of electronics for further improvement of current data-acquisition systems.

CHAPTER 5

STEP-FUNCTION INPUT ON THE VIBRATING RIBBON

5.1 Basic Idea

It is well known from vibration analysis that the response of every linear system to any input can be determined precisely if the response of the system to the step-function input is known.

The development of Tollmien-Schlichting waves in the boundary layer on a flat plate can be considered as the response of a system to an excitation of sinusoidal form which is introduced with the vibrating ribbon. That system will be called "laminar boundary-layer system."

It would be very interesting to apply the methods of vibration analysis to examine the behavior of such a system. Such an analysis must be able to predict the response of the system to any type of excitation. In order to achieve this, the behavior of the system for two types of excitation, the random input and the step-function input, is examined. The response of the system for the case of random excitation is discussed in the previous chapter. In the present chapter the response of the system to step-function input on the vibrating ribbon is examined. Although desirable, the response to the impulse input is not examined because of the difficulties encountered in the production of a signal close to the mathematical definition of impulse function. It has to be mentioned here that although the motion of the vibrating ribbon is of the form of step function, what perturbates the

boundary layer is the motion of it and not its final position. Its motion is of the impulse form.

The vibrating ribbon response to the step-function is shown in Figure 3.3.5. The comparison of that response and the response of the mathematical model is given in chapter 3.

5.2 Experimental Procedure

The introduction of the step-function force on the vibrating ribbon is accomplished by the circuit schematically drawn in Fig. 5.1. Two DC power supplies are used. One is used to provide a constant DC current on the magnets and thus create the constant magnetic field. The other DC power supply is connected in line with a switch and the vibrating ribbon. By closing the circuit through the switch, a DC current passes through the vibrating ribbon and consequently an instant constant force is applied on it. The circuit current is observed on the TEKTRONIC OSCILLOSCOPE and it is very close to step-function form. Thus, the force applied on the vibrating ribbon, according to Lorentz-law must be also of step-function form.

The response of the vibrating ribbon is taken by using the proximitor probe placed under the vibrating ribbon at the midspan of its free length. A sketch of the oscilloscope picture is on Fig. 5.2.

The output of the proximitor probe is connected to the TEKTRONIX OSCILLOSCOPE and to the HP SPECTRUM ANALYSER. The response of the vibrating-ribbon is given in Fig. 3.3.5. In order to preserve that picture on the oscilloscope, the memory screen is used while the response

of the ribbon triggers the oscilloscope. The response in the time domain, using the HP SPECTRUM ANALYSER is obtained through the following steps:

The output of the proximitor probe is connected to the input channels and the trigger channels of the oscilloscope and the spectrum analyser. At the time the vibrating ribbon circuit is closed, the response of the ribbon is obtained by the proximitor probe and it is transformed to a voltage output proportional to the oscillation of the ribbon. The signal generated by the proximitor probe triggers the oscilloscope and the spectrum analyser and the signal is displayed on the screen of the oscilloscope. At the same time it is transformed in the frequency domain in the spectrum analyser. The memory screen of the oscilloscope keeps the signal for a certain time, while it is possible to apply more than once, the step function on the ribbon and then average the response in the frequency domain.

The response of the laminar boundary-layer system to step-function excitation is obtained by using a hot-wire probe placed in the boundary layer at various locations downstream of the location of the ribbon. The signal of the hot-wire probe triggers the oscilloscope and the spectrum analyser and thus the shape of the boundary-layer system response is obtained in the time domain through the memory screen of the oscilloscope and in the frequency domain on the screen of the spectrum analyser. The spectrum analyser mode programming used to obtain the system response is described in Appendix 4.

5.3 Creation of the wave packet

As it is mentioned before the boundary layer sees an impulse-function disturbance, due to the motion of the vibrating ribbon. The memory screen of the oscilloscope indicates the creation of wavepackets when the signal of the hot-wire anemometer is depicted on it. The shape of the wavepacket is schematically shown in Fig. 5.3.

As the hot-wire probe is moved downstream, the amplitude of the wavepacket grows and on the oscilloscope at certain distances downstream the wavepacket form is destroyed by the appearance of spikes as shown in Fig. 5.4. Eventually the wavepacket form is destroyed and distorted forms appear on the oscilloscope.

The spectra of the wavepackets have the form of Figs. 5.4.1, 5.4.10, and 5.4.18 as long as the wavepacket shape remains intact and the wave is growing in amplitude. One observes a broadband of frequencies around 50 Hz. At certain locations downstream (which is 200 cm for U_∞ = 9.0 m/s, 150 cm for U_∞ = 9.1 m/s and 140 cm for U_∞ = 10.5 m/s) an interesting phenomenon is observed. A broadband of frequencies at around 20 Hz starts growing in amplitude and in a short distance of 10 cm its amplitude reaches the amplitude of the broadband of 50 Hz. While the amplitude of 50 Hz remains constant, the amplitude of the broadband at 20 Hz still grows and shortly downstream it is twice the amplitude of the broadband at 50 Hz. This behavior is shown in a sequence of spectra in Figs. 5.4.1 - 5.4.9 for U_∞ = 8.0 m/s, in Figs. 5.4.10 - 5.4.10 - 5.4.17 for U_∞ = 9.0 m/s and in Figs. 5.4.18 -

5.4.25 for U_∞ = 10.5 m/s. The position of the starting point of growth of the 20 Hz spike is given in the stability curve in Fig. 5.5.

The most significant experimental work on the behavior of wavepackets in laminar boundary layers is due to Gaster & Grant (1975). Gaster's work examined the behavior of three-dimensional wavepackets. The packet was artificially generated by a short duration acoustic pulse, which was injected into the boundary-layer flow through a small hole in the plate. A typical power spectrum of the wavepacket produced that way is shown in Fig. 5.7. In Figs. 5.8 and 5.9 the development of the wavepackets is shown. The envelope of the signal is distorted as it moves downstream. Gaster observed and measured the growth of low-frequency modes (Fig. 5.10). He considered non-linear wave interactions as the cause for that growth (Gaster, 1975). He also developed a linear model for the analytical study of the 3-D wavepacket behavior.

The present work deals with two-dimensional wavepackets. For an examination of the phenomena, the results are interpreted with respect to the neutral stability curve. The first observation is that the waves which amplify do not amplify as it is expected from the neutral stability curve. The low frequencies do not grow after they pass the neutral stability point of branch I as the wavepacket moves to higher Reynolds number. They retain their low amplitudes up to the point of the breakdown where, within a distance which corresponds to value of $R = \sqrt{Re}$ of 10, they reach the level of the high-frequency modes and shortly down stream the wavepacket transform into turbulence.

On the oscilloscope, when the growth of the low-frequency broadband is observed sudden spikes appear that destroy the wavepacket envelope. Such a wave form with spikes is presented in Fig. 5.4. Contrary to the low-frequency broadband, the broadband of the higher-frequency waves develops according to the neutral stability curve as if the waves of various frequencies are independent. By examining the growth of waves of particular frequency, they develop a local maximum that corresponds to neutral stability point of the branch II of the neutral-stability curve. For the case of U = 9.0 m/s and 10.5 m/s, the observed neutral stability points that are verified are shown in Fig. 5.5. The position where the growth of low-frequency broadband is started is also indicated on the same figure.

After reviewing the observations of the wavepacket behavior, one can describe the following characteristics. Although the vibrating ribbon strongly excites the low-frequency modes, only a certain broadband of frequencies are excited. The theoretical analysis of chapter 3.2 may explain that behavior. After the formation of the wavepacket, it can be seen from the spectra that it is composed of a band of frequencies around 50 Hz which behaves as independently considered modes, and a part of low frequencies, around 25 Hz, which although initially excited by the vibrating ribbon does not grow, as indicated by the neutral stability curve, but it exhibits an explosive behavior far downstream.

Comparing the behavior of random excitation of the vibrating ribbon with the present step-function excitation, the following possible

conclusions may be made. THe fact that in the case of the random excitation, the individual modes grow or decay according to the neutral stability curve while in the case of step-function excitation only a certain band exhibits such a behavior, leads to the conclusion that the wavepacket structure prohibits the development of modes other than those developed to form the wavepacket.

If this is the case, the wavepacket acts as a structure that absorbs energy from the freestream for its growth but prevents the growth of any other mode. In such a case, the sudden growth of low-frequency modes while the wavepacket form remains intact can be considered as the final stage of the wavepacket structure and the beginning of its destruction by being transformed into abnormal form. The mechanism that leads to the development of low-frequency band may be a nonlinear wave interaction.

CHAPTER 6

CONCLUDING REMARKS

In practice, the disturbances present in the laminar boundary layer are not sinusoidal but either random or in the form of discrete steps as in the case of an insect stuck on the surface of a wing. Thus, the importance of the results presented in the previous two chapters is significant since they represent the response of boundary--layer system to random and impulsive inputs.

From the results of the random excitation response, it is obvious that it can be considered as the response to infinite number of sinusoidal waves of different frequency, each considered separately.

The results of the step-function force input to the vibrating ribbon are more interesting since they represent the behavior of a wavepacket created by an impulsive input to the boundary-layer system. From the data, it is deduced that the wavepacket grows as an ensemble with no preference to any particular frequency, that is it maintains its structure through the period of growth. The fact that the low-frequency disturbances present in a wavepacket do not grow, although they are in the amplified region of the neutral stability curve, shows that waveforms which consist of frequencies of specific amplitude ratio are much more stable than if the waves of different frequencies were independent. The breakdown to turbulence happens because of the sudden growth of waves of frequencies much lower than the lower limit

of the wavepacket broadband and the process of transition is not gradual as in the case of sinusoidal waves but rather explosive.

The previous results introduce some new aspects in the general problem of transition whose closer examination may lead to new consideration of the problem.

REFERENCES

Bradshaw, P. 1965. The effect of wind-tunnel screens on nominally two-dimensional boundary layers. J. Fluid Mech. vol. 22, pp. 679-

Gaster, M. 1965. On the generation of spatially growing waves in a boundary-layer, J. Fluid Mech. 22, 3, pp. 433-441.

Gaster, M. 1968. The development of three-dimensional wavepackets in a boundary layer. J. Fluid Mech. vol. 32, pp. 173-184.

Gaster, M. and Grant, I. 1975. Experimental investigation and development of a wave packet in a laminar boundary layer. Proc. R. Soc. Lon. A. 347, pp. 253-269.

Gaster, M. 1975. A theoretical model of a wave packet in the boundary layer on a flat plate. Proc. R. Soc. Lon. A. 347, pp. 271-289.

Hama, F. R. and Nutant, J. 1963. Detailed flow observations in the transition process in a thick boundary layer. Proc. 1963, Heat Transfer and Fluid Mech. Institute, Stanford Univ. Press, pp. 77-93.

Kachanov, Yu. S., Kozlov, V. V., and Levchenko, V. Ya. 1980. Experimenta on nonlinear interactions of waves in boundary layers. I.U.T.A.M. Symposium on Laminar-Turbulent Transition, Springer 1980.

Klebanoff, P. S. and Tidstrom, K. D. 1959. Evolution of amplified waves leading to transition in a boundary layer with zero pressure gradient, NASA, TN. D-195.

Klebanoff, P. S., Tidstom, K. D. and Sargent, L. M. 1962. The three-dimensional nature of boundary-layer instability. J. Fluid Mech. 12, pp. 1-

Kovasznay, L. S. A., Komoda, H. and Vasudeva, B. R. 1962. Detailed flow field in transition. Proc. 1962 Heat Transf. & Fluid Mech. Instit., pp. 1-

Reynolds, G. A. 1979. Experiments on the stability of the Blasius boundary-layer. M.S. Thesis, Engineering Science and Mechanics, VPI & SU.

Ross, T. A., Barns, F. H., Burns, J. G., and Ross, M. A. S. 1970. The flat plate boundary layer, Part 3, comparison of theory with experiment. J. Fluid Mech. 43, 819.

Saric, W. S. and Nayfeh, A. H. 1977. Nonparallel stability of boundary layers with pressure gradients and suction, AGARD Symposium "Laminar-Turbulent Transition" Conf. Proceeding 224.

Saric, W. S., Reynolds, G. A. 1980. Experiments on the stability of nonlinear waves in a boundary layer I.U.T.A.M. Symposium on Laminar-Turbulent Transition Springer. 1980.

Schlichting, H. 1933. Zur Entstehung der Turbulenz bei der Plattenströmung. Nachr. Wiss. Göttingen Math. - phys. Klasse, pp. 181-208.

Schubauer, G. B. and Skramstad, H. K. 1947. Laminar boundary layer oscillations and transition on a flat plate. J. Res. Nat. Bureau of Standards, 38, p. 251.

Strazisar, A. J., Prahl, J. M., and Reshotko, E. 1975. Experimental study of the stability of heated laminar boundary layers in water. Case Western Researve Univ., Dept. Fluid Thermal Aerosp. Sci. FTAS/TR-75-113.

Tollmien, W. 1929. Über die Entstehung der Turbulenz. Nach. Ges. Wiss. Göttingen, Math. - phys. Klasse, pp. 21-44.

Wortmann, F. X., 1955. "Untersuchung instabiler Grenzschicht schwingungen in einem Wasserkanal mit der Tellurmethode," 50 Hajre Grenzschichtforschung, Braunschweig, F. Vieweg & Sohn, 1955, pp. 460-470.

TABLE 2.1 FREE STREAM TURBULENCE LEVELS

m/s	%
U_∞	$\lvert u \rvert / U_\infty$
9	.018
12	.018
15	.022
20	.028
30	.045

Table 4.1. Neutral stability points found by random excitation of the vibrating ribbon and comparison with theoretical values of non-parallel theory for U_∞ = 16 m/s

Conditions: U_∞ = 16 m/s

$\nu = 1.658 \times 10^{-5} m^2/s$

Vibrating ribbon tension . . . . . T = 6.5 lb
Current on the magnets . . . . . I = 2.5 A
RMS voltage on the ribbon. . . . . V = 12 V
Distance of Vibrating ribbon from plate. . t = 0.165 mm

y-position of H.W.: $u/U_\infty = 0.95$

$F \times 10^6$	R		
	Experiment	Theory	
16.2	1282	1171	Branch I
20.3	1160	1017	
46.6	1243	1287	
44.5	1282	1303	Branch II
42.5	1330	1384	

y-position of H.W.: $u/U_\infty = 0.4$

$F \times 10^6$	R		
	Experiment	Theory	
46.5	1282	1286	
48.6	1243	1248	Branch II
50.6	1203	1219	

Table 4.1. (Continued)

y-position of H.W.: $u/U_\infty = 0.3$

$F \times 10^6$	$R = \sqrt{Re}$		
	Experiment	Theory	
20.25	1243	1017	Branch I
22.2	1282	970	
46.5	1243	1286	Branch II
50.6	1203	1219	

y-position of H.W.: $u/U_\infty = 0.15$

$F \times 10^6$	$R = \sqrt{Re}$		
	Experiment	Theory	
16.2	1243	1191	Branch I
55.0	1160	1139	
50.0	1203	1219	Branch II
47.5	1243	1260	
42.5	1282	1350	

Table 4.2 Neutral-Stability points found by random excitation of the vibrating ribbon and comparison with theoretical values of nonparallel theory for U_∞ = 15 m/s

Conditions: U_∞ = 15 m/s

$\nu = 1.735 \times 10^{-5}$ m^2/s

Voltage on the Vibrating ribbon . . V = 8.5 Volts (RMS)
Current on the magnets. . . . . I = 3.5 A
Position of the V.R . . . . . R_{VR} = 1018

y-location of the H.W.: u/U_∞ = 0.95

$F \times 10^6$	$R = \sqrt{Re}$ Experiment	Theory	
19.5	1281	1050	
21.8	1212	1010	
24.2	1176	920	Branch I
26.6	1139	900	
44.0	1313	1321	
46.2	1281	1274	
49.0	1248	1221	
53.3	1212	1153	Branch II
55.6	1139	1139	
60.8	1058	1069	

Table 4.2 (continued)

y-location of the H.W.: $u/U_\infty = 0.4$

$F \times 10^6$	R		
	Experiment	Theory	
19.3	1212	1050	
21.7	1139	1000	Branch I
24.1	1100	910.4	
26.7	1058	910.4	
43.7	1281	1320	
47.0	1248	1250	
52.0	1139	1160	Branch II
55.0	1176	1121	
59.0	1100	1070	
64.0	1058	1010	

Table 4.2 (Continued)

$F \times 10^6$	$R = \sqrt{Re}$ Experiment	Theory	
y-location of the H.W.: $u/U_\infty = 0.3$			
19.4	1176	1060	
21.7	1139	993	Branch I
24.1	1100	920	
26.8	1058	900	
47.0	1212	1259	
53.0	1139	1153	
58.2	1212	1076	Branch II
60.5	1100	1052	
64.0	1058	1006	
y-location of the H.W.: $u/U_\infty = 0.15$			
19.3	1248	1030	
21.8	1139	991	Branch I
24.3	1058	920	
46.0	1248	1278	
49.5	1212	1202	Branch II
59.3	1100	1061	
64.5	1058	1004	

Table 4.3 Neutral-Stability points found by random excitation of the vibrating ribbon and comparison with theoretical values of non-parallel theory for U_∞ = 10 m/s

Conditions: U_∞ = 10 m/s

ν = 1.699 m^2/s

Position of the V.R.
R_{VR} = 840

y-location of the H.W.: u/U_∞ = 0.95

$R = \sqrt{Re}$	$F \times 10^6$ Experiment	Theory	
1040	67.0	66	
1009	72.4	64.2	Branch II
946	78.0	68.9	

y-location of the H.W.: u/U_∞ = 0.4

978	62.1	66	
946	67.6	68	Branch II
914	72.8	73	

y-location of the H.W.: u/U_∞ = 0.3

1009	62.0	64.2	
978	67.3	66	Branch II
946	72.8	68.9	

y-location of the H.W.: u/U_∞ = 0.15

1009	62.0	64.2	
978	67.3	66.0	Branch II
946	72.8	68.9	
914	78.0	73.0	

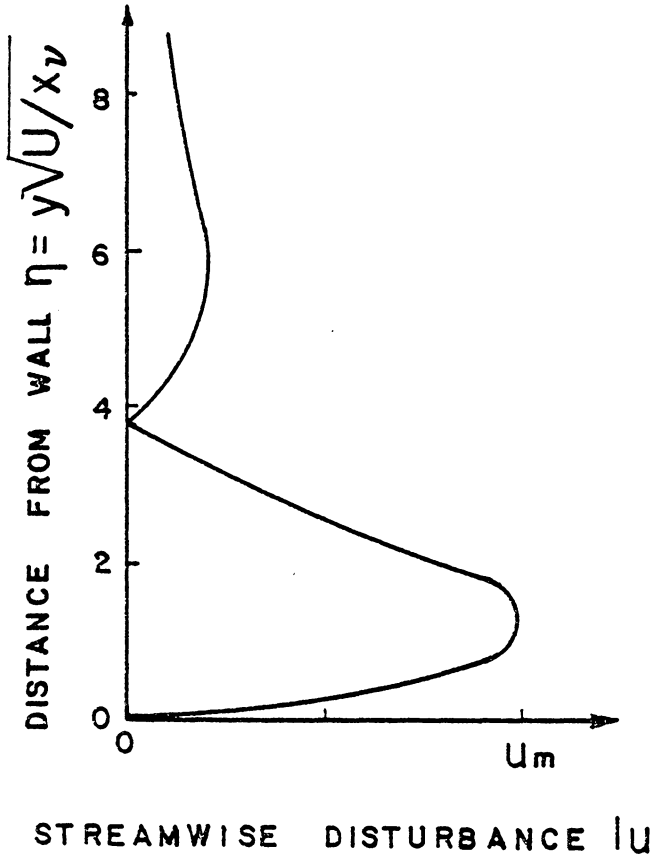

Figure 1.1 Example of streamwise disturbance velocity for the case of F = 86 x 10^{-6}, R = 440.

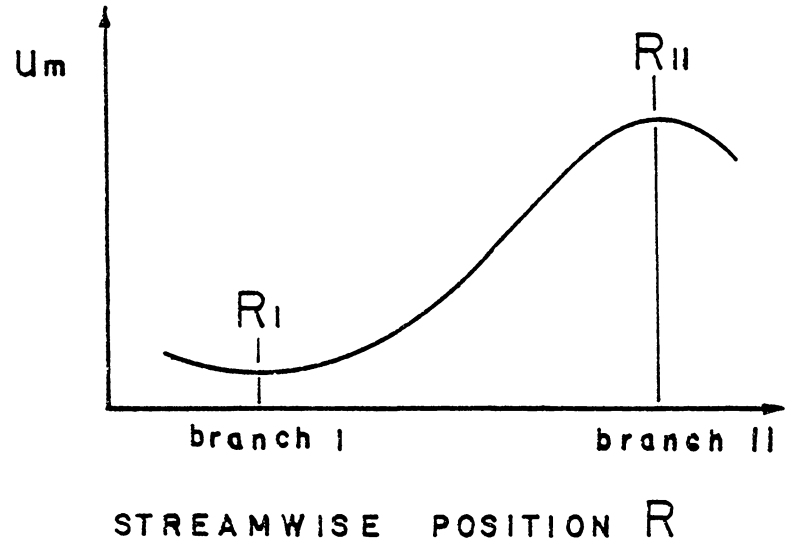

Figure 1.2 Schematic of amplitude growth and neutral stability point determination.

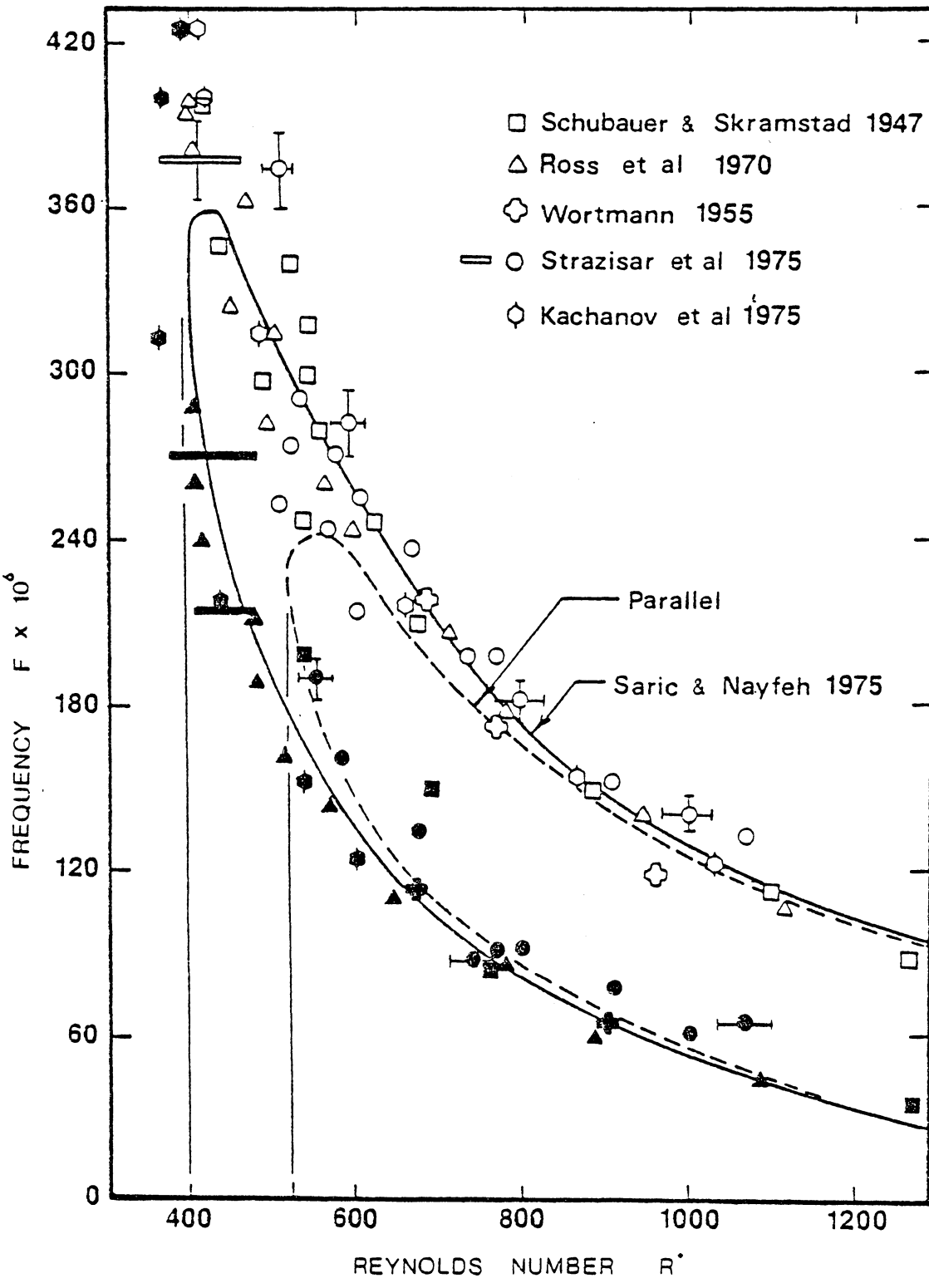

Figure 1.3 Neutral stability curve for Blasius boundary layer.

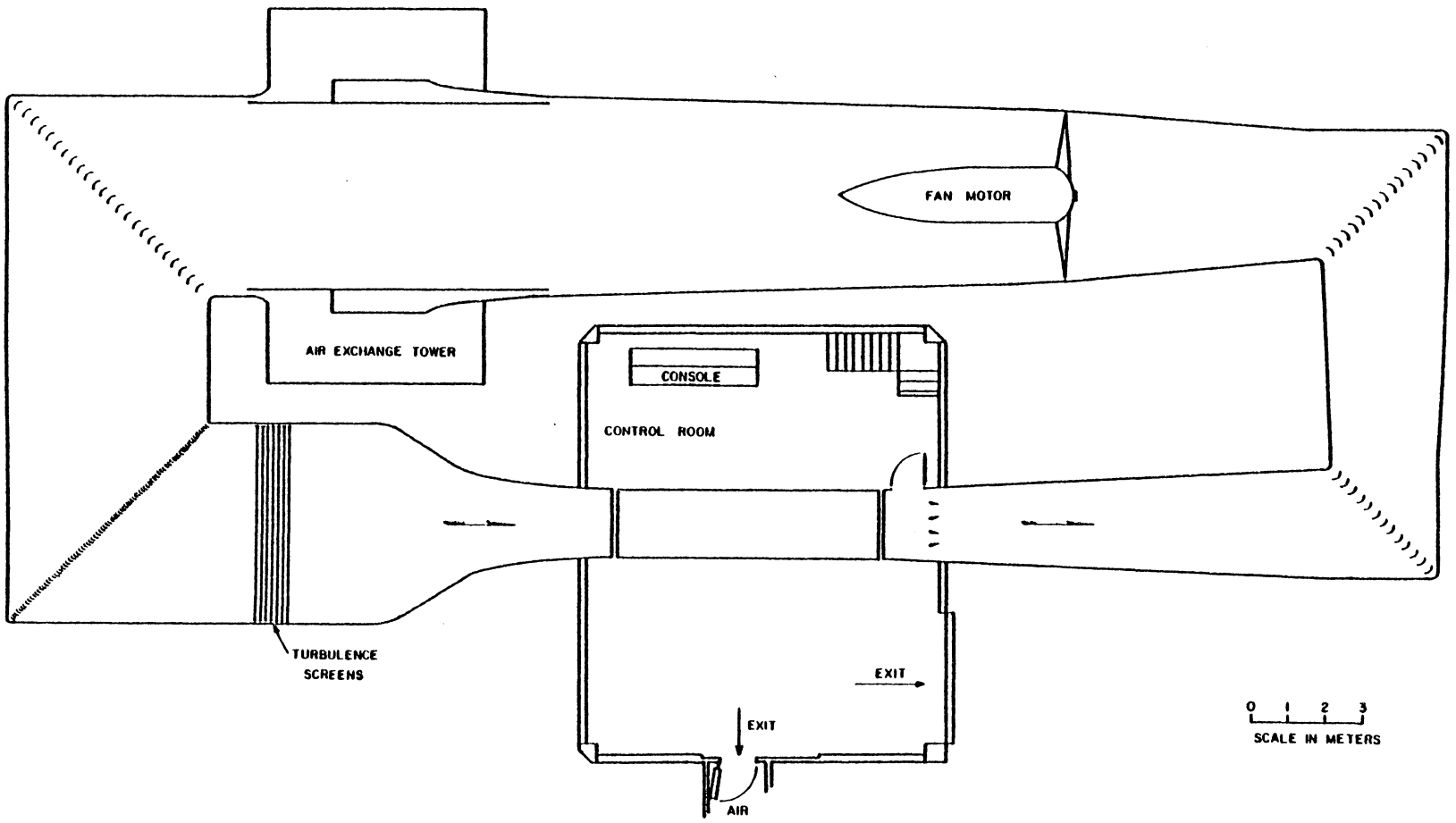

Figure 2.1 VPI & SU Stability Wind Tunnel.

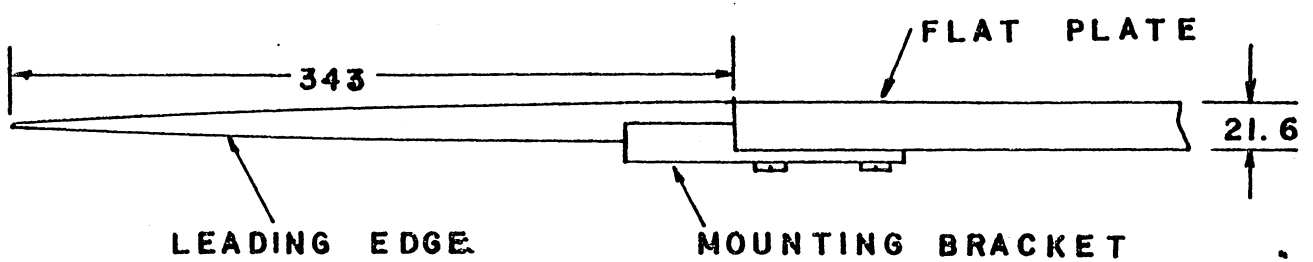

Figure 2.2 Leading edge-flat plate junction. All dimensions in millimeters.

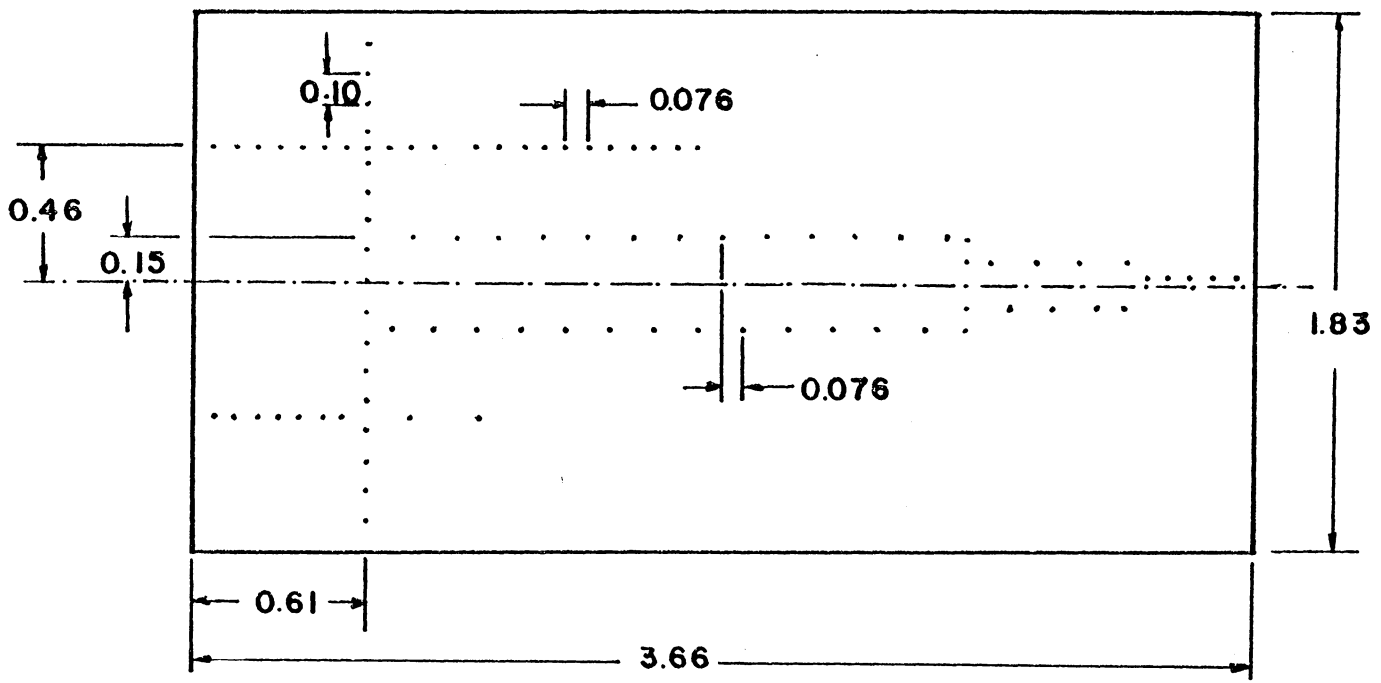

Figure 2.3 Flat plate model and location of pressure ports. All dimensions in meters.

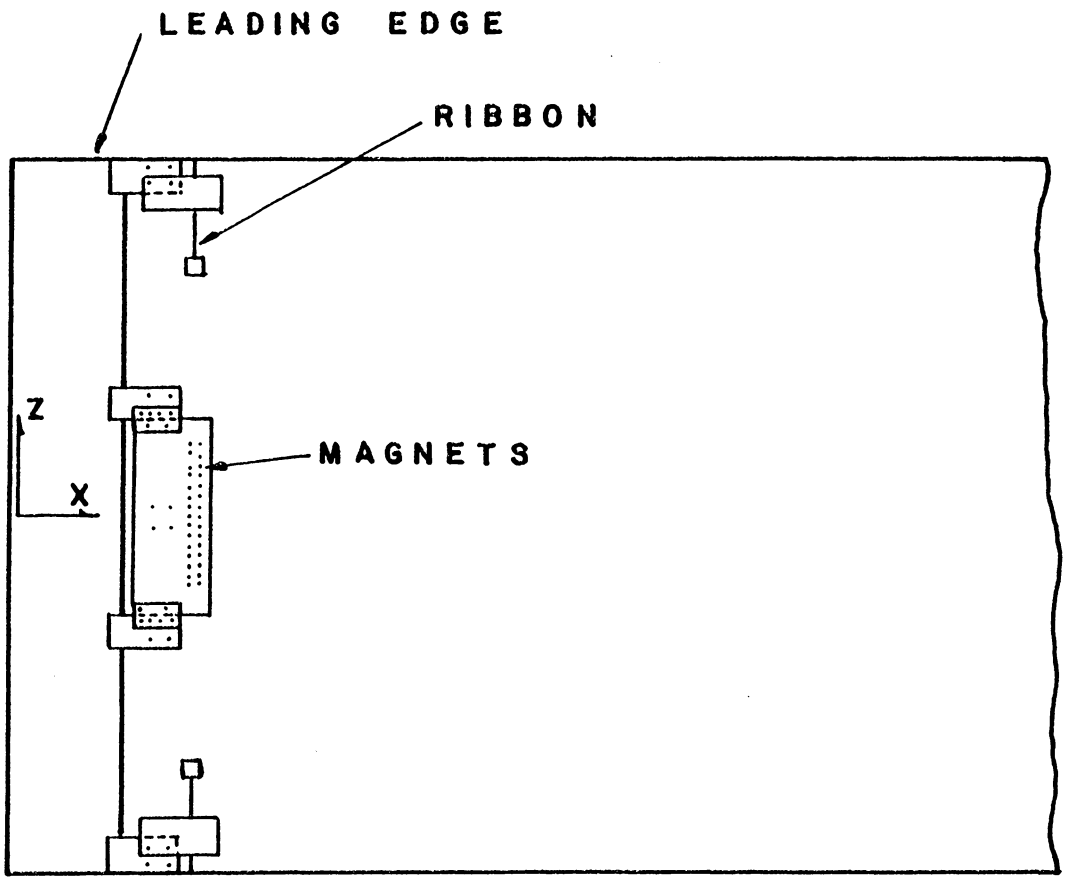

Figure 2.4 Electro-magnet configuration.

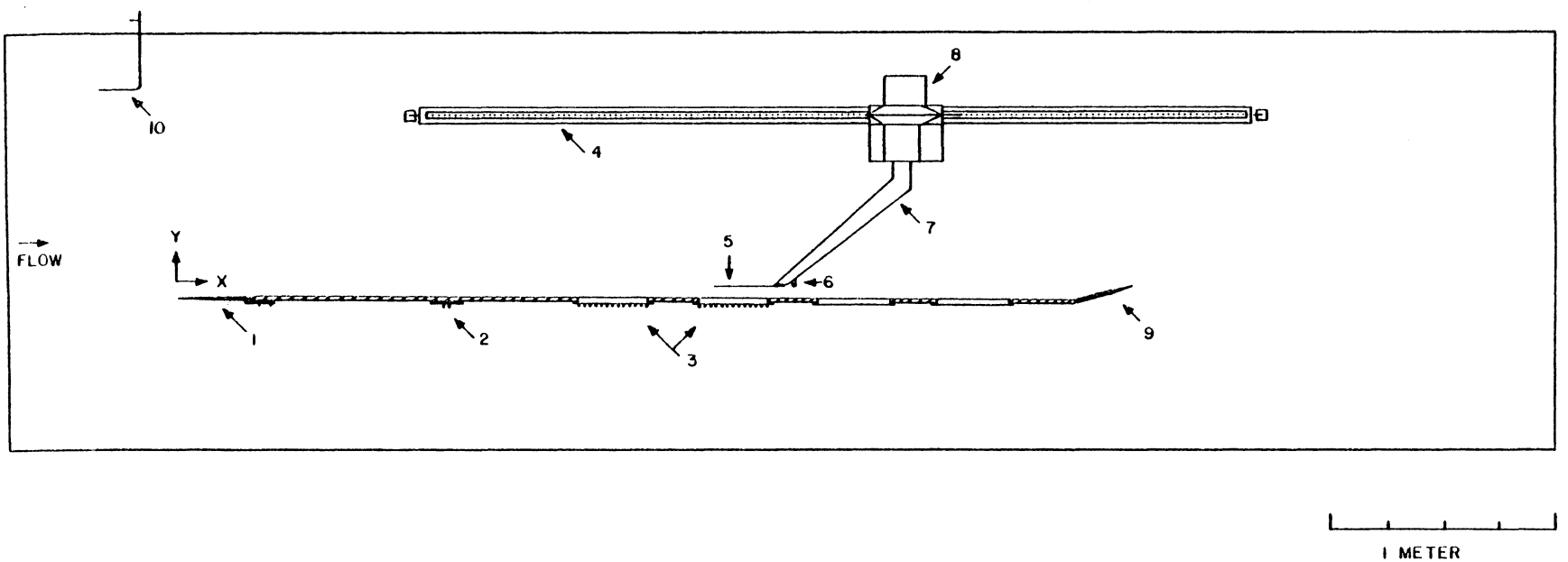

Figure 2.5 Test-section lay-out for experiments on the flat plate model using the 2-D traversing mechanism. The items noted are (1) Elliptical leading edge; (2) Electro-magnets for the vibrating ribbon; (3) Pressure port tubing bundles; (4) Support channel and guide rod for x-traverse; (5) Hot-wire probe extension tube; (6) Proximity probe; (7) Hot-wire probe sting; (8) 2-D traversing mechanism; (9) Trailing-edge flap; (10) Pitot tube.

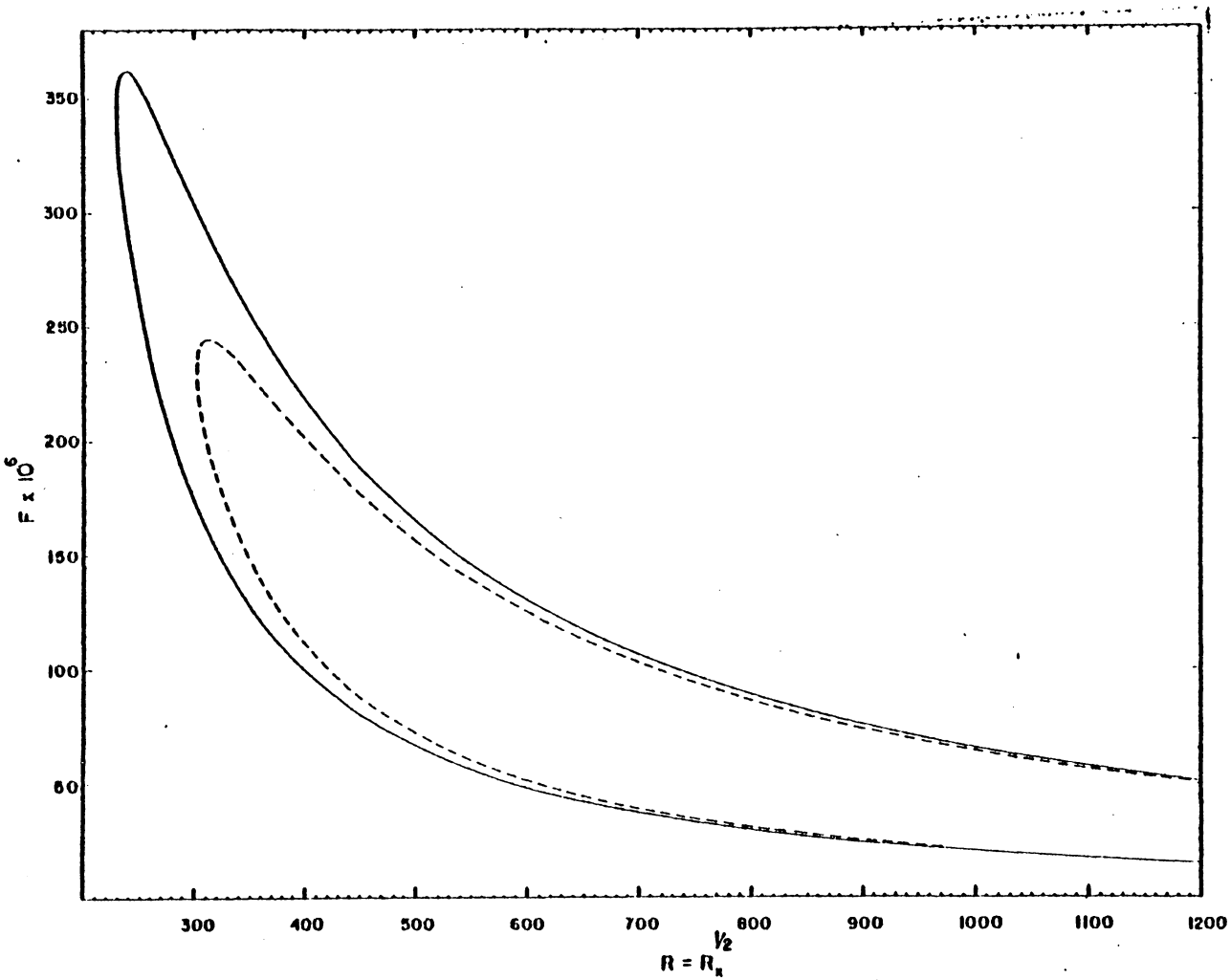

Figure 3.1. Neutral stability curves.

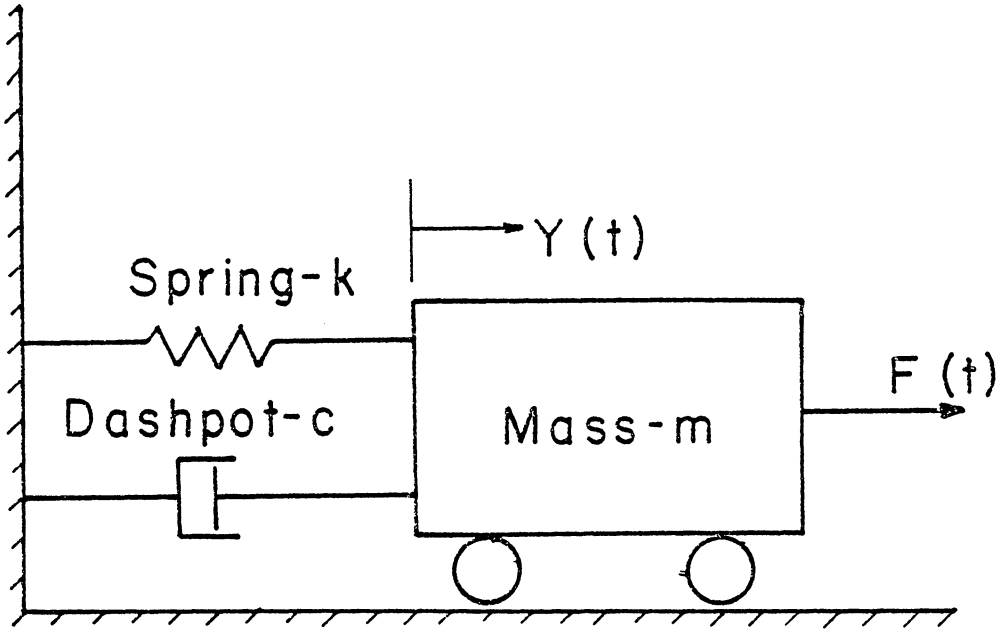

Figure 3.3.1. Vibrating-ribbon model.

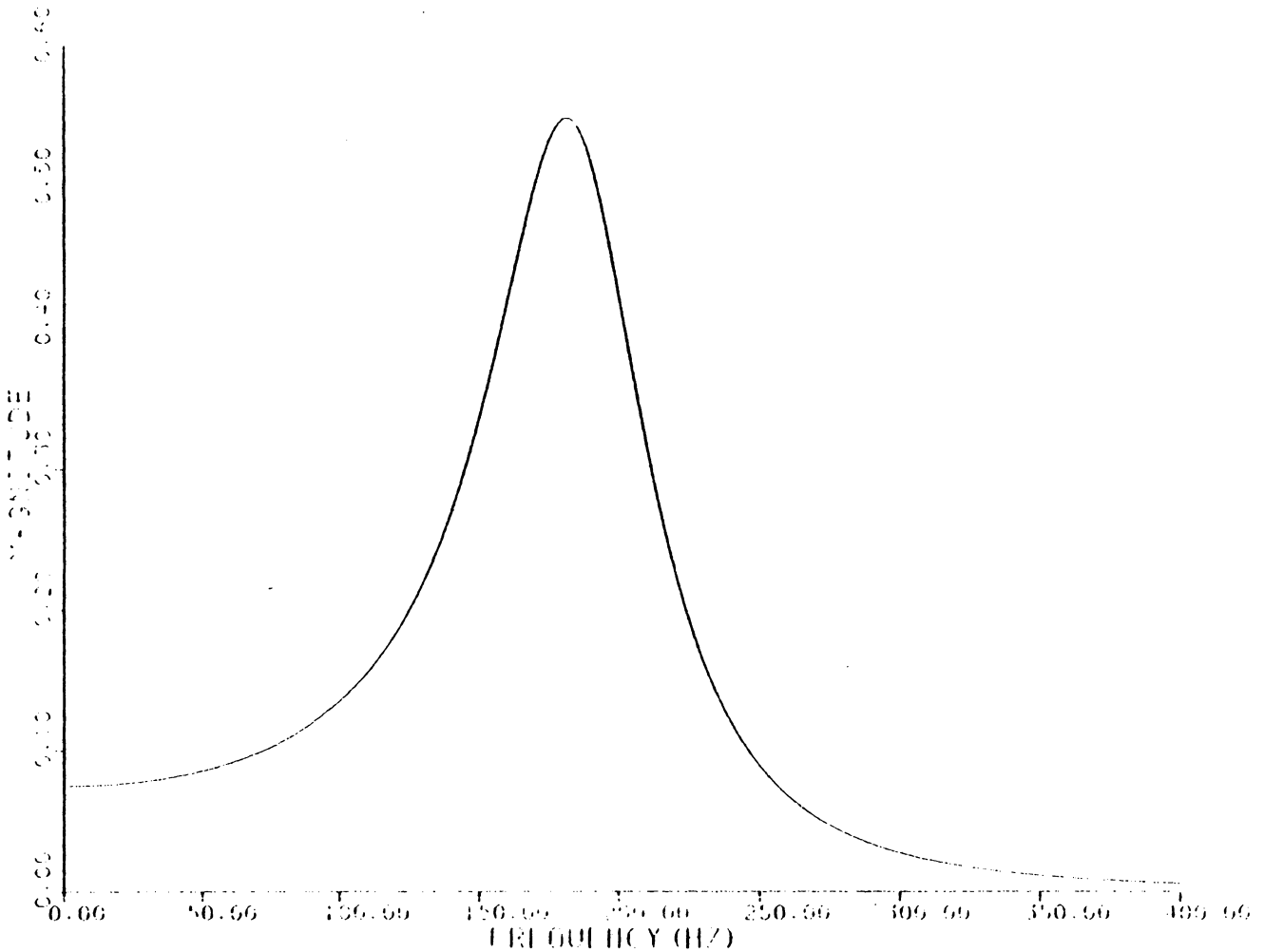

Figure 3.3.2. Response of the model of the vibrating ribbon due to random excitation.

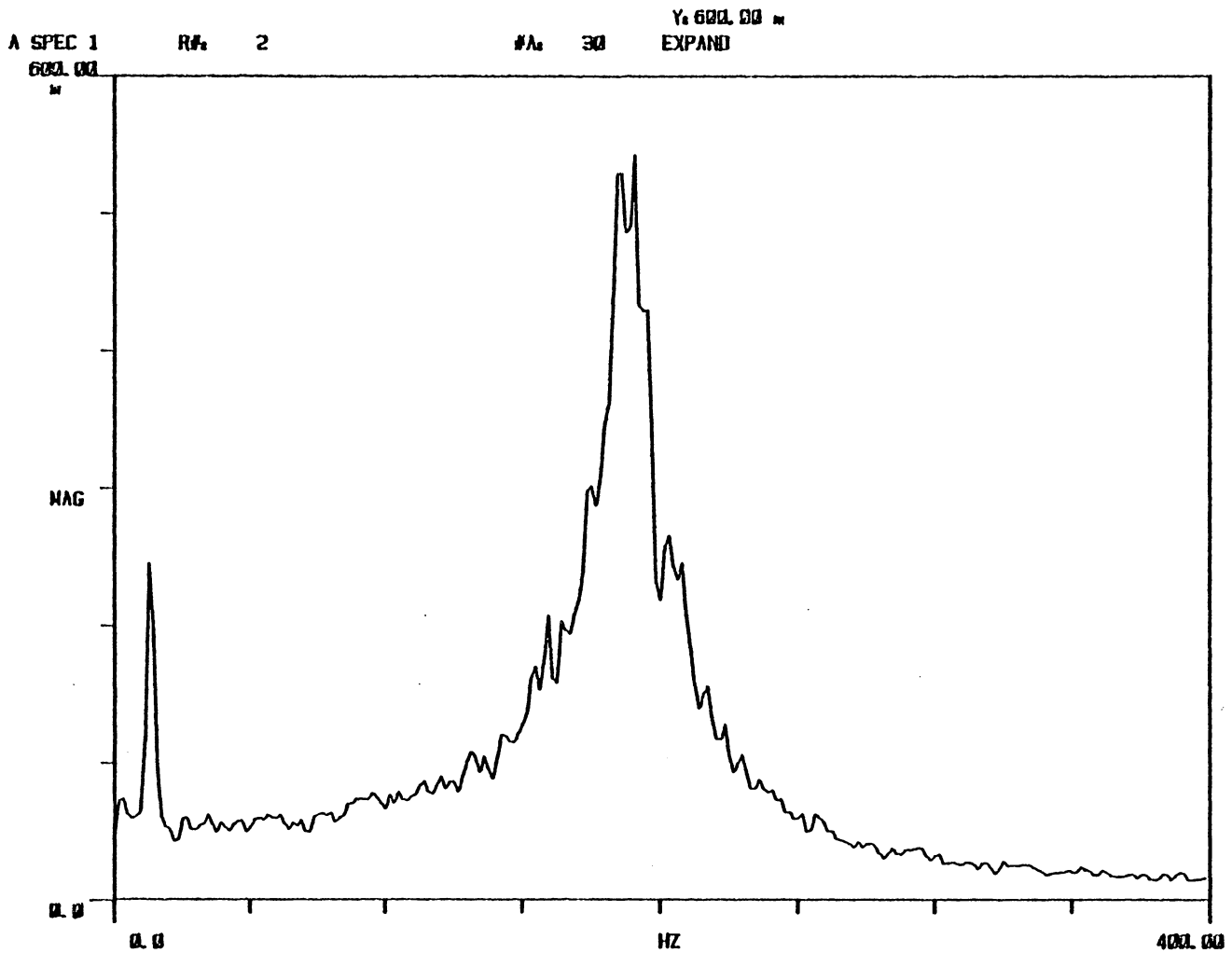

Figure 3.3.3. Vibrating ribbon response due to random excitation.

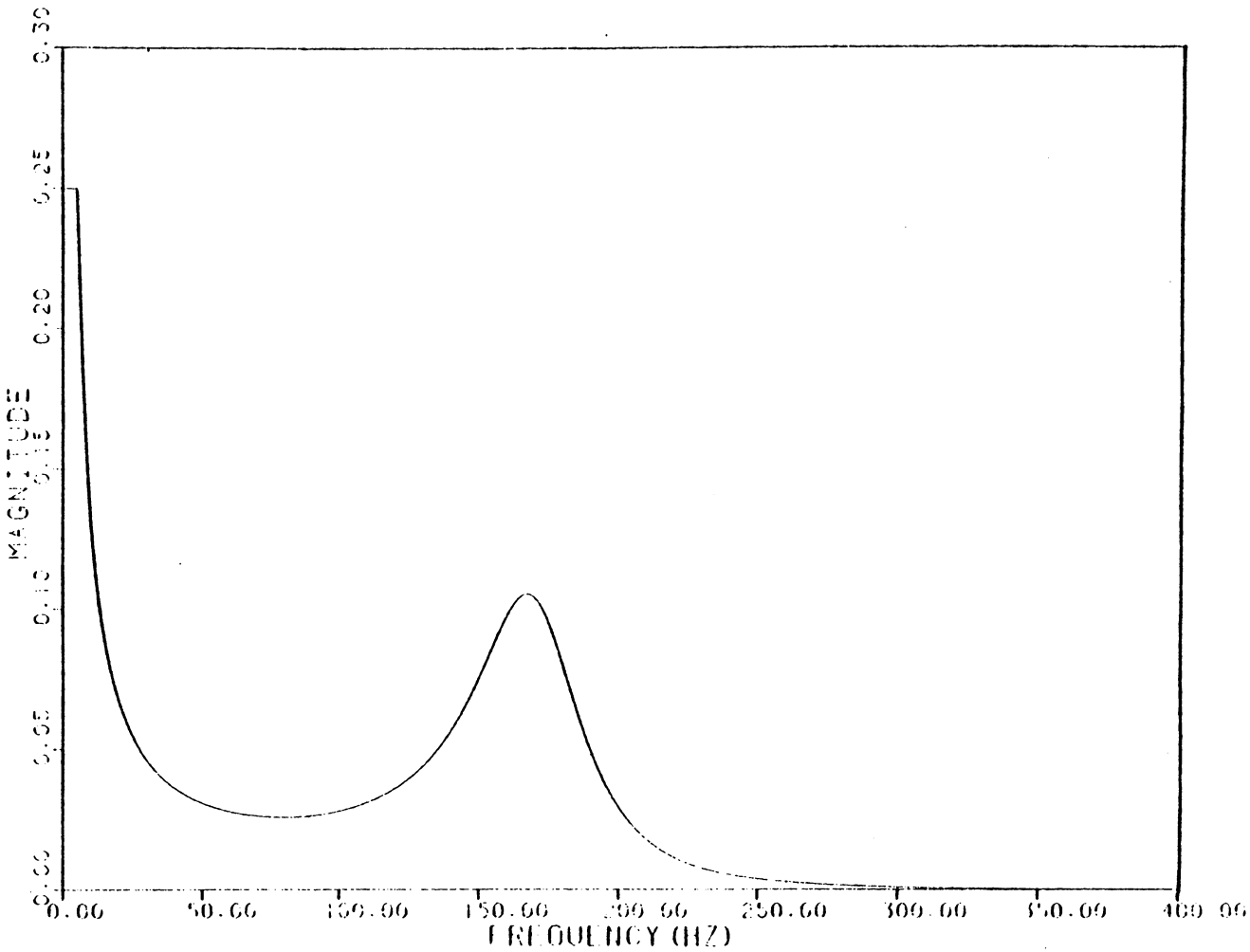

Figure 3.3.4. Frequency response of the model of the vibrating ribbon due to step-form excitation.

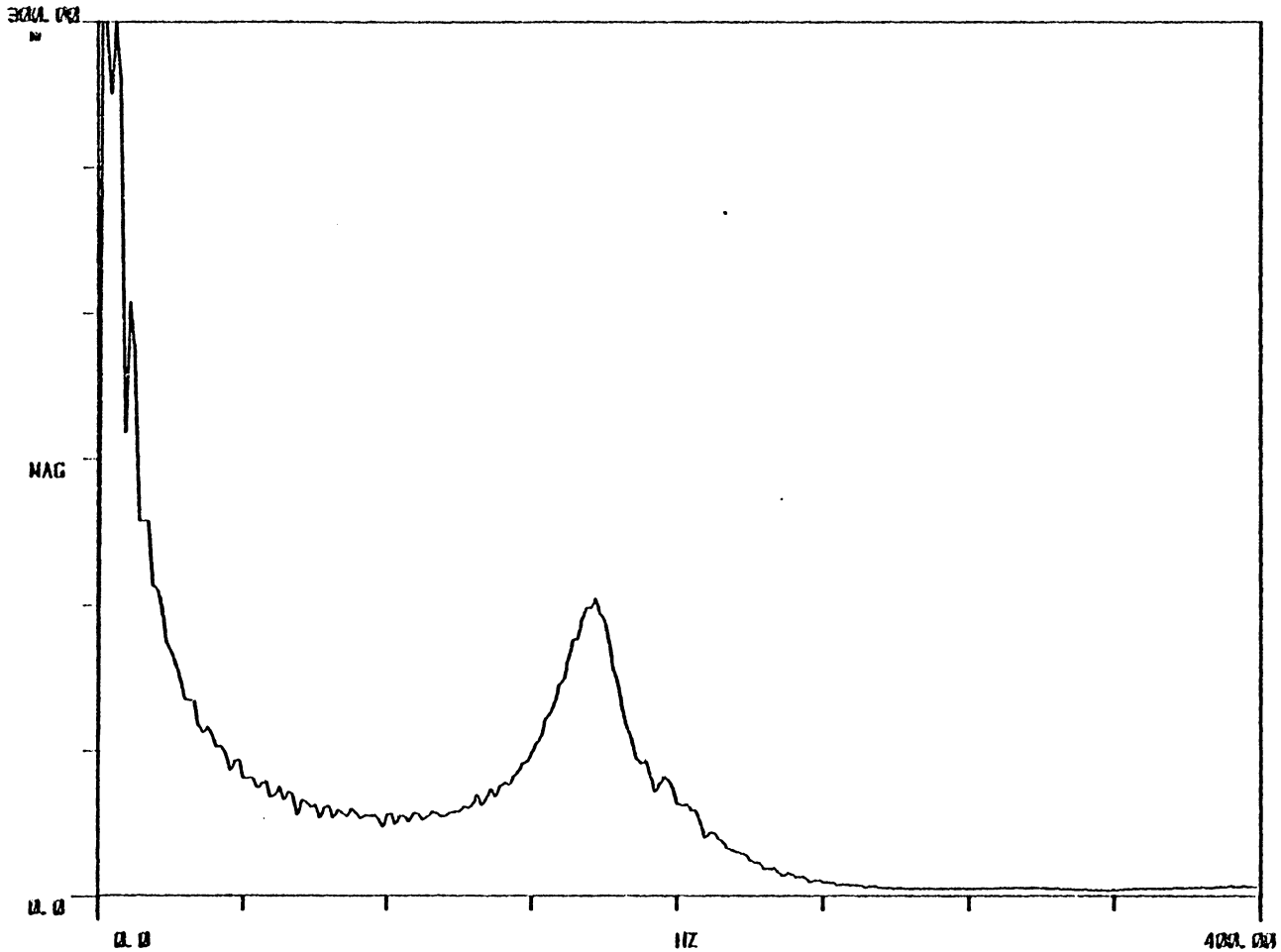

Figure 3.3.5. Frequency response of the vibrating ribbon due to step-form excitation.

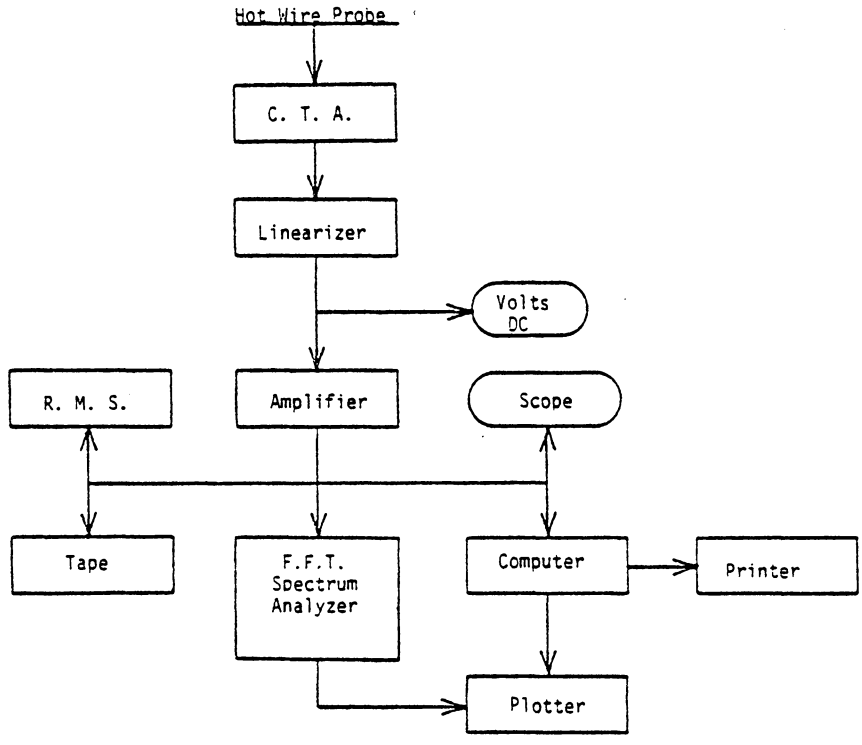

Figure 4.1 Data aquisition instrumentation.

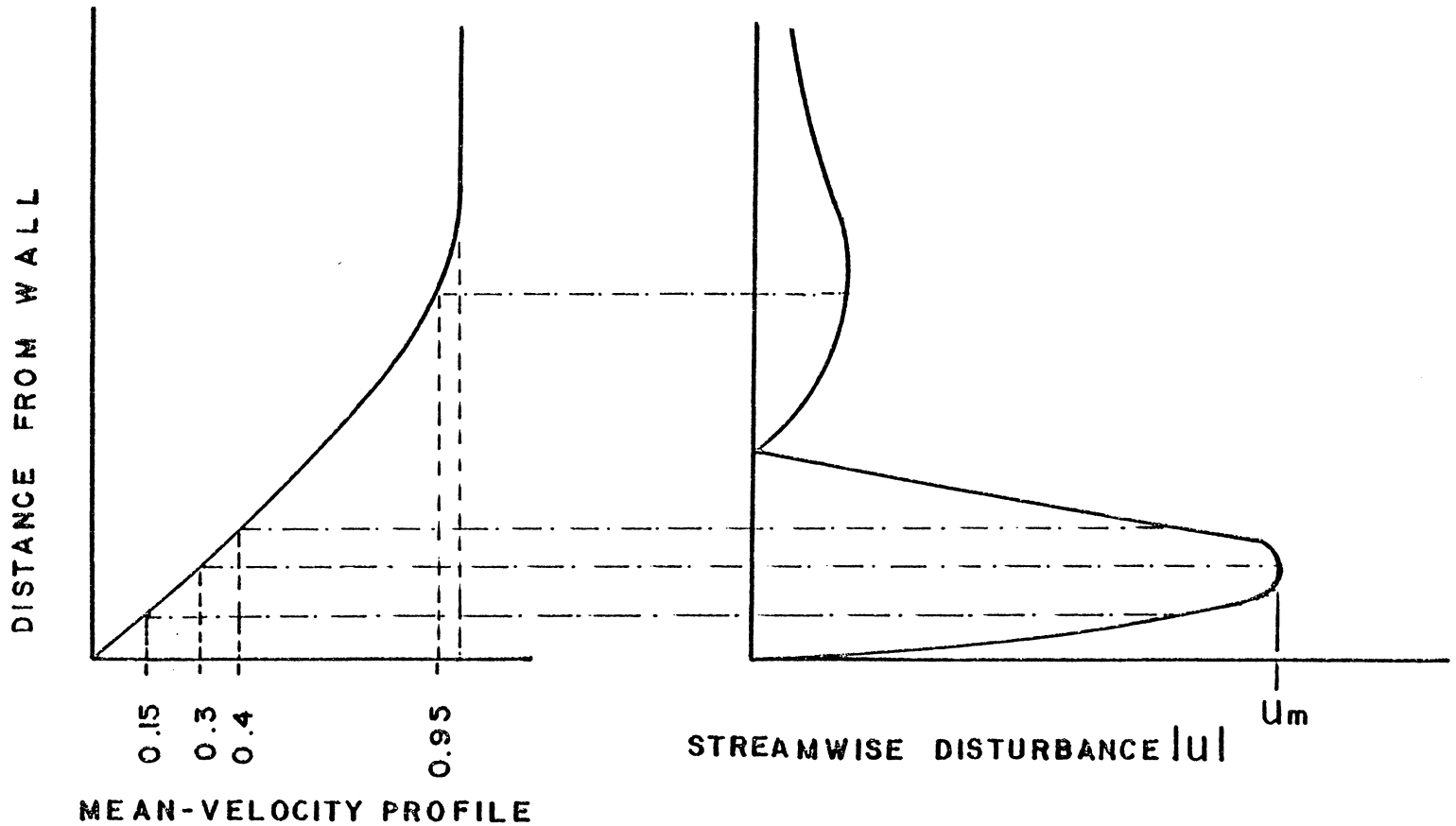

Figure 4.2 Positions in y-direction where measurements were taken for the case of random excitation response.

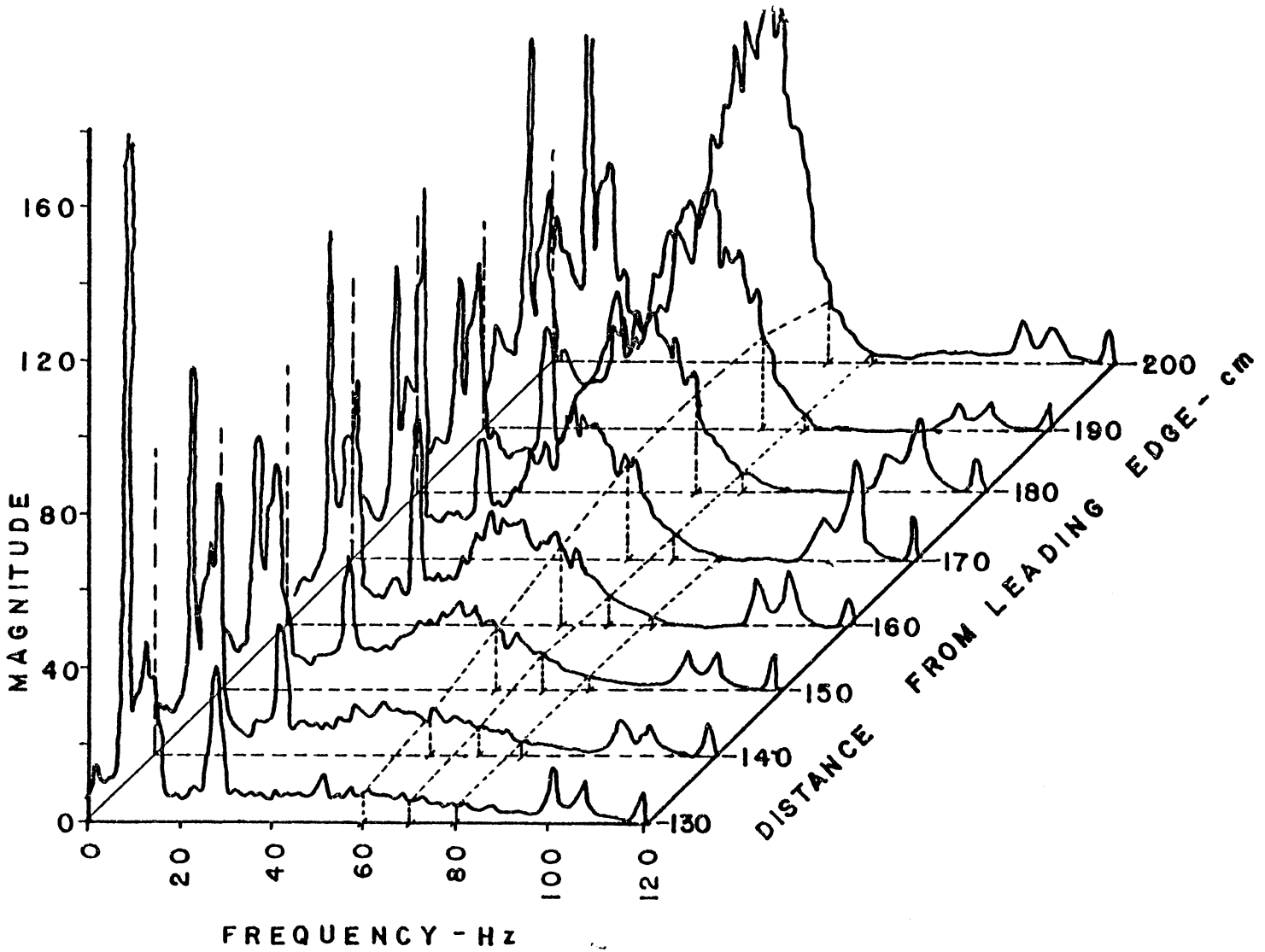

Figure 4.3 Aquisition of constant frequency curves from the random-excitation output spectra.

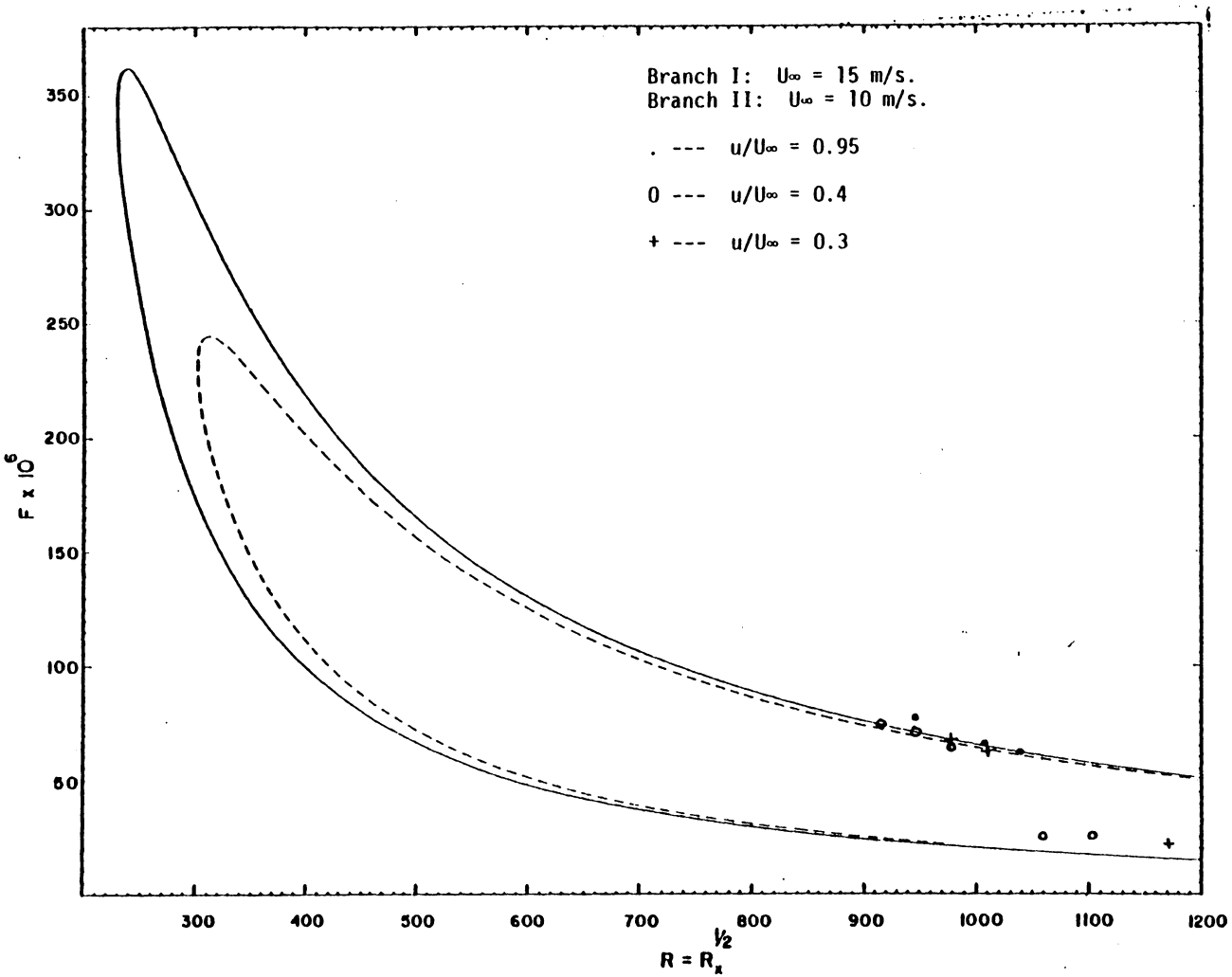

Figure 4.4 Experimentally found neutral stability points.

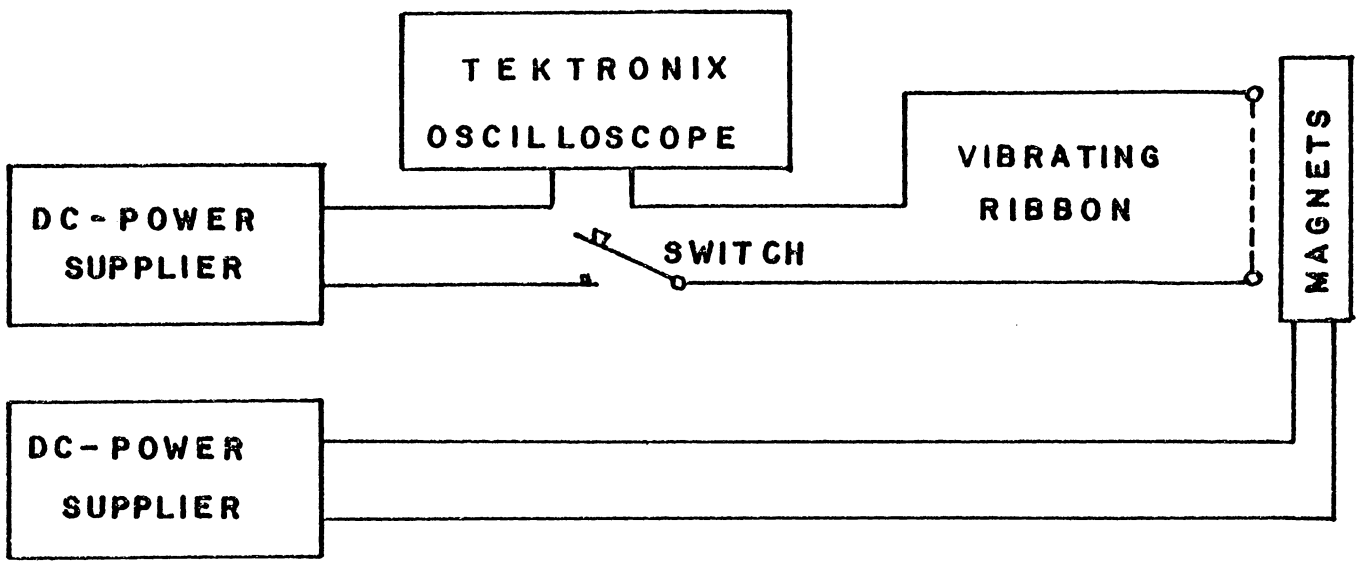

Figure 5.1 Circuit for the introduction of step-function input force to the vibrating ribbon.

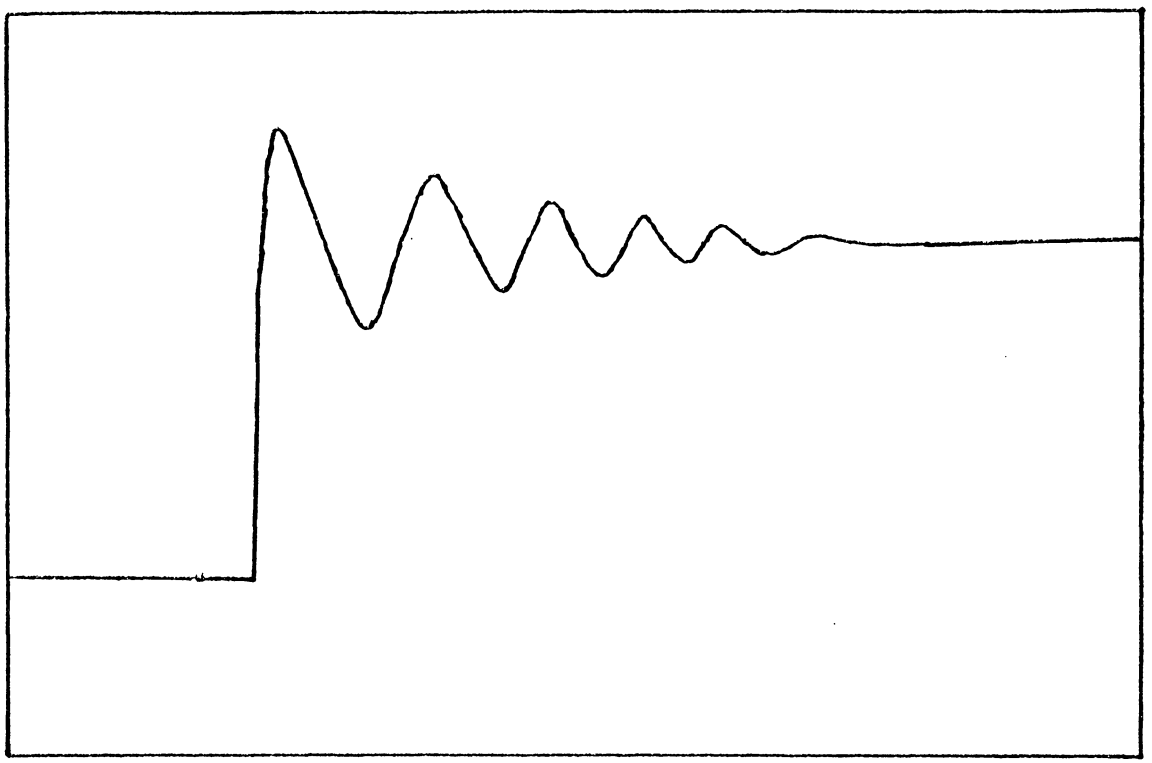

Fig. 5.2 Response of the vibrating ribbon on the osciloscope screen.

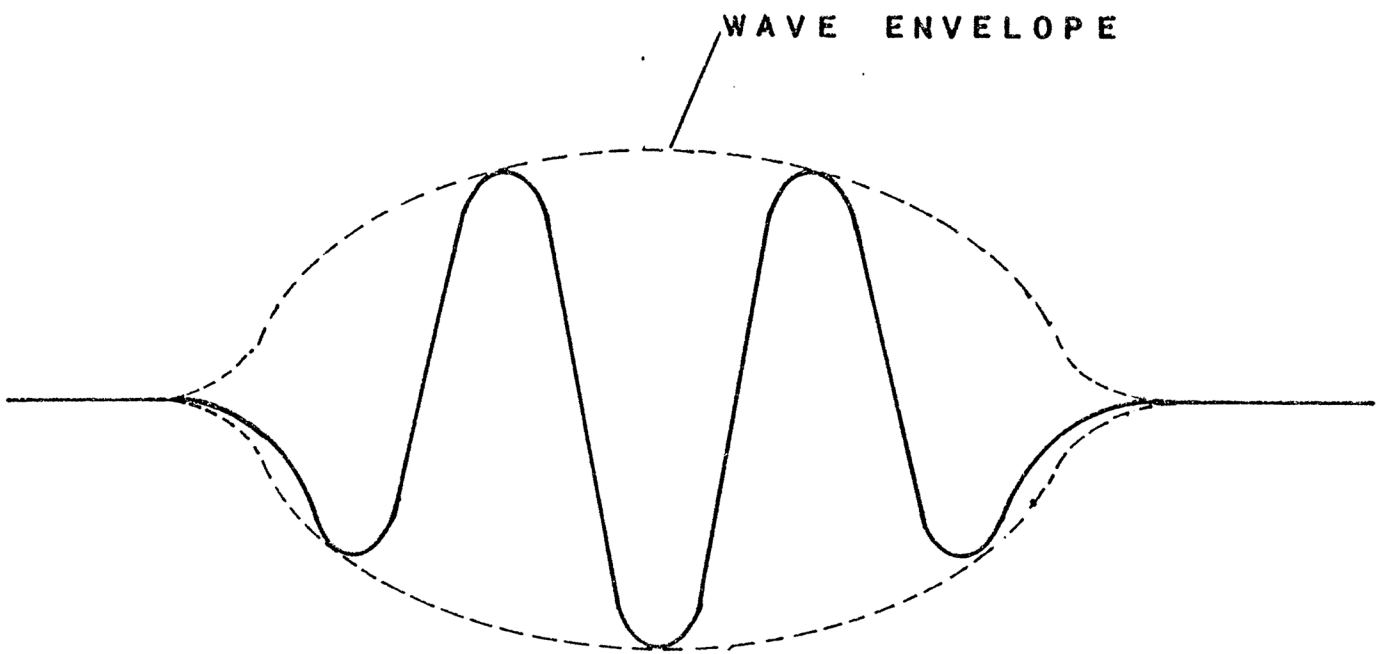

Figure 5.3 Shape of the wavepacket as seen in the osciloscope.

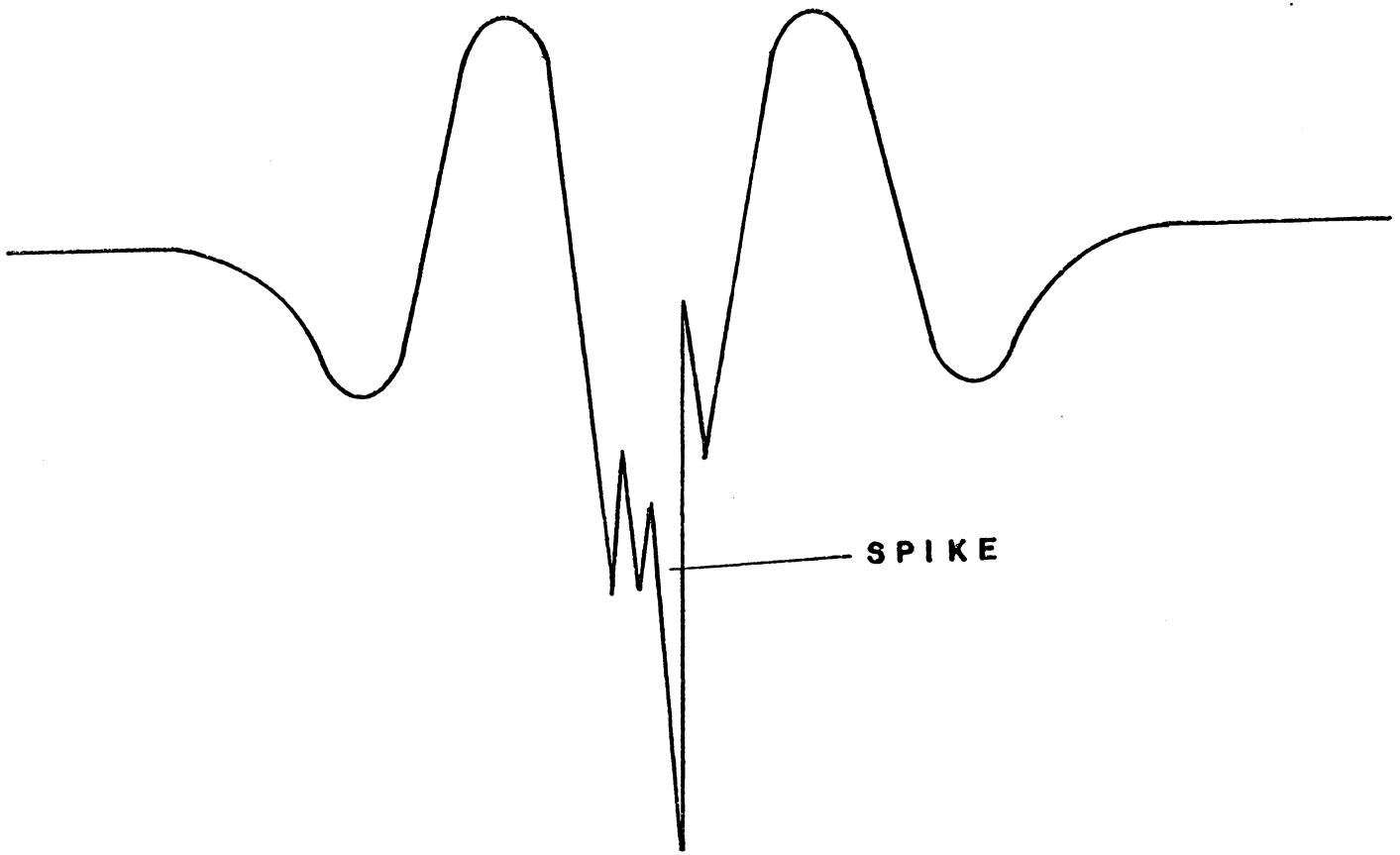

Figure 5.4 Distorted wavepacket form due to appearance of turbulent spikes.

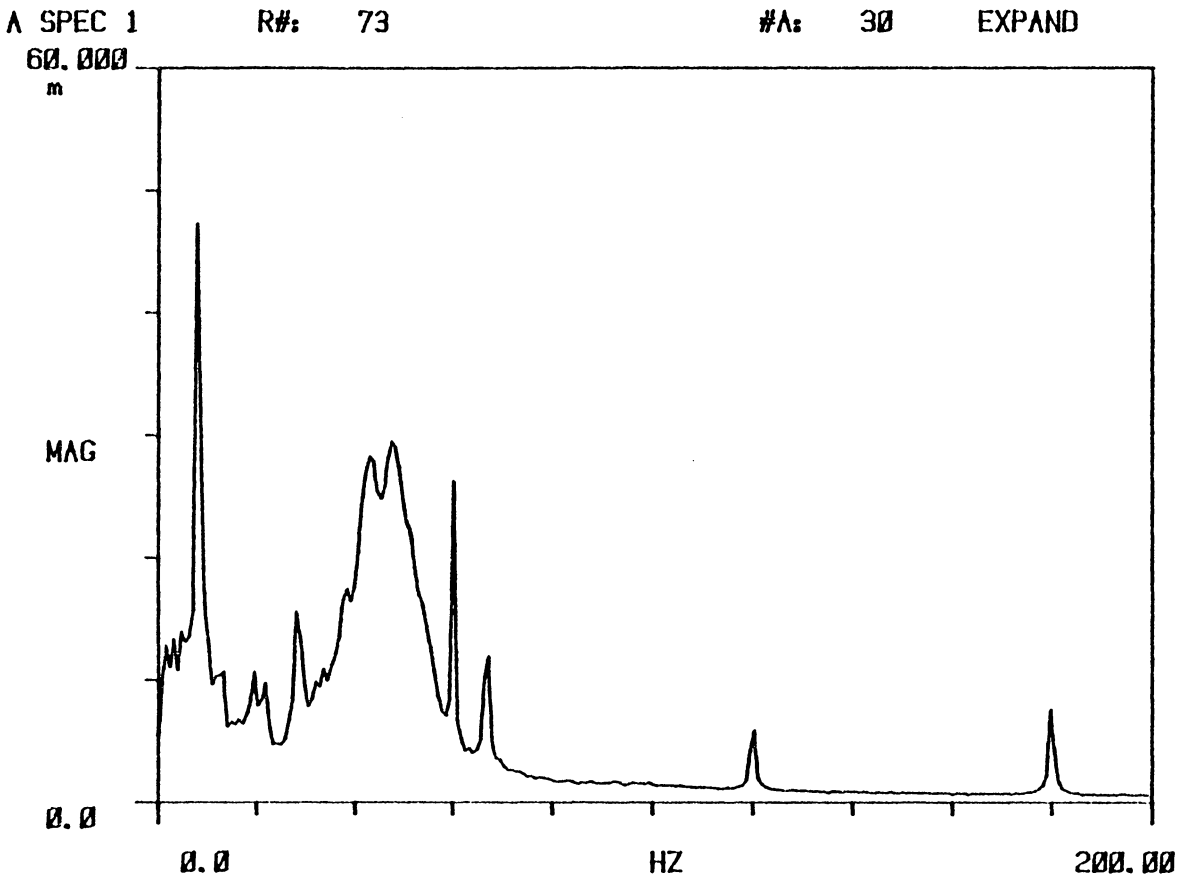

Figure 5.4.1 Boundary-layer system response to step-function excitation U_∞ = 9.0 m/sec.

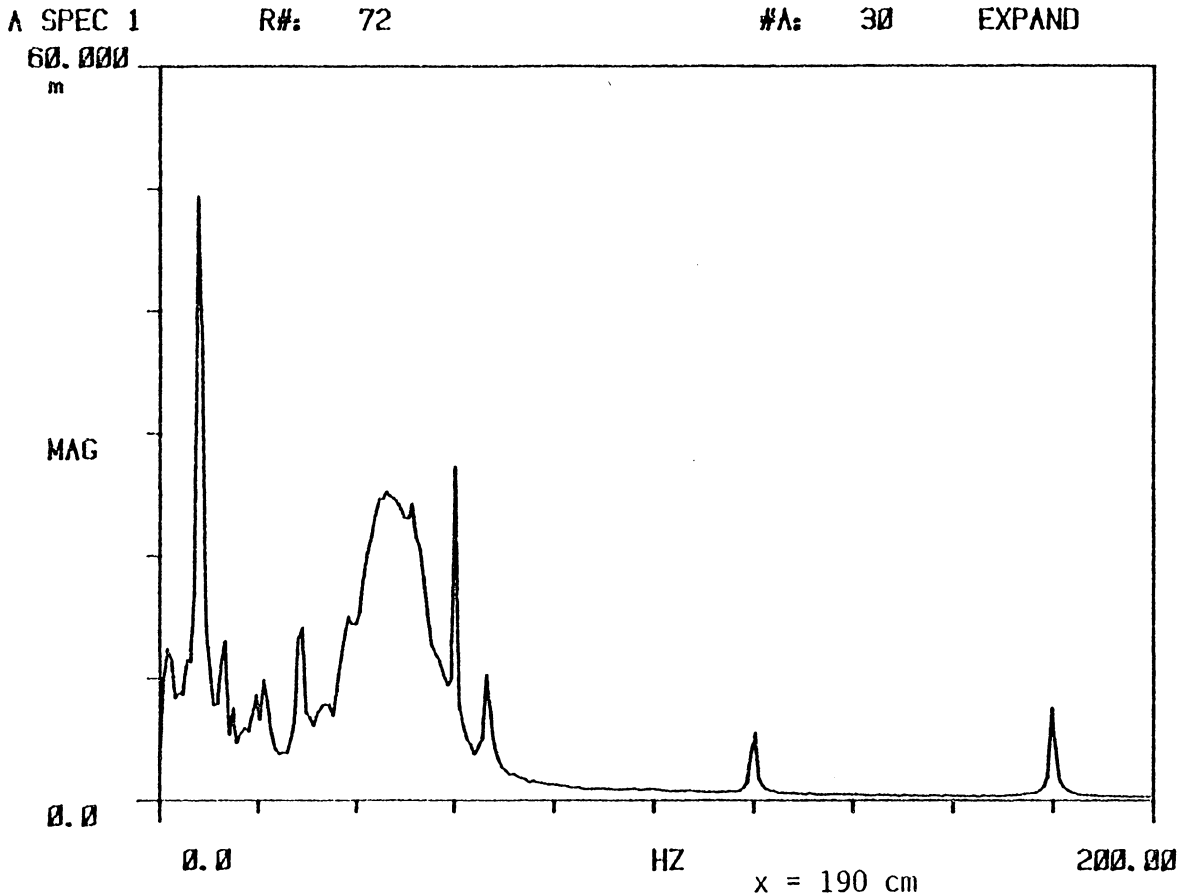

Figure 5.4.2. Boundary-layer system response to step-function excitation U_∞ = 9.0 m/sec.

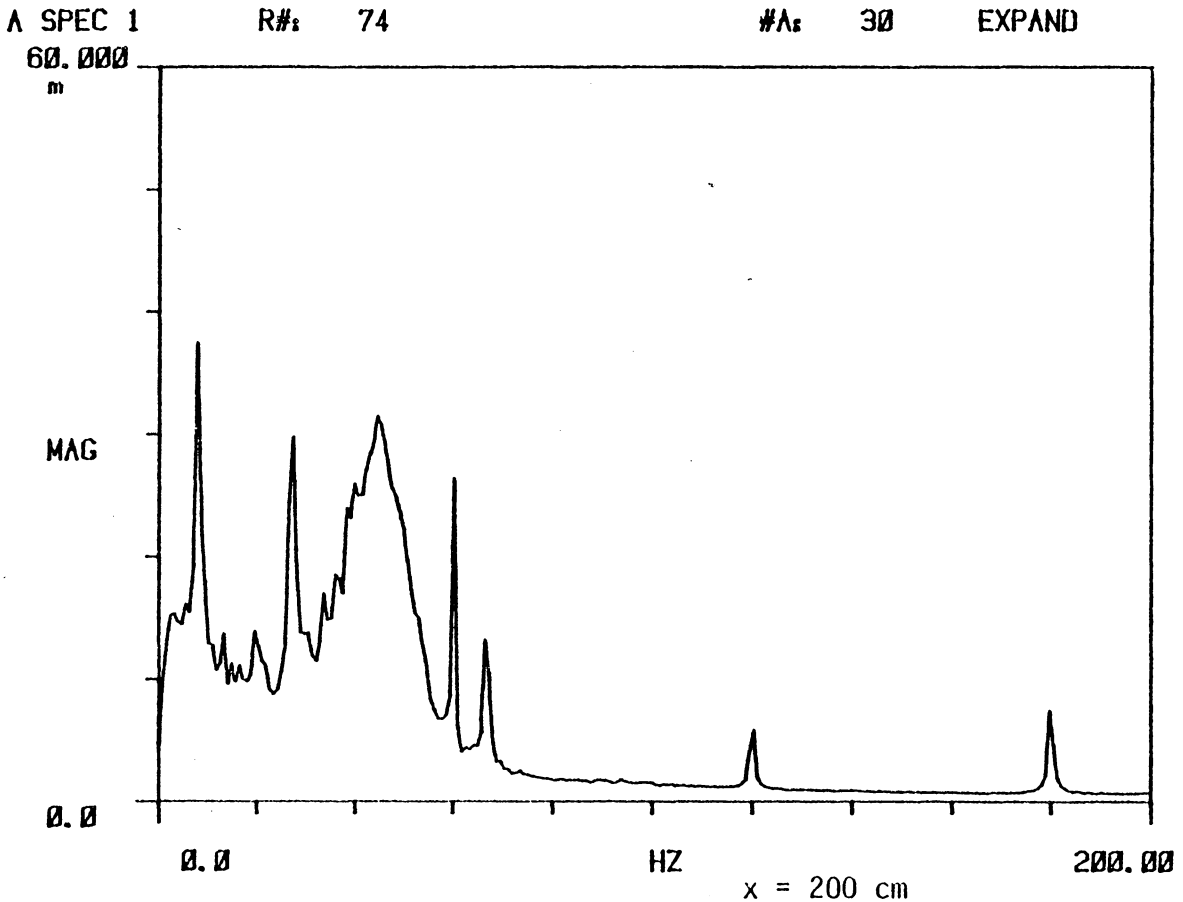

Figure 5.4.3 Boundary-layer system response to step-function excitation U_∞ = 9.0 m/sec.

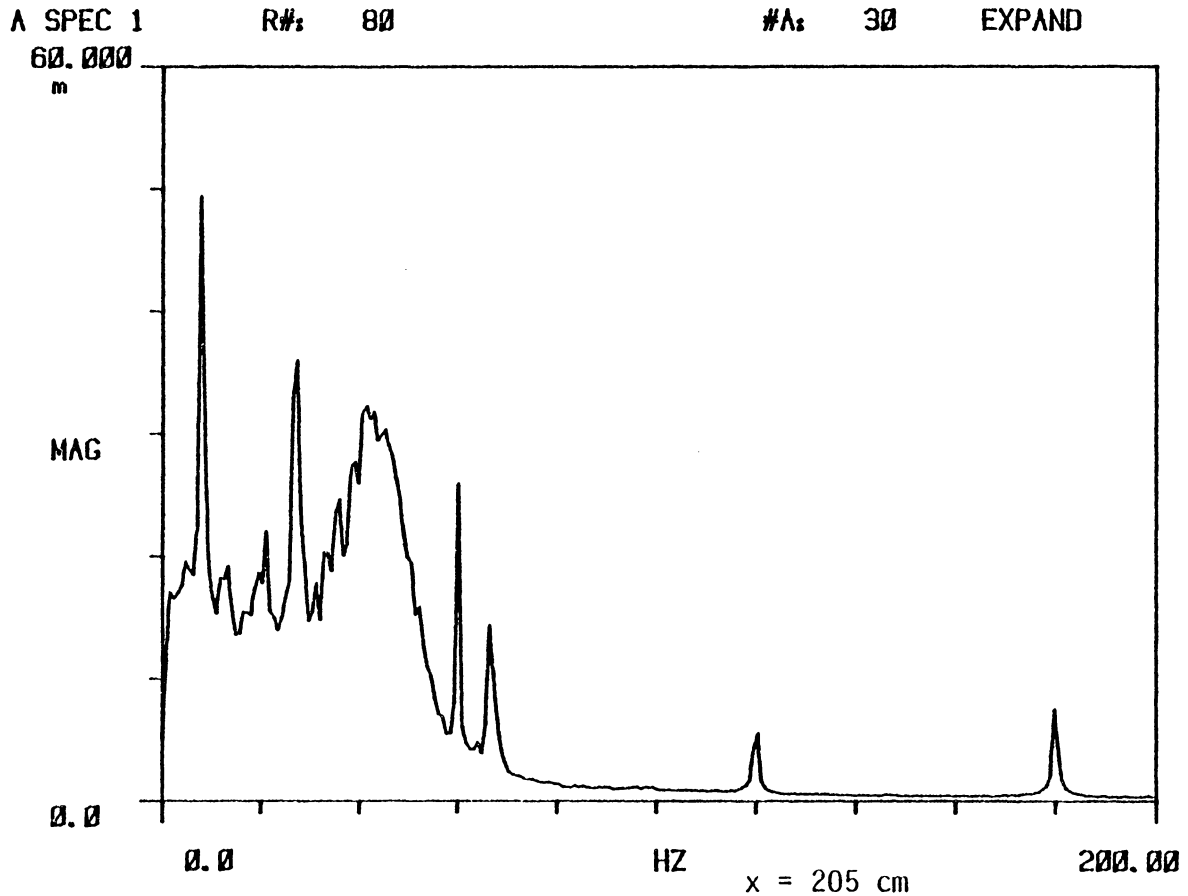

Figure 5.4.4 Boundary-layer system response to step-function excitation U_∞ = 9.0 m/sec.

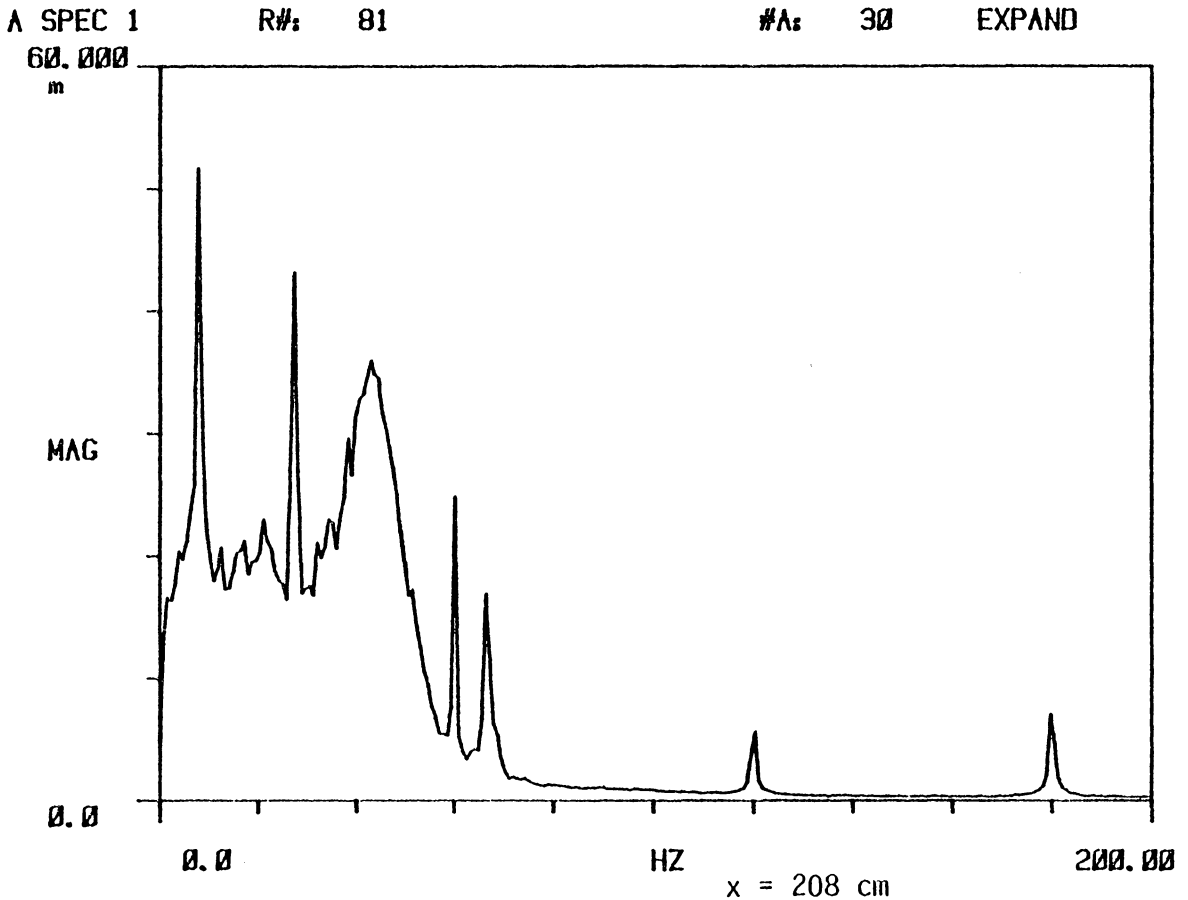

Figure 5.4.5 Boundary-layer system response to step-function excitation U_∞ = 9.0 m/sec.

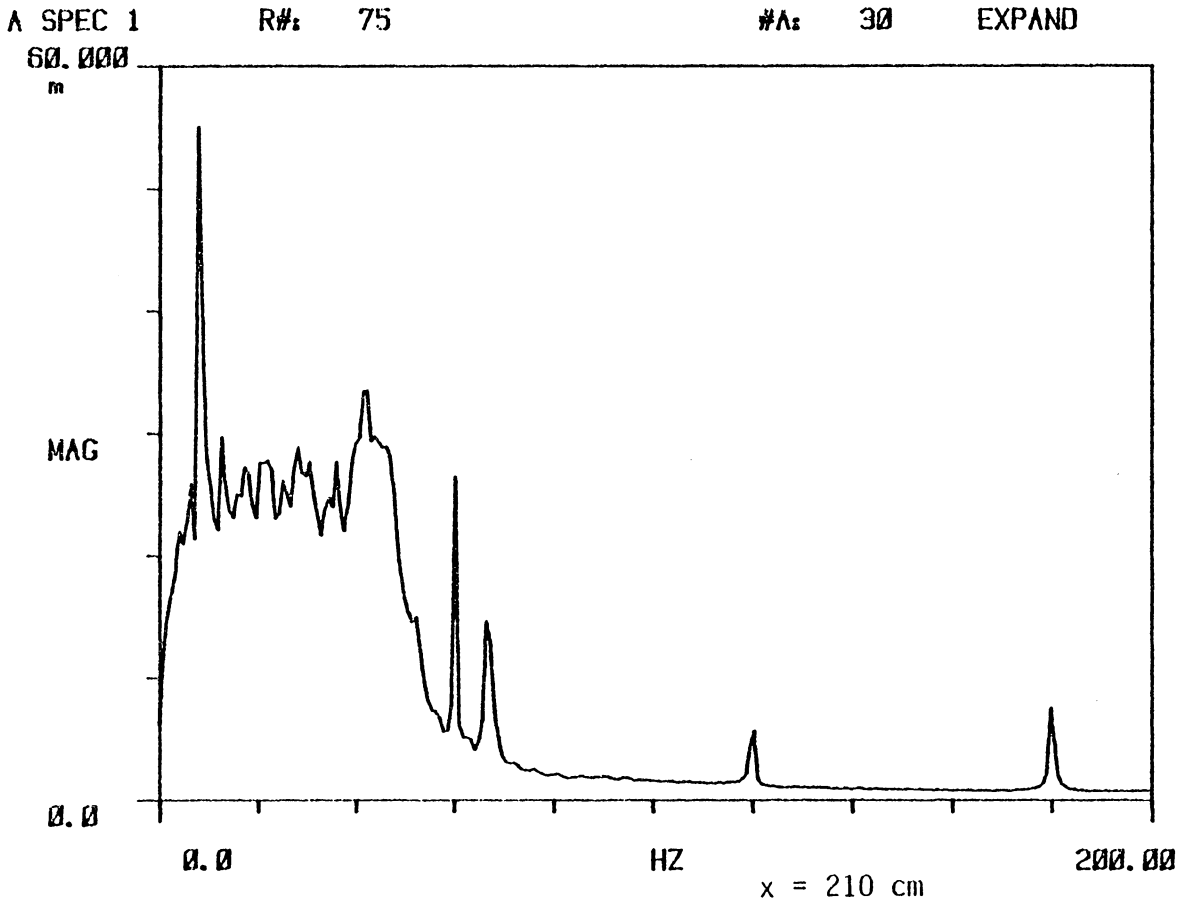

Figure 5.4.6 Boundary-layer system response to step-function excitation U_∞ = 9.0 m/sec.

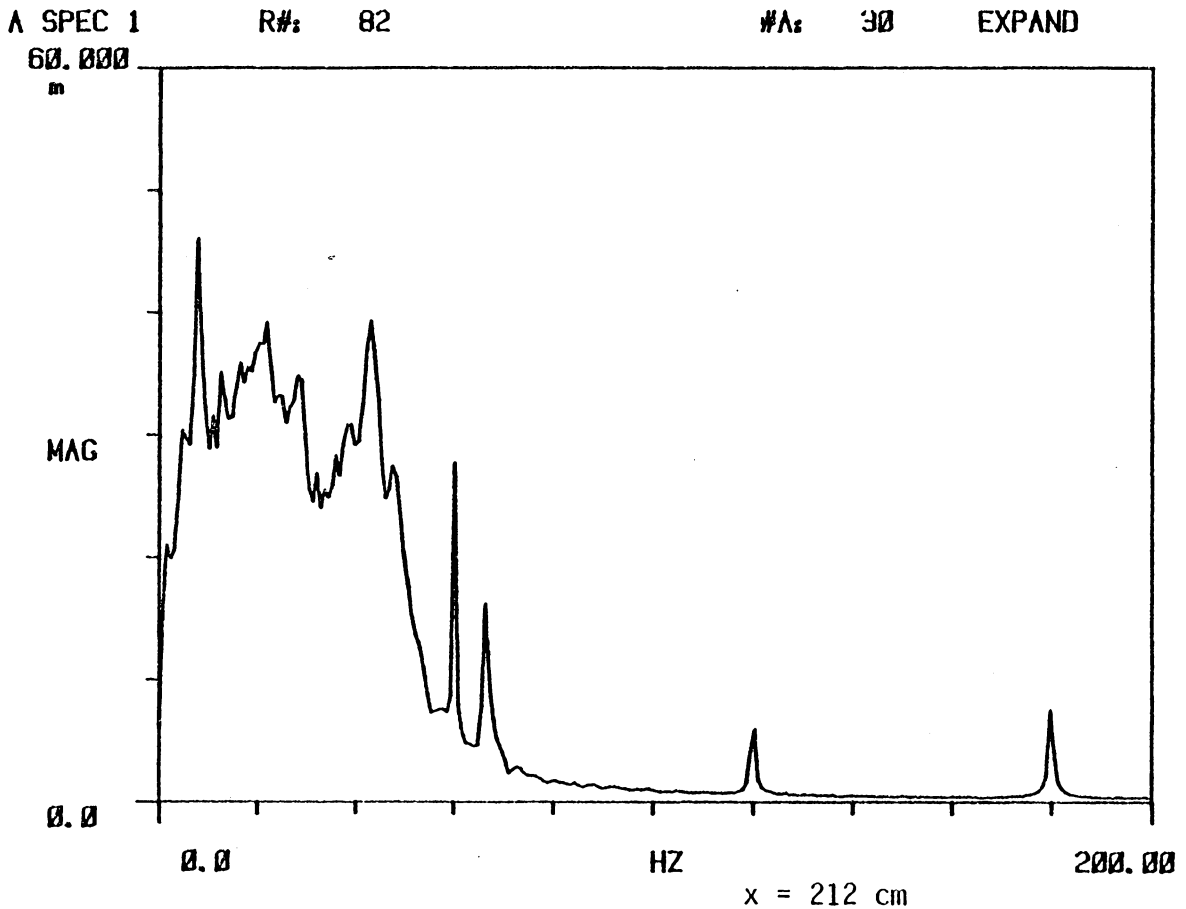

Figure 5.4.7 Boundary-layer system response to step-function excitation U_∞ = 9.0 m/sec.

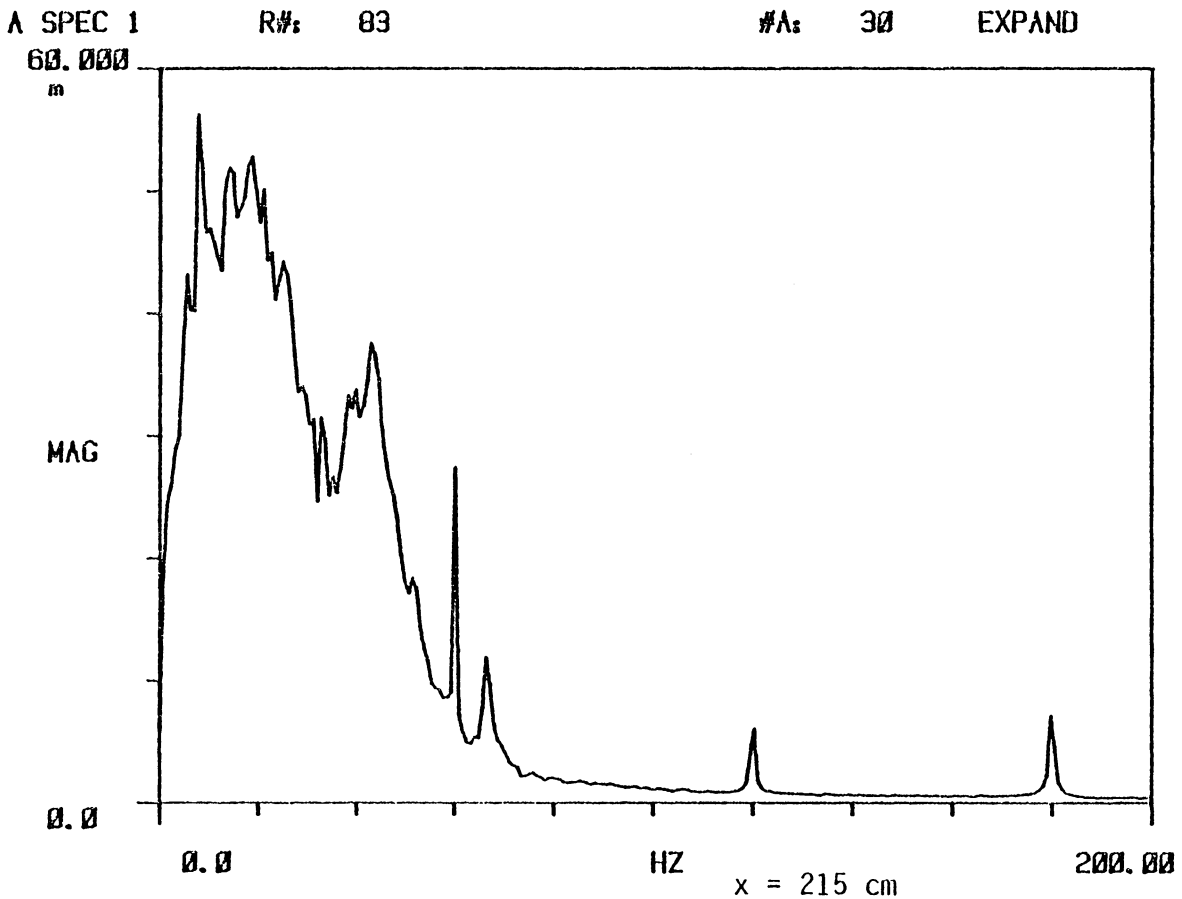

Figure 5.4.8 Boundary-layer system response to step-function excitation U_∞ = 9.0 m/sec.

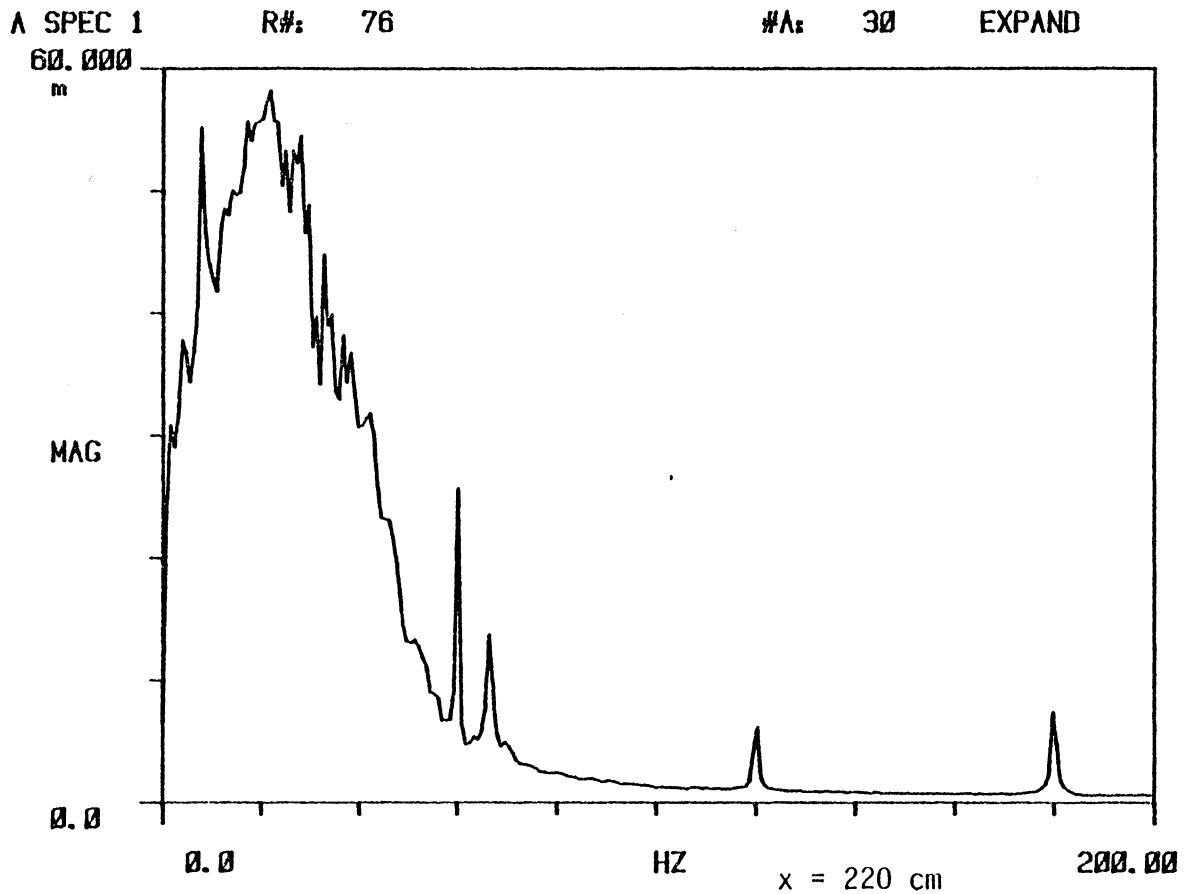

Figure 5.4.9 Boundary-layer system response to step-function excitation U_∞ = 9.0 m/sec.

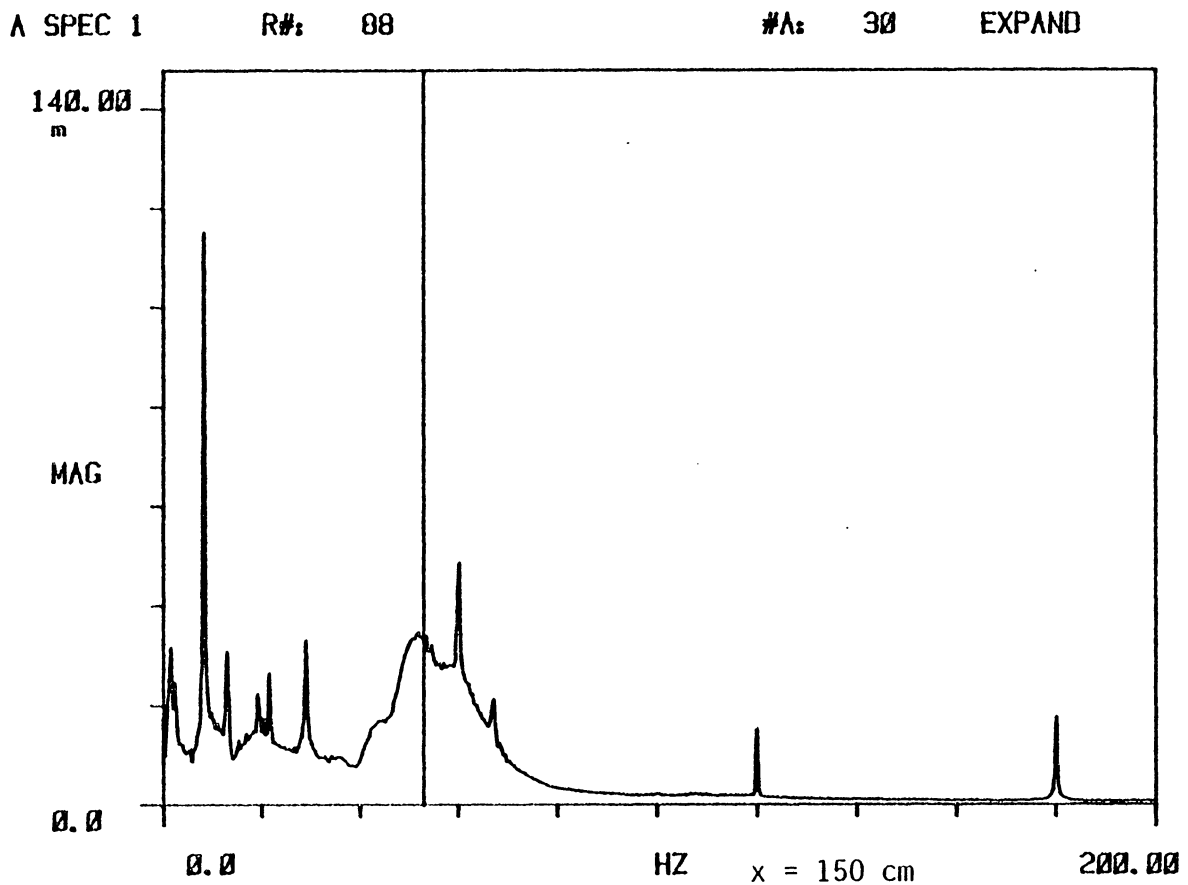

Figure 5.4.10 Boundary-layer system response to step-function input U_∞ = 9.1 m/sec.

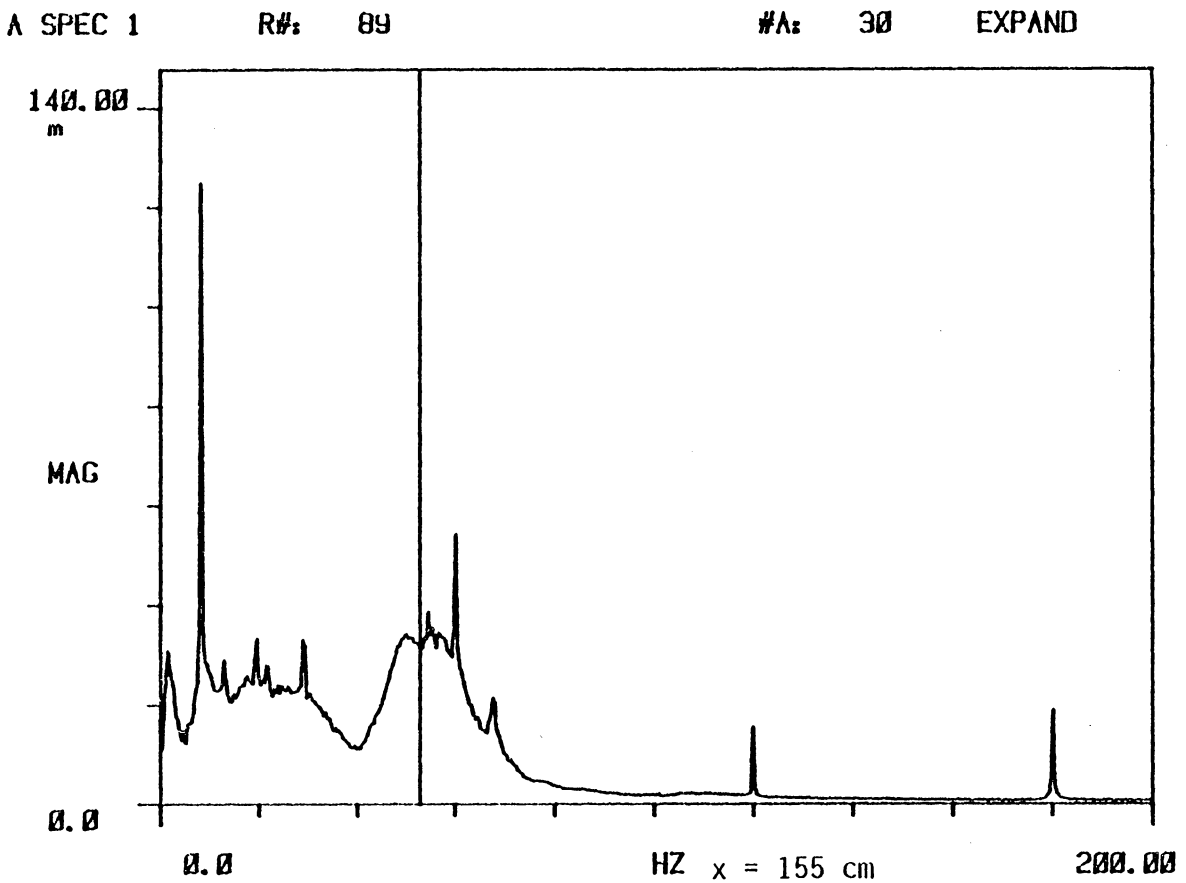

Figure 5.4.11 Boundary-layer system response to step-function input U_∞ = 9.1 m/sec.

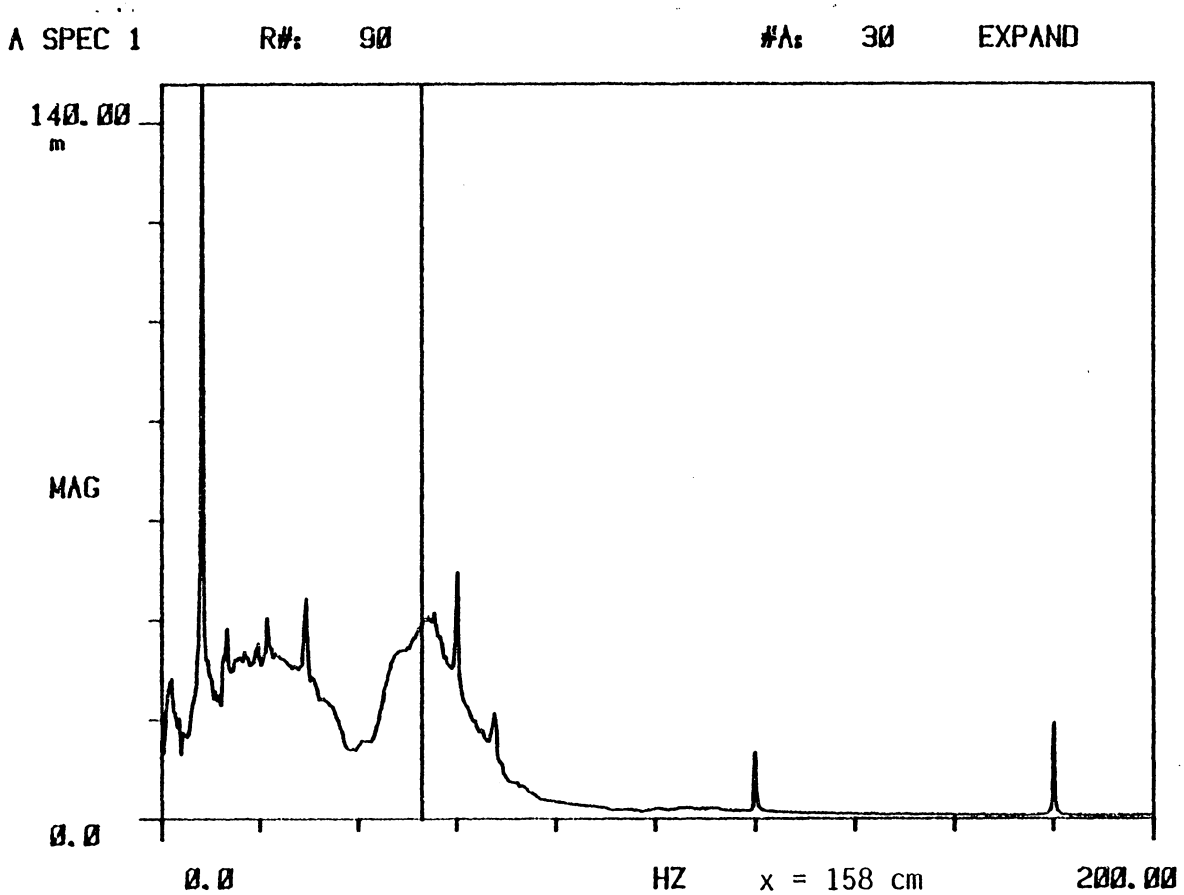

Figure 5.4.12 Boundary-layer system response to step-function input U_∞ = 9.1 m/sec.

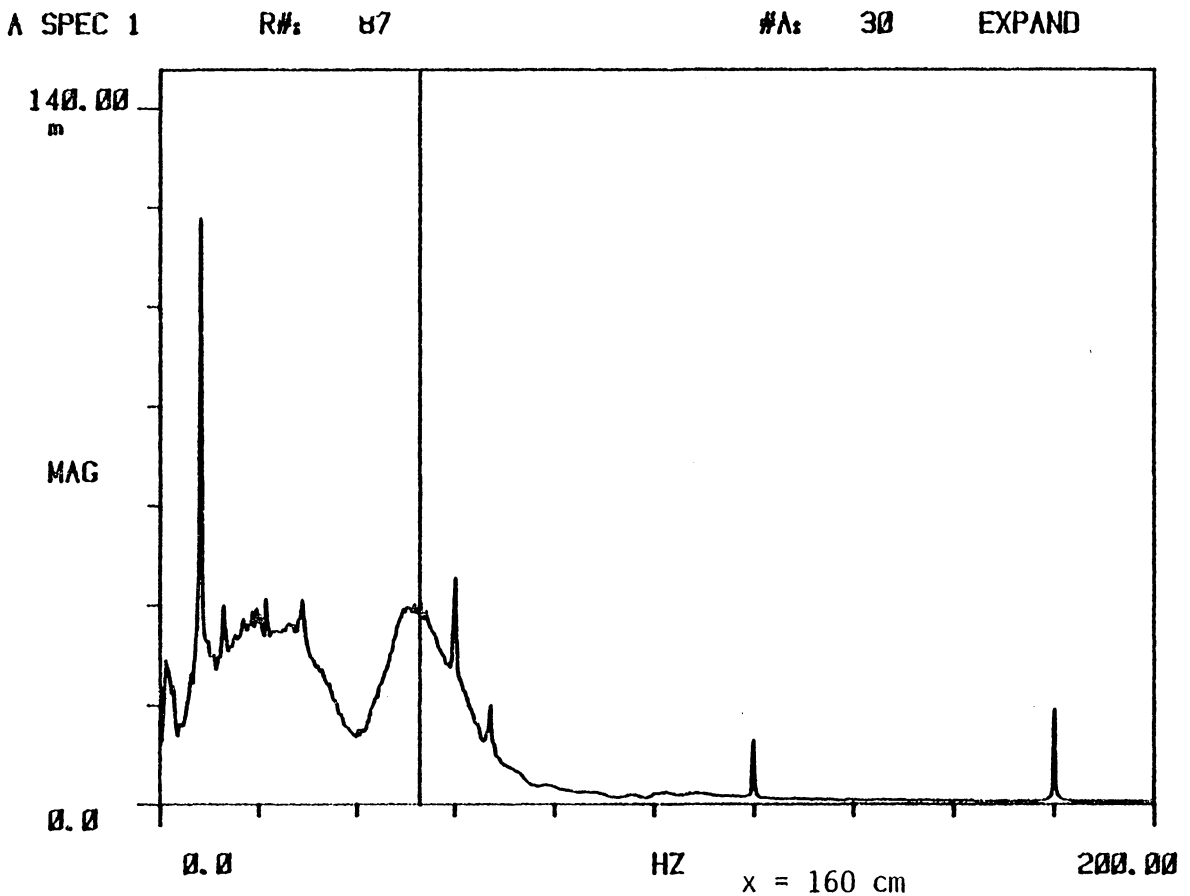

Figure 5.4.13 Boundary-layer system response to step-function input U_∞ = 9.1 m/sec.

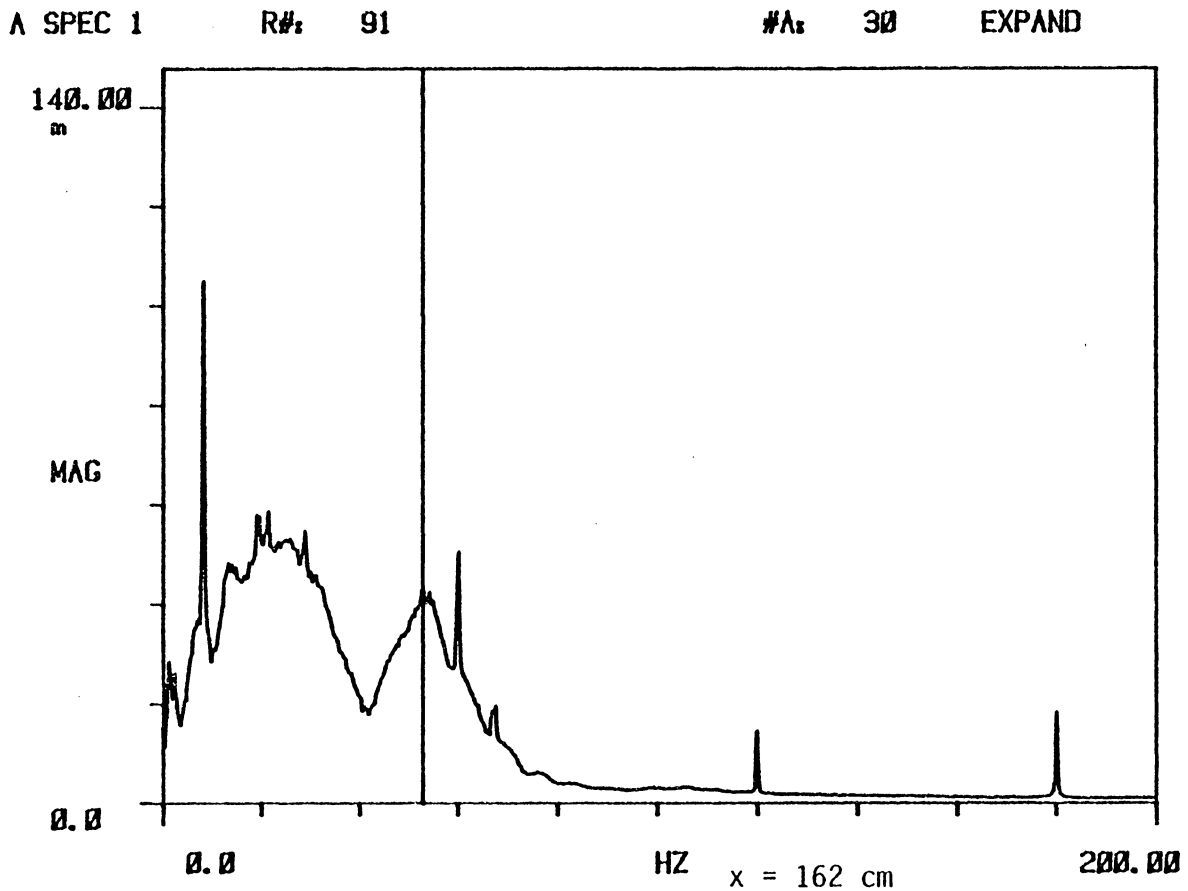

Figure 5.4.14 Boundary-layer system response to step-function input U_∞ = 9.1 m/sec.

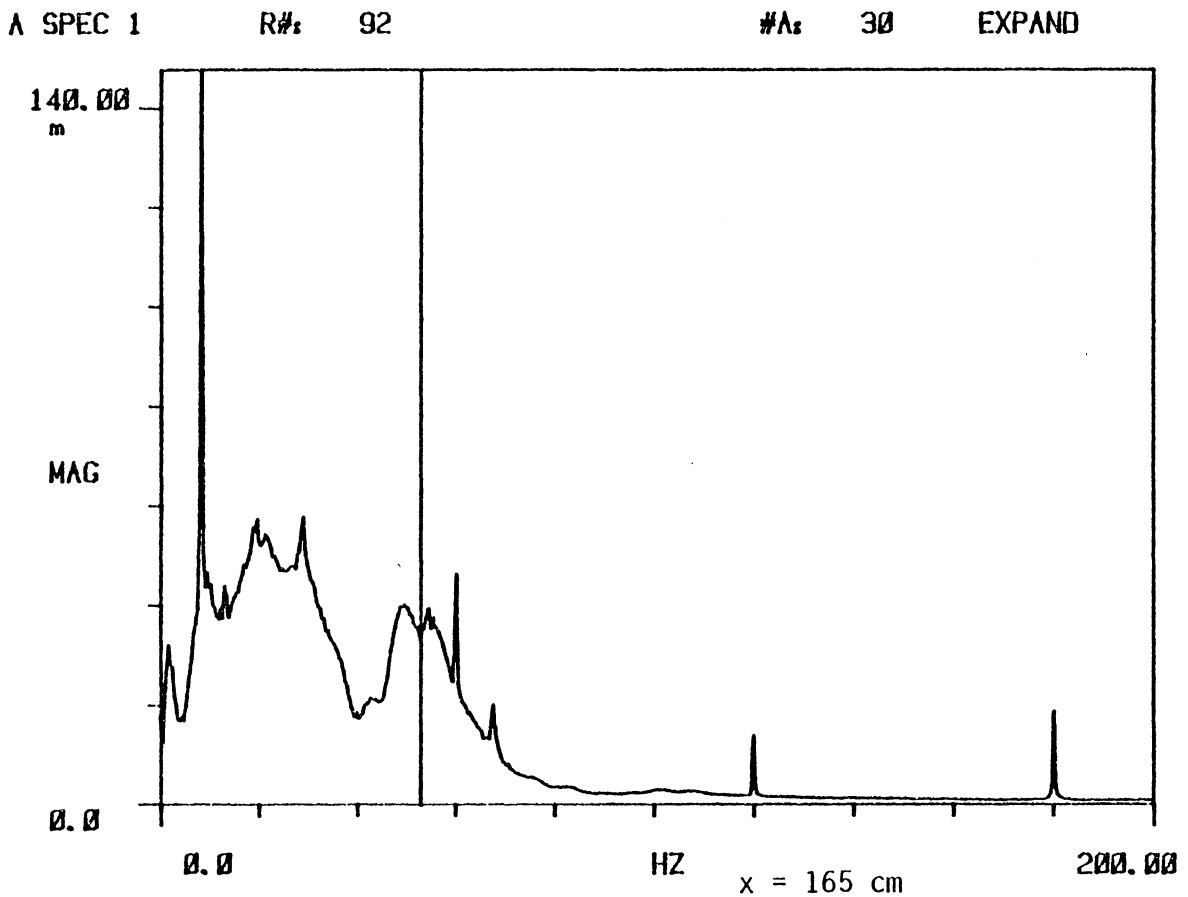

Figure 5.4.15 Boundary-layer system response to step-function input U_∞ = 9.1 m/sec.

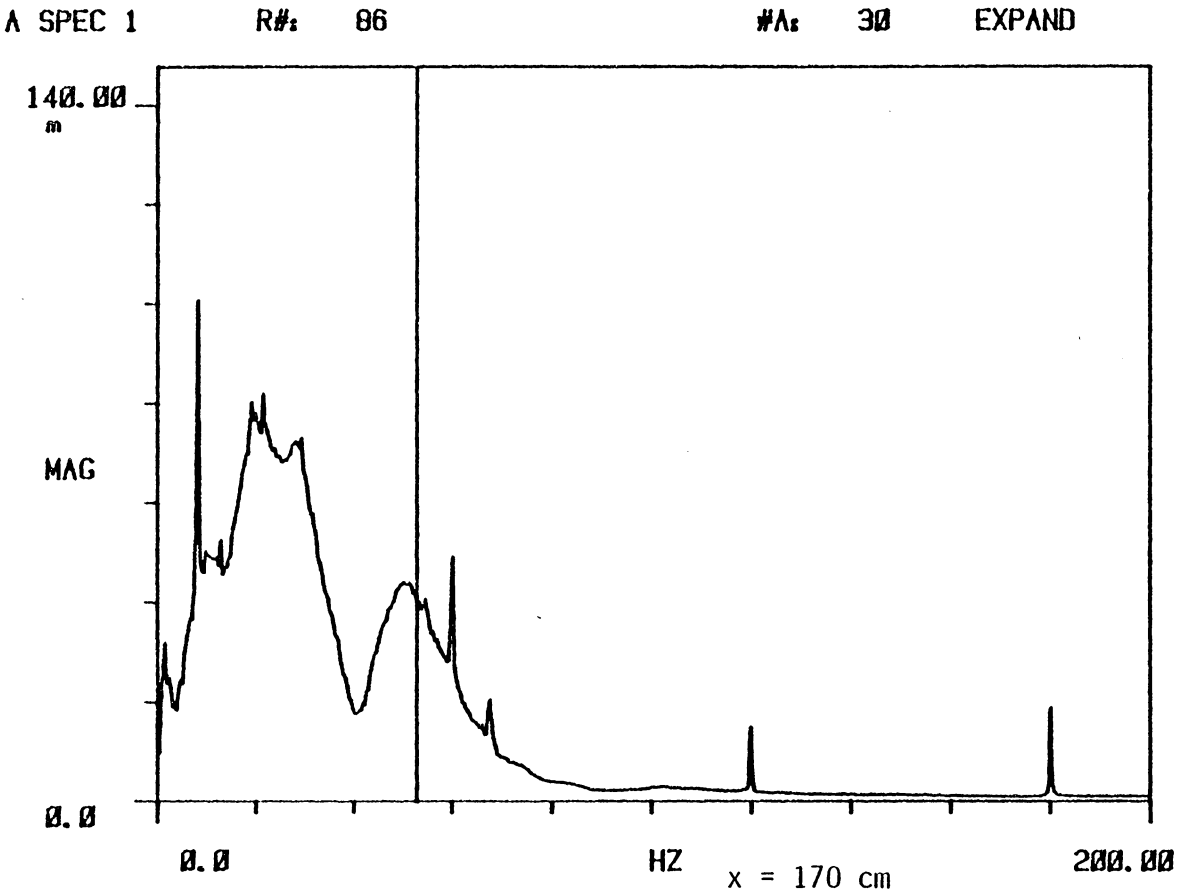

Figure 5.4.16 Boundary-layer system response to step-function input U_∞ = 9.1 m/sec.

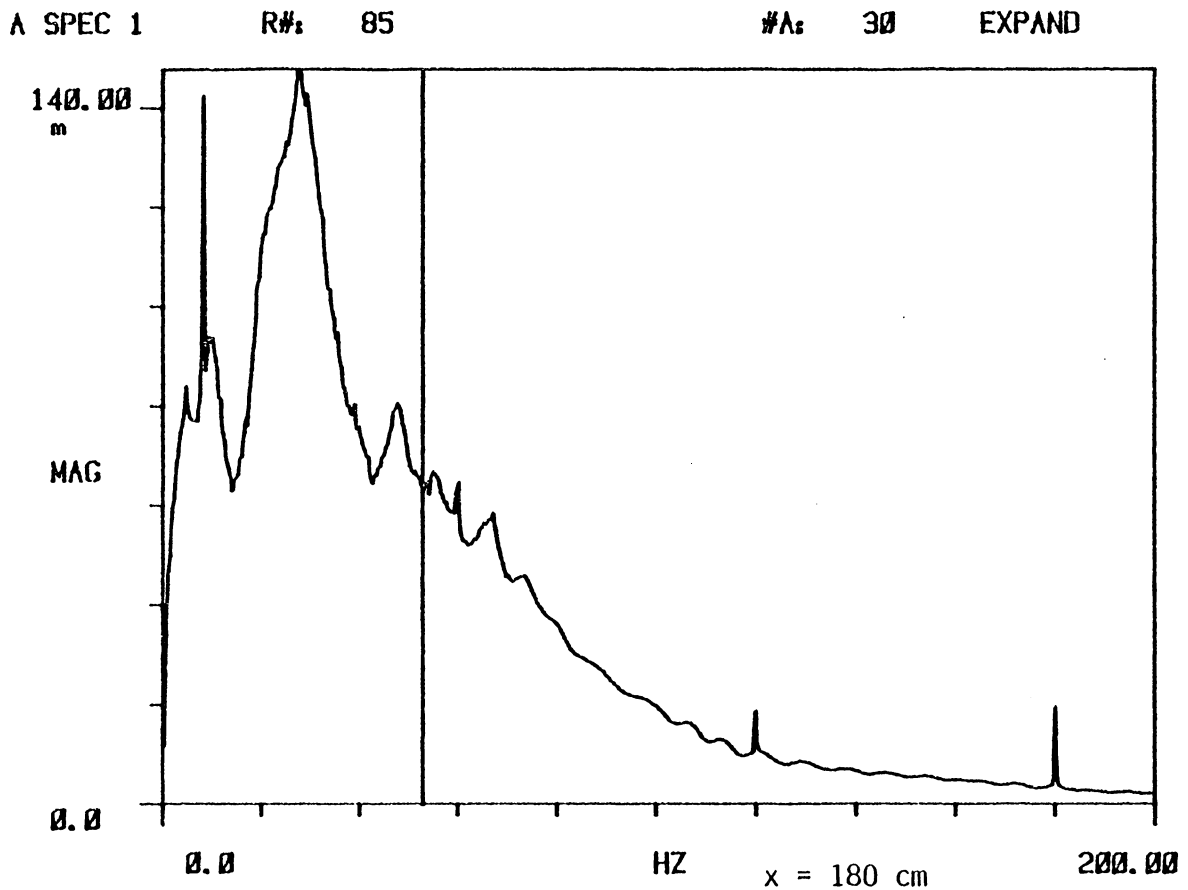

Figure 5.4.17 Boundary-layer system response to step-function input U_∞ = 9.1 m/sec.

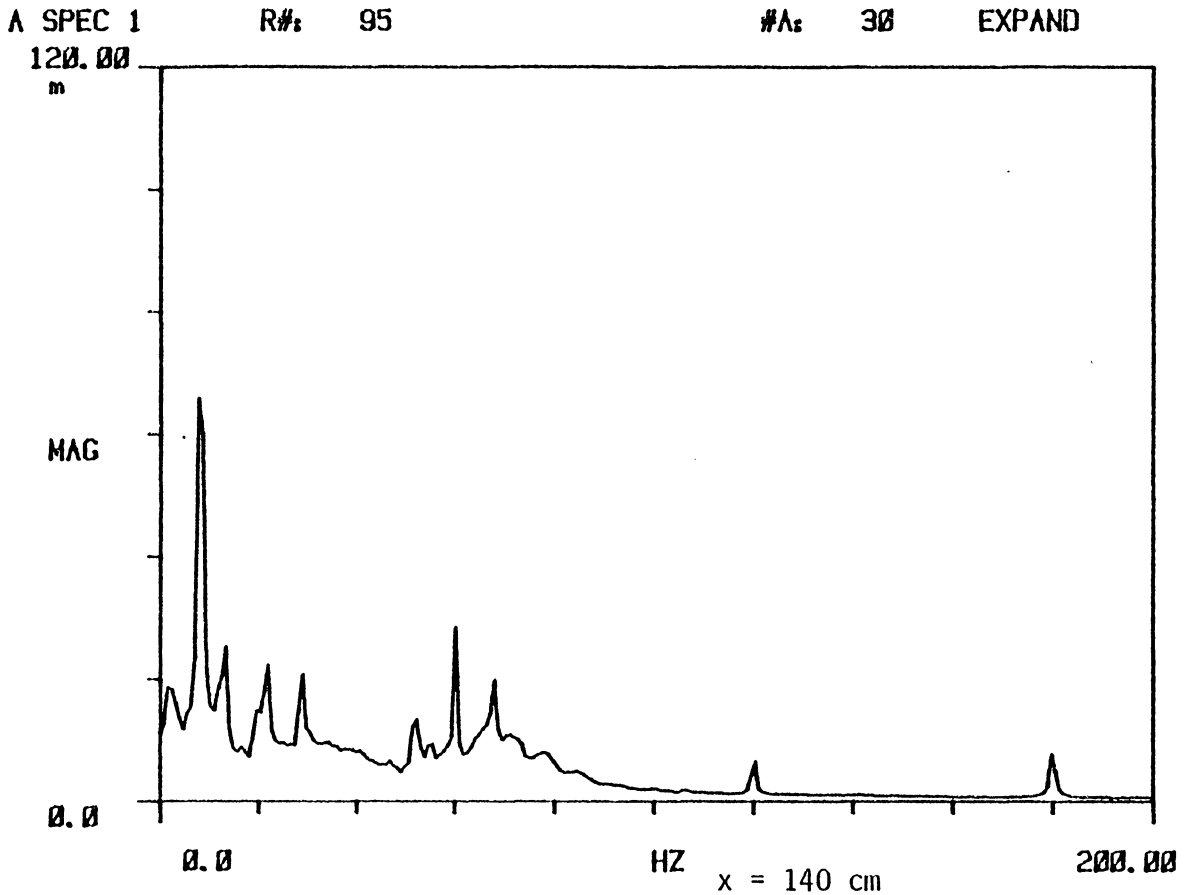

Figure 5.4.18 Boundary-layer system response to step input-excitation U_∞ = 10.5 m/s.

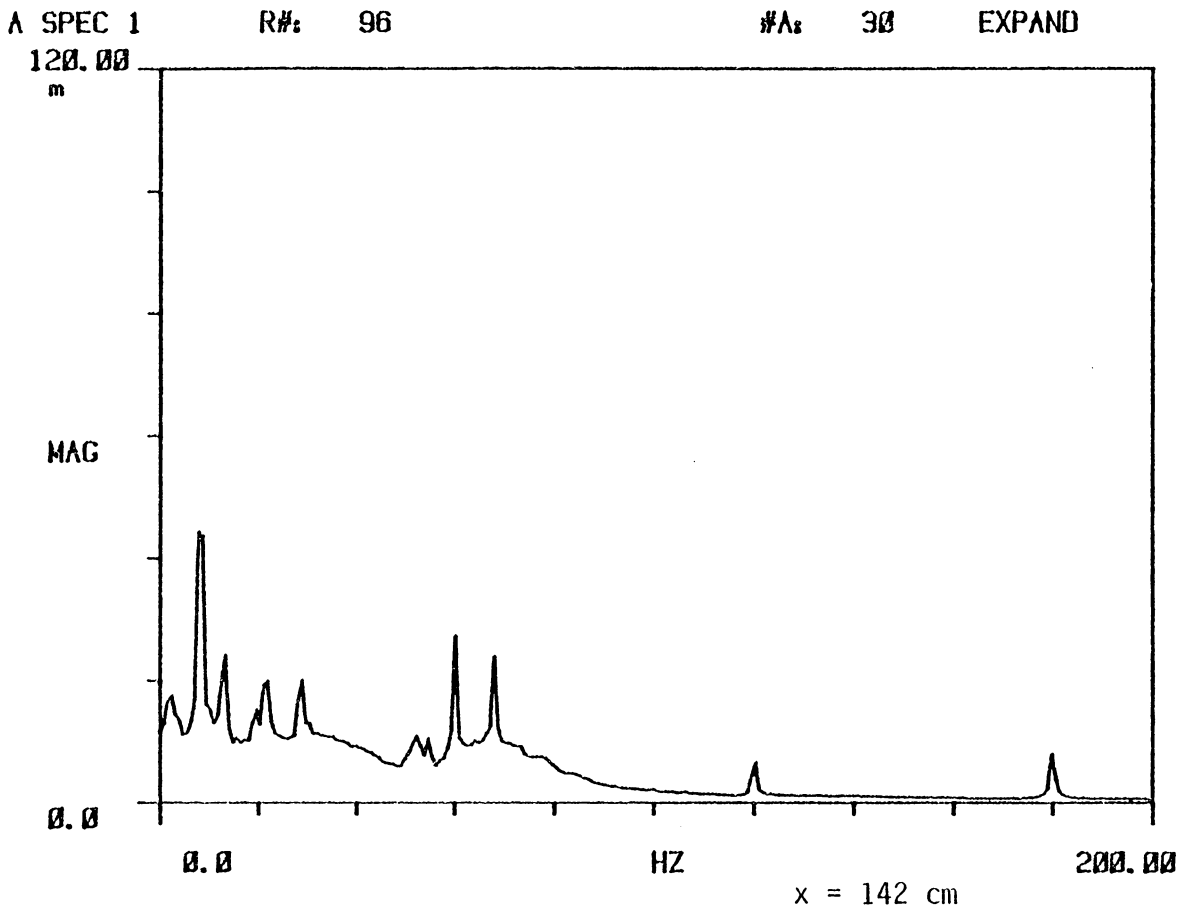

Figure 5.4.19 Boundary-layer system response to step input-excitation U_∞ = 10.5 m/s.

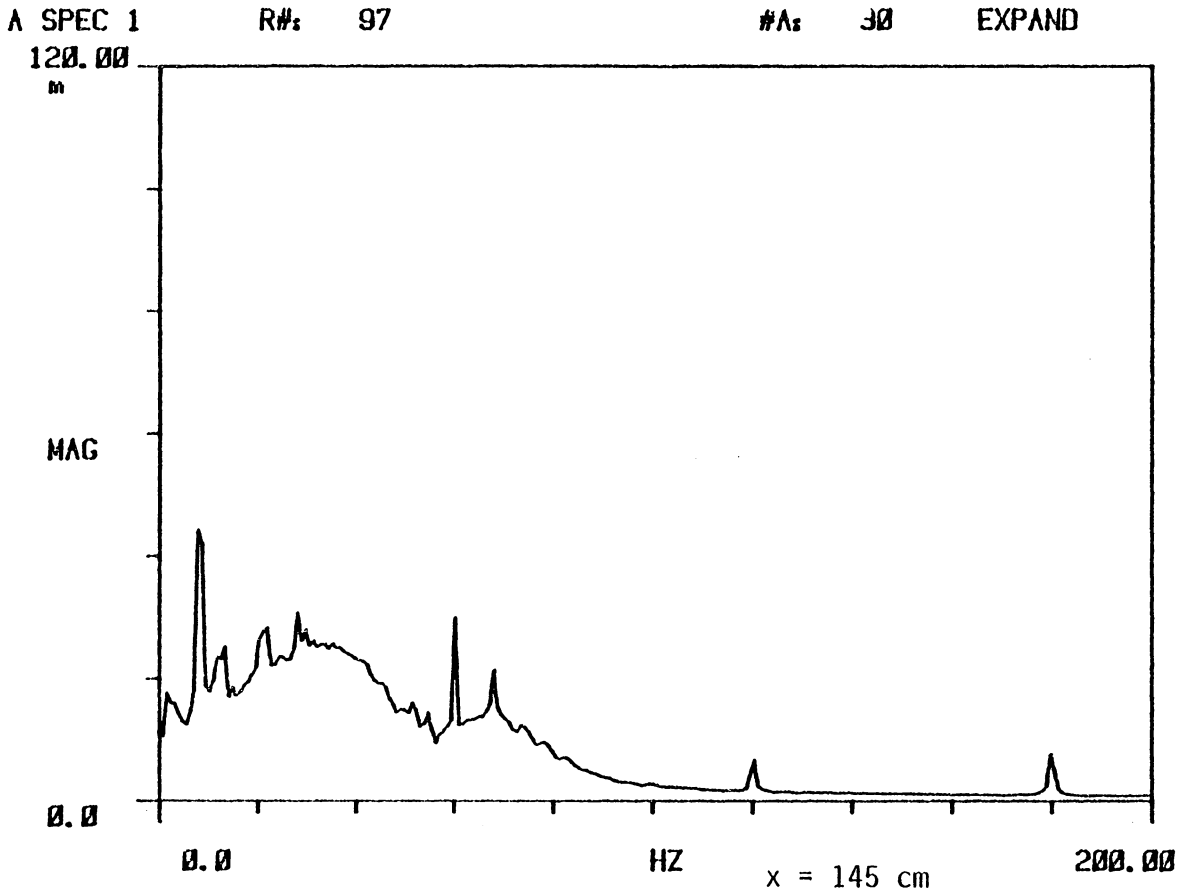

Figure 5.4.20 Boundary-layer system response to step input-excitation U_∞ = 10.5 m/s.

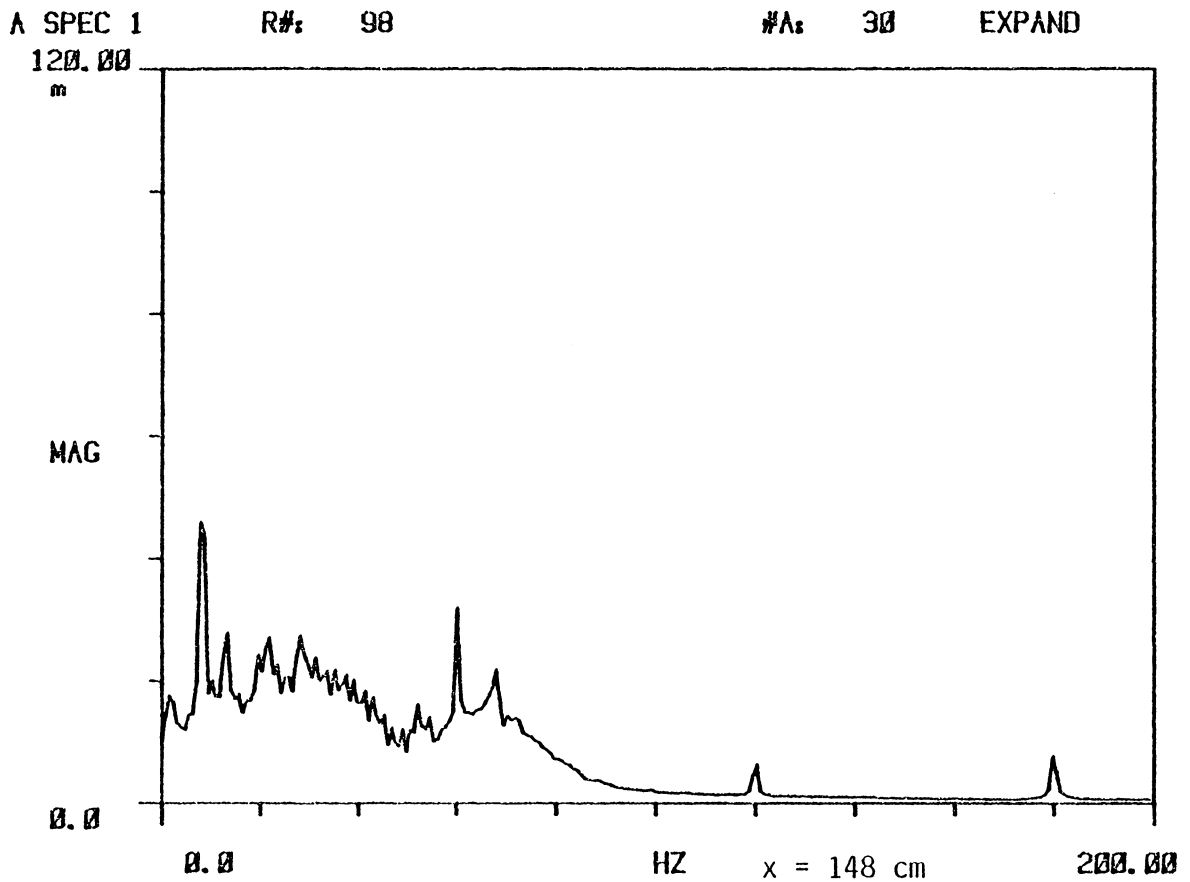

Figure 5.4.21 Boundary-layer system response to step input-excitation U_∞ = 10.5 m/s.

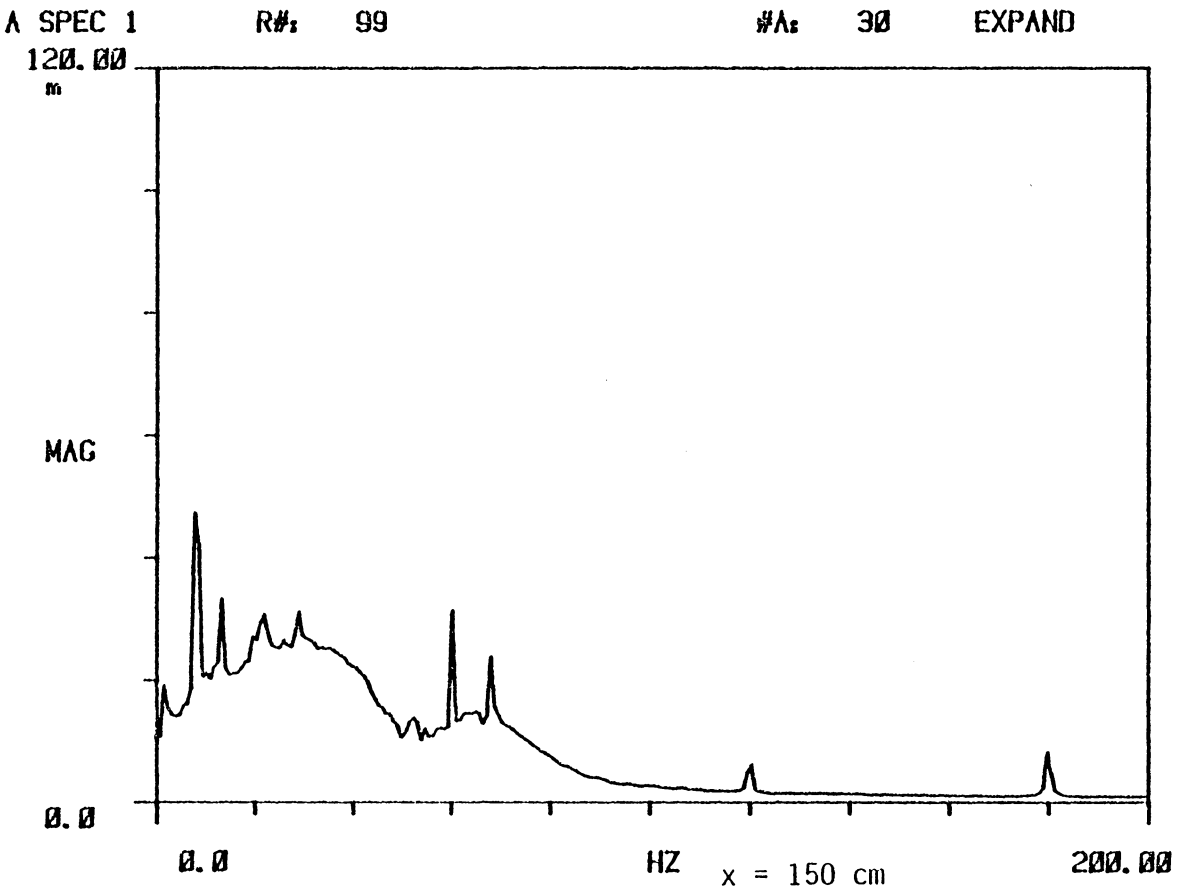

Figure 5.4.22 Boundary-layer system response to step input-excitation U_∞ = 10.5 m/s.

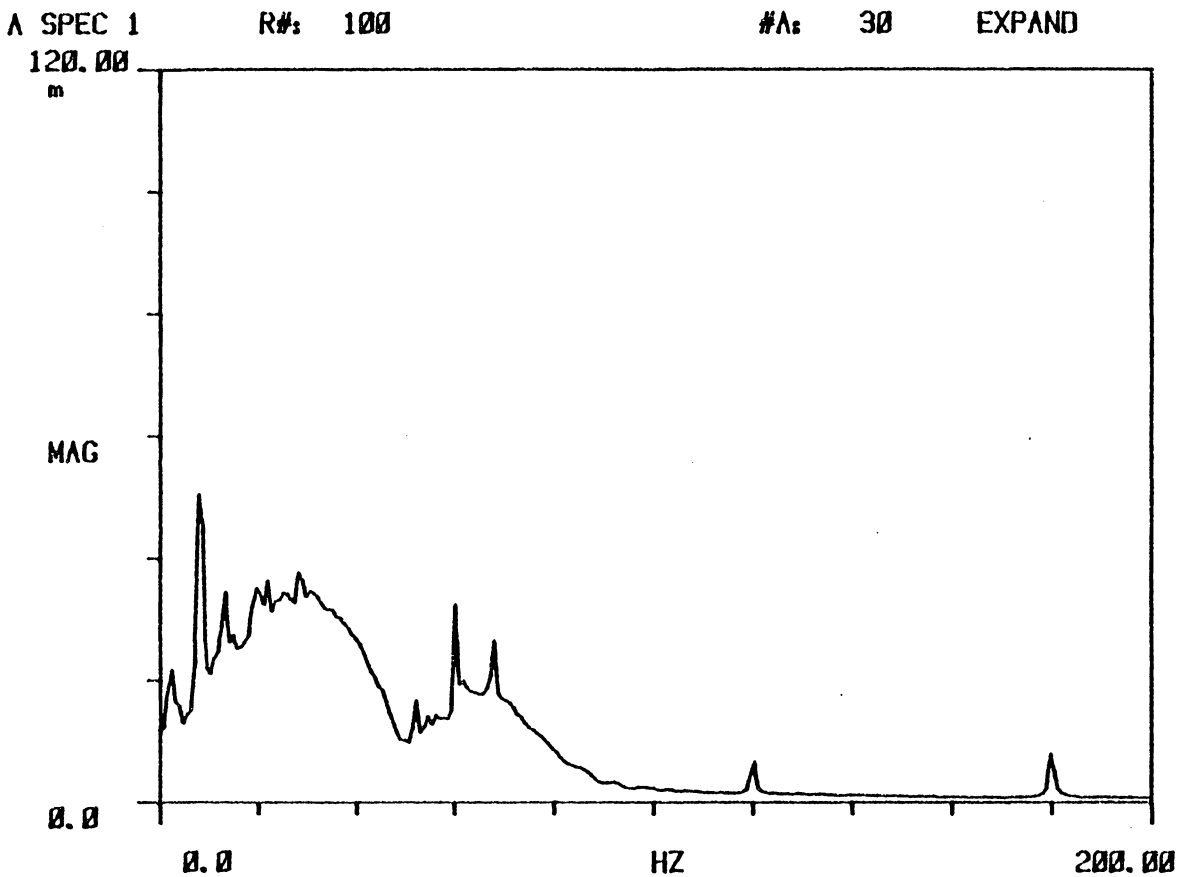

Figure 5.4.23 Boundary-layer system response to step input-excitation U_∞ = 10.5 m/s.

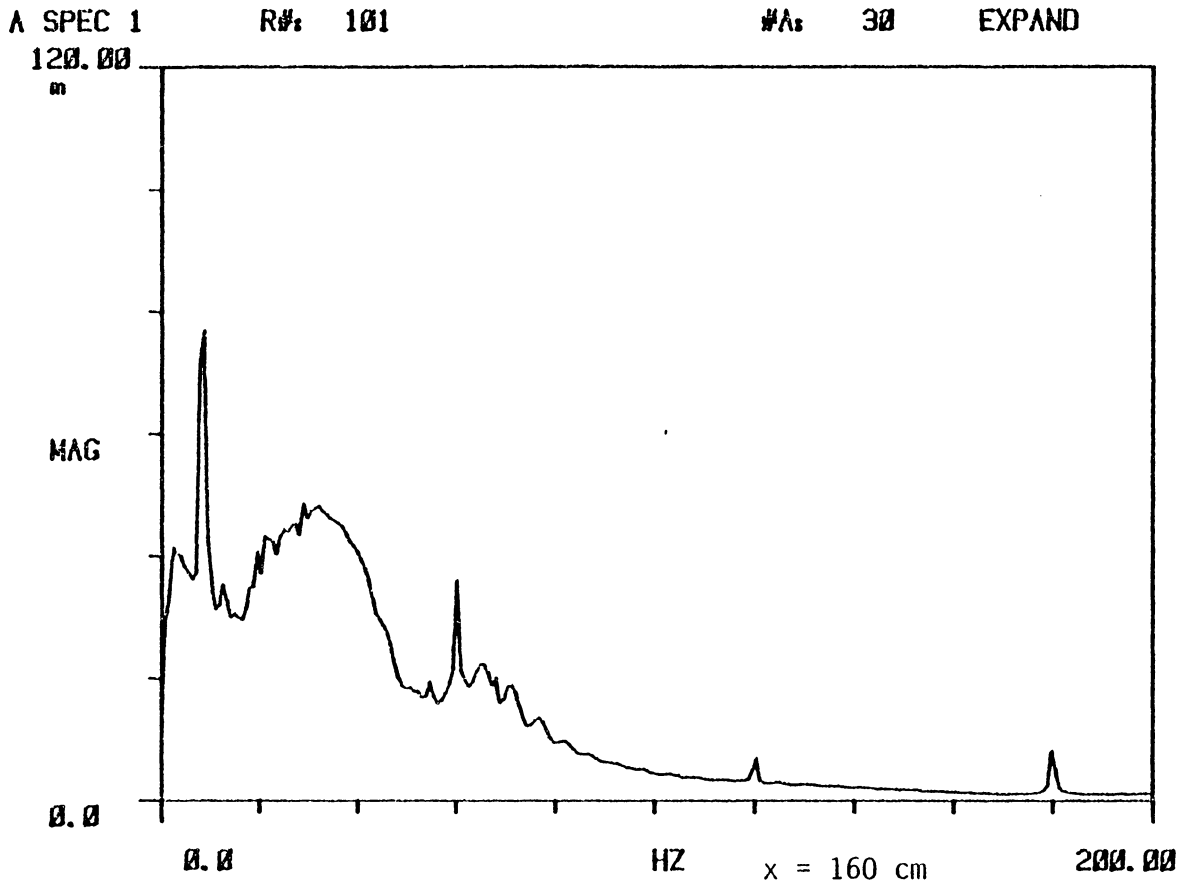

Figure 5.4.24 Boundary-layer system response to step input-exitation U_∞ = 10.5 m/s

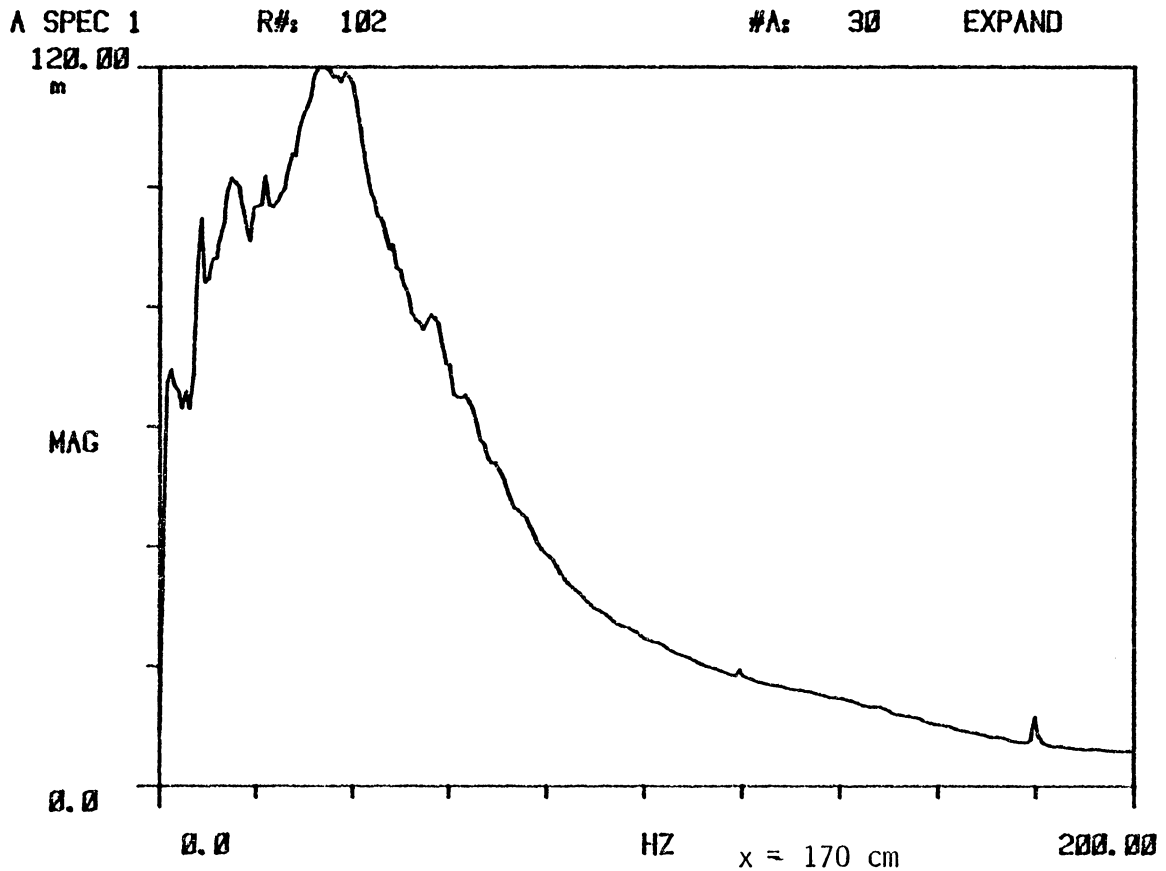

Figure 5.4.25 Boundary-layer system response to step input-excitation U_∞ = 10.5 m/s.

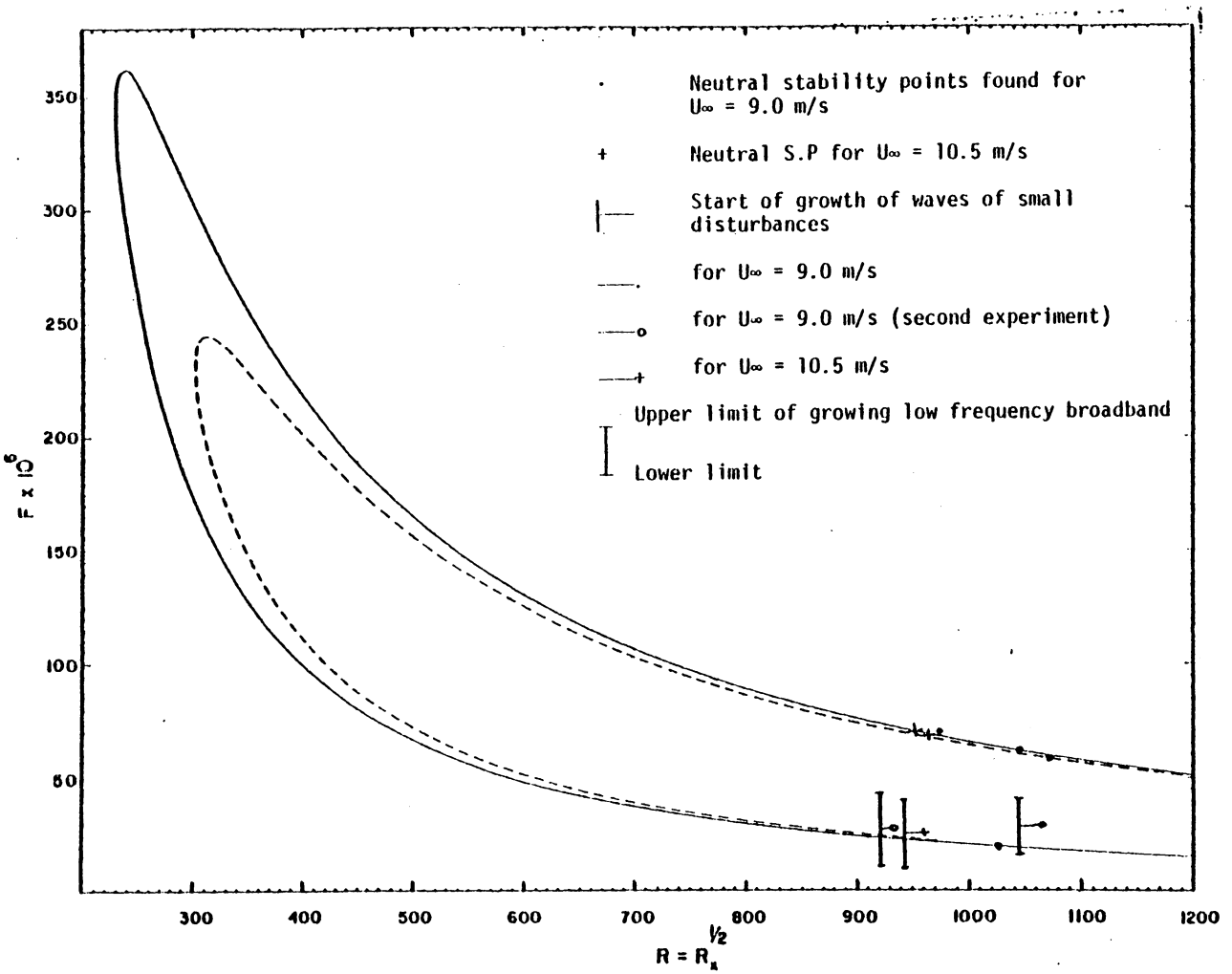
Neutral stability points found for U∞ = 9.0 m/s
Neutral S.P for U∞ = 10.5 m/s
Start of growth of waves of small disturbances
for U∞ = 9.0 m/s
for U∞ = 9.0 m/s (second experiment)
for U∞ = 10.5 m/s
Upper limit of growing low frequency broadband
Lower limit
F x 10^6
350
300
250
200
150
100
50
300
400
500
600
700
800
900
1000
1100
1200
R = R_δ*^1/2

Figure 5.5

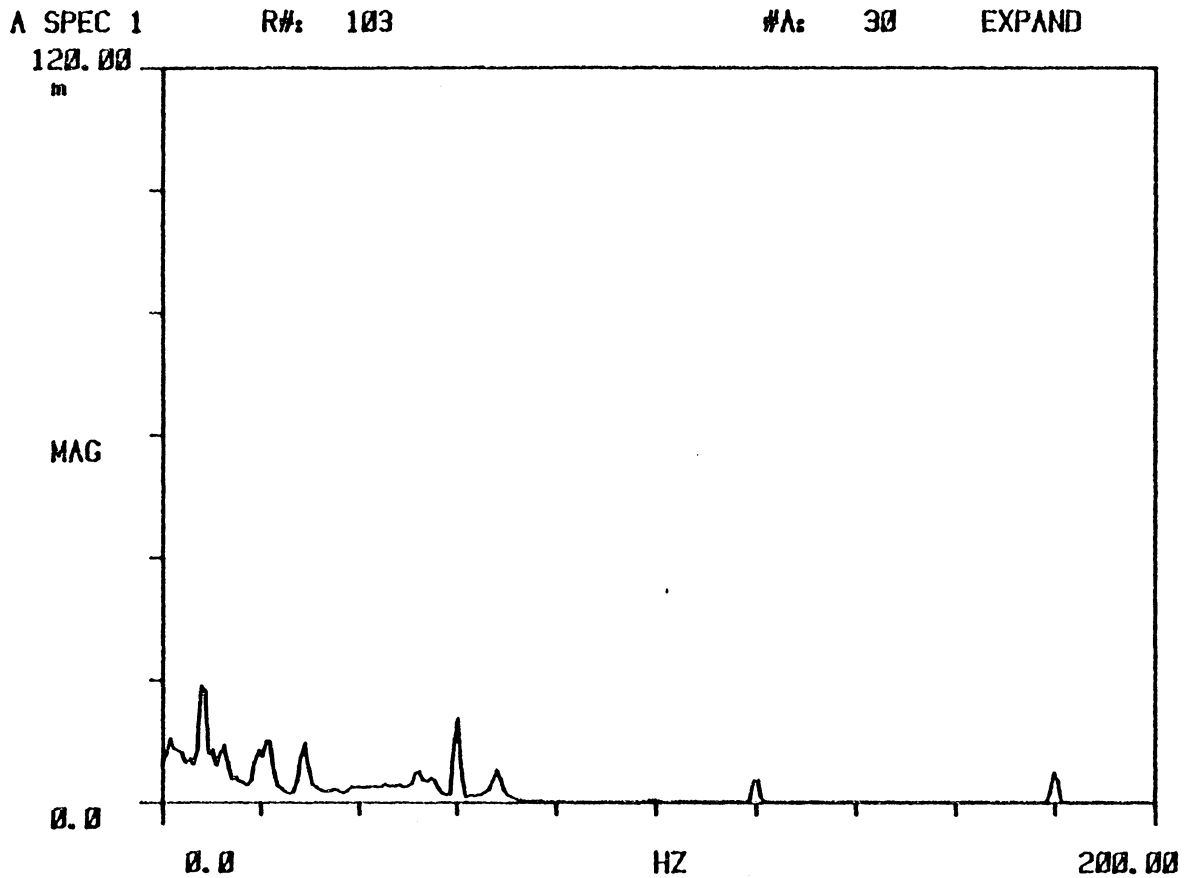

Figure 5.6 Boundary-layer system response without step-function input at U_∞ - 10.5 m/s.

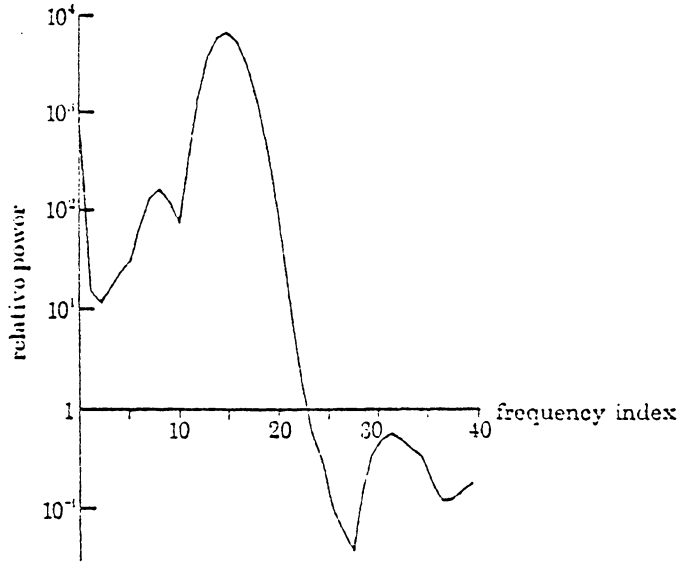

Figure 5.7 Typical wave-packet spectrum given by Gaster & Grant (1975).

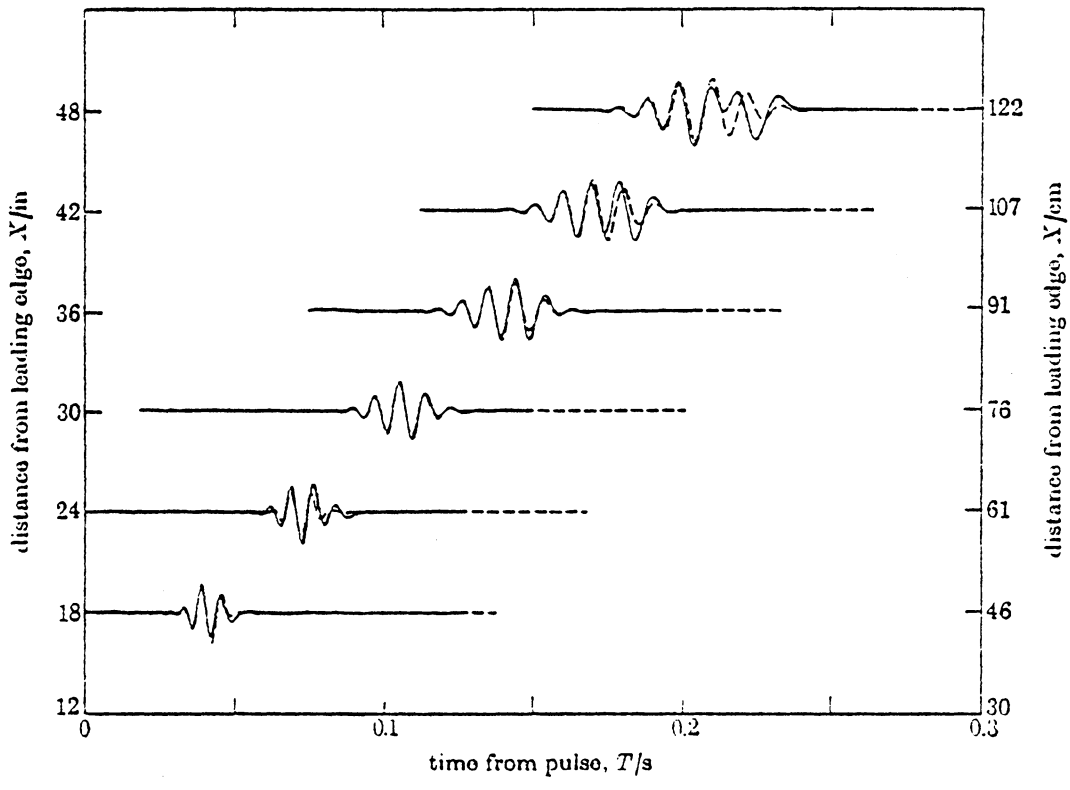

Figure 5.8 Comparison of model and experimental records along the center line ---, theory; ____, experiment (Gaster, 1975)

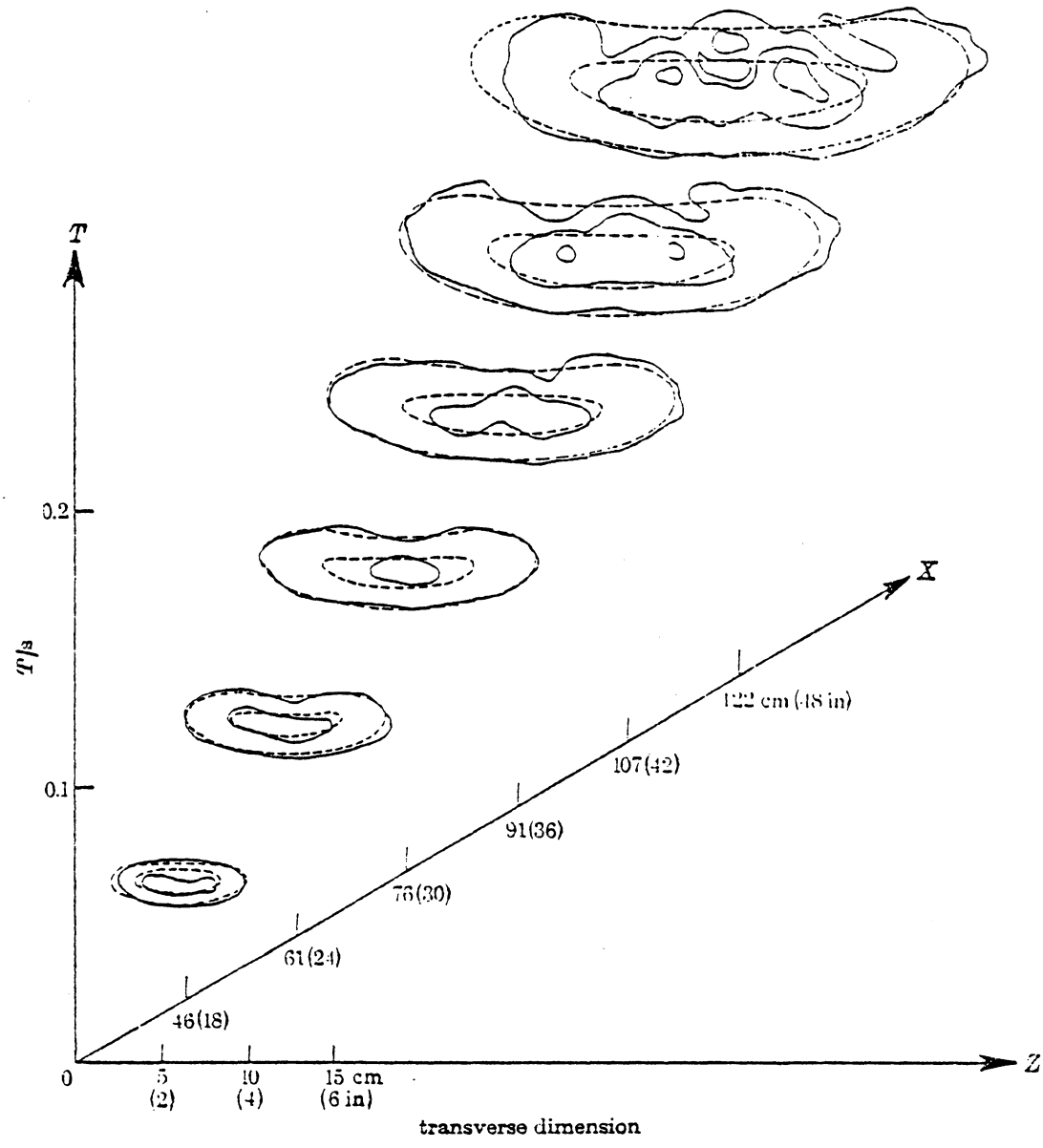

Figure 5.9 Comparison of measured and computed envelope contours (Gaster, 1975).

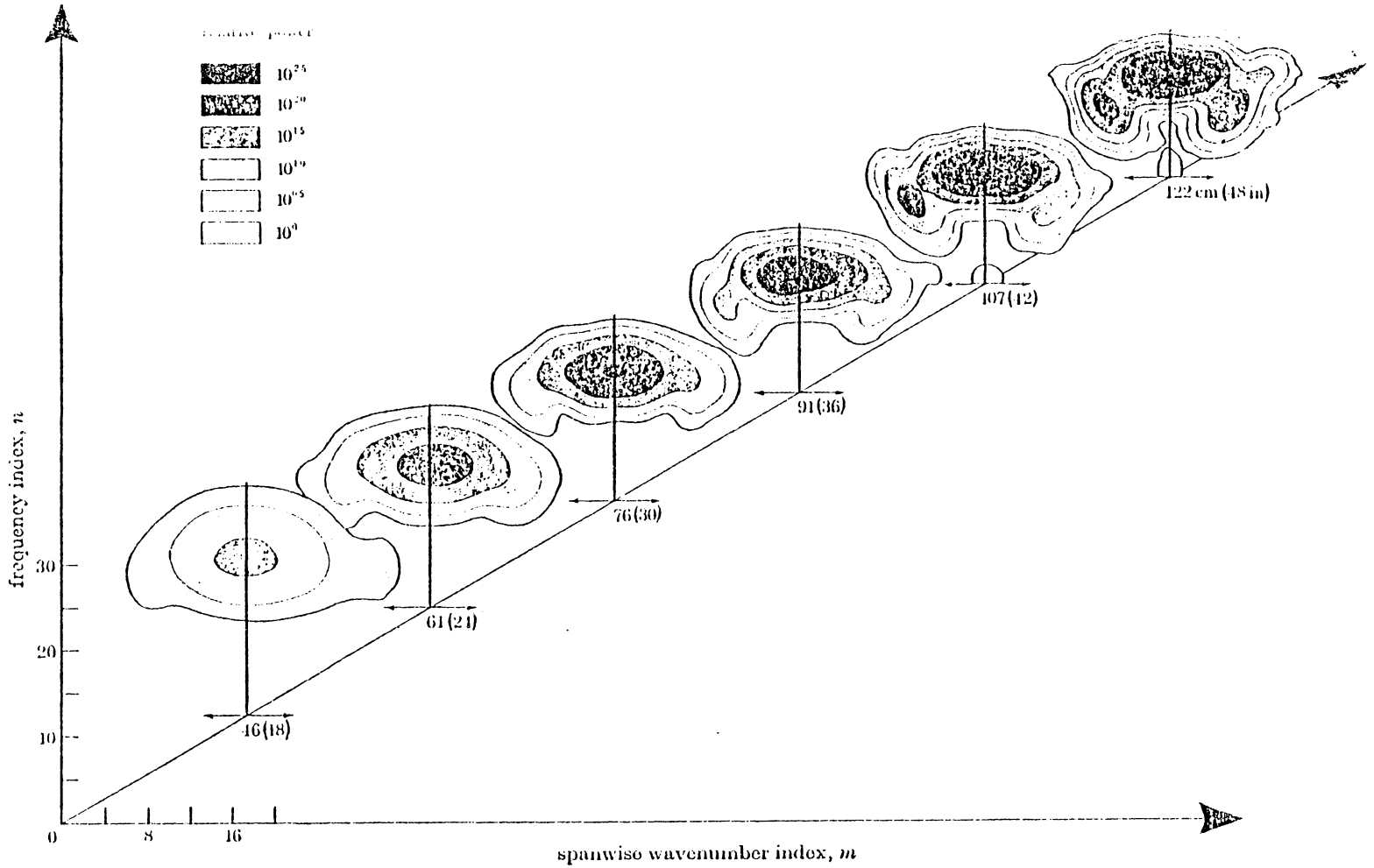

Figure 5.10 Wavenumber against frequency spectra of record arrays at different downstream locations.
$\omega\nu/U^2 = 5.29 \times 10^{-6} n$; $b\nu/U = 19.4 \times 10^{-6} m$. (Gaster, 1975)

APPENDIX 1. ELECTRONIC EQUIPMENT

A.1. DISA ANEMOMETRY. Six independent anemometry channels are available. Each channel consists of:

A.1.1. DISA 55D0L Constant Temperature Anemometer (CTA). The anemometer is operated with a bridge ratio of 1:20, using a probe cable length of 5m. For high resolution measurement of low-level signals, the hot wires and cables are balanced at a gain of 11 and operated at a gain of 7. The hot wires are calibrated through the data acquisition system.

A.1.2. DISA 55D10 Linearizer. All anemometer outputs are processed through this unit to obtain a voltage signal which is linearly proportional to the velocity being measured. The unit is calibrated through the data acquisition system.

A.1.3. DISA 55D35 RMS Voltmeter. A true r.m.s. and squared r.m.s. is obtained in the range -60 dB to 50 dB over one volt. The integrator time constant is variable in the range 0.3 to 100 seconds.

A.2. DISA HOT-WIRE PROBES

A.2.1. DISA 55P05 Boundary-Layer Probe. The sensor consists of a 5 μm diameter Platinum-plated tungsten wire with an overall length of 3 mm and a sensitive wire length of 1.25 mm (L/D = 250). Sensor-support prong isolation is provided by a copper and gold plating at the wire ends to a diameter of approximately 30 μm.

A.2.2. DISA 55P71 Parallel-Array Turbulence Probe. This is a two wire probe with parallel sensors separated by 0.4 mm. The probe sensors measure free-stream turbulence at essentially the same point and thus allow elimination of electronic noise from the two independent channels.

A.2.3. DISA 55P02 Slant-Wire Probe. This is used in conjunction with another probe to measure the w' fluctuations.

A.3. HP 3052 AUTOMATIC DATA ACQUISITION SYSTEM. This system provides high speed, 40 channel, data sampling capabilities. In addition, data processing capabilities are provided by the calculator with output via magnetic tape, paper tape, or digital plotting. All hot-wire calibrations, mean-flow measurements, proximitor calibrations, free-stream turbulence levels, and boundary-layer disturbance measurements are interfaced into the data-acquisition system. The signals from the constant-temperature hot-wire anemometers are conditioned using the usual assortment of linearizers, oscillators, tracking filters, phase meters, r.m.s. meters, and log converters described below. The traverse mechanism and the spectrum analyzer are also operated with this unit in either a programmed fashion or in response to the hot-wire signal. The system consists of:

A.3.1. HP 3455A High Accuracy/High Resolution DVM.

A.3.2. HP 3495A Input Multiplexer.

A.3.3. HP 9825A High Performance Calculator and ROMS.

A.3.4. HP 9872A Four-Pen Digital Plotter.

A.4. BRUEL & KJAER 4133 CONDENSOR MICROPHONES. Four of these units exist at VPI & SU. They have the following specifications: sensitivity 12.5 mv/Pa, Frequency range 3.9 Hz-40 KHz, Diameter 12.7 mm. Each are equipped with model 2619 preamplifier and Model 2801 power supply.

A.5. RION UC-29 CONDENSOR MICROPHONES. Ten of these units exist at VPI & SU and ten additional units will be added during the contract. They have the following specifications: sensitivity 4.5 mv/Pa, Frequency range 5Hz to 90 KHz, Diameter 6.3 mm. Each is equipped with a preamplifier and ganged power supply.

A.6. HP 5420A DIGITAL SIGNAL ANALYZER. This is a two channel digital FFT spectrum analyzer which provides time and frequency domain analysis of analog signals in the range of DC to 26 kHz. Analog data is input through the HP 54410A Analog/Digital Converter and anti-aliasing is provided by a HP 54470 Digital Filter. Unfiltered hot-wire signals are analyzed in conjunction with the data acquisition system. Both steady and triggered modes are possible.

A.7. HP 3960 INSTRUMENTATION TAPE RECORDER. This unit is a portable, 4 channel, 3-speed tape recorder which uses 6.35 mm magnetic tape. The recorder could be operated in either FM mode or direct record mode. It is used in FM mode which provides a DC to 5 kHz frequency bandwidth.

A.8. HONEYWELL MODEL 5600B TAPE RECORDER. Two of these units provide 24 channels of either direct- or FM-mode continuous records. These units, when used with the VPI & SU MINC Computer system, gives a back-up to the real-time data analysis.

A.9. SPECTRAL DYNAMICS SD121 TRACKING FILTER. This unit is a phase-locked servo, narrow-band pass filter which is tuned to a reference signal input. It is used with a bandwidth of 1 Hz, while bandwidths of 2, 10, 50, 100, 200 Hz are also available (three channels are available).

A.10. SPECTRAL DYNAMICS SD131 PHASE METER. Relative phase between any two measured signals is monitored with this unit. Typical usage is the measurement of the phase between the vibrating ribbon signal and the anemometer signals.

A.11. TRAVERSE CONTROLLER. Pulses to all three traversing mechanism stepping motors are provided by a Superior Electric ST103 Translator. This unit is supplemented by a controller/counter which provides convenient selection of motor stepping modes available through the ST103. These include half step/full step, low speed/high speed, and continuous run/single step options. Motor steps are also counted by the Traverse Controller and are output in a binary led display as well as front panel mounted DVM and corresponding analog voltage output. This unit is also operated by the data acquisition system.

A.12. TEKTRONIX MODEL 5113 OSCILLOSCOPE. This is an 8-channel scope with 2-channel storage capabilities.

A.13. HP 5300A/5302A FREQUENCY COUNTER. This counter provides frequency measurements with a resolution of 0.1 Hz for a ten second sample period.

A.14. BRUEL & KJAER 2427 AUTORANGING DIGITAL VOLTMETER. This voltmeter provides a true r.m.s., average, or peak reading for input signals in the range 0.5 Hz to 500 kHz.

A.15. SETRA-SYSTEMS MODEL 239E DIFFERENTIAL PRESSURE TRANSDUCER. This is a ± 0.01 psid transducer which provides a linear DC output of ± 2.5 volts. It is used for the static pressure measurements on the plate surface.

A.16. BENTLY-NEVADA SERIES 190 PROXIMITOR PROBE/SERIES 3000 SIGNAL CONDITIONER. This is an inductance type probe which has a linear measuring range of 0 - 1.1 mm with a nominal output of 0.0 to - 14 vdc. The frequency response is DC to 10 Hz, ± 1%. Two of these transducers are used to monitor sting vibration and ribbon vibration.

A.17. SCANIVALVE MODEL D. This solenoid operated mechanism provides for serial sampling of 48 pressure inputs. The selected pressure input is then available for pressure transducer measurement. Two of these units are used for 96 pressure ports.

A.18. MISCELLANEOUS. The usual collection of multimeters, strip-chart recorders, Kronhite: low-pass, high-pass, and band-pass filters, differential amplifiers, signal generators, power supplies, and (x,y,y') analog plotters are available.

```
                C$JOB     WATFIV
0001                DIMENSION X(402),Y(402),Y1(402),Y2(402)
0002                P=3.14159
0003                X0=8.17
0004                SY0=75.0E-03
0005                SYN1=5.294E-01
0006                SYN2=100.97E-03
0007                OMEGN1=188.
0008                OMEGN2=172.27
0009                DO 1 I=1,400
0010                X(I)=FLOAT(I)
0011                Y(I)=SY0/((1.-X(I)**2/(OMEGN1**2))**2+
                   $(SY0/SYN1)*(X(I)/OMEGN1)**2)
0012                Y1(I)=(X0/(2.*P*X(I)))/((1.-X(I)**2/(OMEGN2**2))**2+
                   $X0*X(I)**2/(SYN2*2.*P*OMEGN2**3))
0013                IF(I.LE.5) Y1(I)=0.250
0014                WRITE(6,11) X(I),Y(I),Y1(I)
0015             11 FORMAT(5X,3F15.5)
0016              1 CONTINUE
0017                F1=3.0
0018                F2=1.0
0019                G1=12.0
0020                G2=F2
0021                E1=21.0
0022                E2=F2
0023                CALL PLOTS(0,0,50)
0024                CALL PLOT(F1,F2,-3)
0025                CALL SCALE(X,8.,400,1)
0026                CALL SCALE(Y,6.,400,1)
0027                CALL SCALE(Y1,6.,400,1)
0028                CALL SCALE(Y2,6.,400,1)
0029                CALL AXIS(0.,0.,13HFREQUENCY(HZ),-13,8.,0.,X(401),X(402))
0030                CALL AXIS(0.,0.,9HMAGNITUDE,+9,6.,90.,Y(401),Y(402))
0031                CALL LINE(X,Y,400,1,0,1)
0032                CALL PLOT(G1,0.0,-3)
0033                CALL AXIS(0.,0.,13HFREQUENCY(HZ),-13,8.,0.,X(401),X(402))
0034                CALL AXIS(0.,0.,9HMAGNITUDE,+9,6.,90.,Y1(401),Y1(402))
0035                CALL LINE(X,Y1,400,1,0,1)
                C   CALL PLOT(E1,0.0,-3)
                C   CALL AXIS(0.,0.,13HFREQUENCY(HZ),-13,8.,0.,X(401),X(402))
                C   CALL AXIS(0.,0.,9HMAGNITUDE,+9,6.,90.,Y2(401),Y2(402))
                C   CALL LINE(X,Y2,400,1,0,1)
0036                CALL PLOT(21.,4.,999)
0037                STOP
0038                END
```

APPENDIX 2

Vibrating-Ribbon Model Program

SETUP STATE

MEASUREMENT : HI-RES AUTO SPECTRUM

AVERAGE : 20 , STABLE

SIGNAL : SINUSOIDAL

TRIGGER : FREE RUN , CHNL 1

CENT FREQ : 0.0 HZ

BANDWIDTH : 200.000 HZ

TIME LENGTH : 2.56000 S

dF : 390.625 mHZ dT : 1.25000 mS

ADC CHNL	RANGE	AC/DC	DELAY	CAL(C1/C2)
* 1	5 V	AC	0.0 S	1.00000
2	10 V	DC	0.0 S	1.00000

APPENDIX 3
SETUP STATE OF THE H-P SPECTRUM ANALYSER FOR RANDOM EXCITATION

SETUP STATE

MEASUREMENT : TRANSFER FUNCTION

AVERAGE : 30 , EXPONENTIAL DECAY

SIGNAL : TRANSIENT

TRIGGER : EXTERNAL AC , CHNL 1

CENT FREQ : 0.0 HZ

BANDWIDTH : 200.000 HZ

TIME LENGTH : 1.28000 S

dF : 781.250 mHZ dT : 1.25000 mS

ADC CHNL	RANGE	AC/DC	DELAY	CAL(C1/C2)
* 1	5 V	AC	0.0 S	1.00000
2	10 V	DC	0.0 S	1.00000

APPENDIX 4

SETUP STATE OF THE SPECTRUM ANALYSER FOR STEP-FUNCTION FORM OF EXCITATION

The vita has been removed from the scanned document

EXCITATION OF WAVE PACKETS AND RANDOM DISTURBANCES IN A BOUNDARY LAYER

by

CHRISTOPHER E. COSTIS

(ABSTRACT)

A study on the behaviour of wave-packets and random disturbances, introduced by the vibrating-ribbon technique in a Blasius boundary layer, is presented. The experiments were conducted in the VPI & SU low turbulence wind tunnel. The flat plate model was constructed from an aluminum-paper honeycomb laminate and an aluminum leading edge with an elliptical profle.

A theoretical model was developed to verify the random and step-function-form motion of the vibrating ribbon. In the case of random-disturbance introduction it was found that the random disturbances behave like infinite number, single-frequency waves and measurements of their growth made possible to verify regions of the neutral-stability curve.

In the case of wave-packet creation it was found that the wave-packets behave like a structure that consists of waves of certain frequencies that grow or decay not necessarily according to the stability curve but in that way as to maintain the wave-packet structure.

Their growth as they move downstream and their quick destruction into turbulence was compared to previously published data.